

3D Printing of SelfHealing Materials

*Original*

3D Printing of SelfHealing Materials / Roppolo, Ignazio; Caprioli, Matteo; Pirri, Candido F.; Magdassi, Shlomo. - In: ADVANCED MATERIALS. - ISSN 0935-9648. - 36:9(2024). [10.1002/adma.202305537]

*Availability:*

This version is available at: 11583/2995435 since: 2024-12-16T12:04:33Z

*Publisher:*

John Wiley and Sons

*Published*

DOI:10.1002/adma.202305537

*Terms of use:*

This article is made available under terms and conditions as specified in the corresponding bibliographic description in the repository

*Publisher copyright*

(Article begins on next page)

# 3D Printing of Self-Healing Materials

Ignazio Roppolo,\* Matteo Caprioli, Candido F. Pirri, and Shlomo Magdassi

This review article presents a comprehensive overview of the latest advances in the field of 3D printable structures with self-healing properties.

Three-dimensional printing (3DP) is a versatile technology that enables the rapid manufacturing of complex geometric structures with precision and functionality not previously attainable. However, the application of 3DP technology is still limited by the availability of materials with customizable properties specifically designed for additive manufacturing. The addition of self-healing properties within 3D printed objects is of high interest as it can improve the performance and lifespan of structural components, and even enable the mimicking of living tissues for biomedical applications, such as organs printing. The review will discuss and analyze the most relevant results reported in recent years in the development of self-healing polymeric materials that can be processed via 3D printing. After introducing the chemical and physical self-healing mechanism that can be exploited, the literature review here reported will focus in particular on printability and repairing performances. At last, actual perspective and possible development field will be critically discussed.

manufacturing (CAM) relies on the deposition of materials in a layer-by-layer fashion creating models by selective and successive addition of material, until completion, to reproduce the designed virtual model in a single-step fabrication process.<sup>[2]</sup> Unlike traditional manufacturing processes, AM tools can produce arbitrarily complex shapes characterized by hierarchical and intricate architectures with hollow features and graded or multi-material structures, thanks to the controlled spatial arrangement of the starting material within the final object.<sup>[3]</sup> Furthermore, 3DP allows on-demand fabrication of tailored products in a cost-effective manner, which is particularly effective for limited productions, thanks to the ease in personalizing CAD files and fabricating parts consequently.<sup>[4]</sup>

Among the various classes of AM techniques, polymeric 3DP is the most relevant part of the market. The geometric freedom and precise control of 3DP, combined with the development of polymers specifically

## 1. Introduction

Three-dimensional printing (3DP), also known as additive manufacturing (AM), has emerged as an advanced, versatile technology for the rapid on-demand manufacturing of solid objects created through a build-up process starting from a virtual CAD model of the geometry to be printed.<sup>[1]</sup> This computer-aided


designed for AM, enable the fabrication of smart materials and structures, not achievable through conventional manufacturing methods.<sup>[5]</sup> Among the various properties that materials can possess, one of particular interest is stimuli-responsiveness, which describes the conversion into measurable macroscopic responses of small environmental variations determined by the specific nature of the constituent elements.<sup>[6]</sup> The combination of 3D manufacturing and stimuli responsiveness is called 4D printing, and nowadays this approach is at the forefront of the research, holding tremendous promise for potential high-performance applications in existing and emerging fields.<sup>[7]</sup> The key is the intimate and synergistic integration between structure and functionalities, which provides the ability to alter particular properties in a controlled and often reversible manner.<sup>[8]</sup>

On the other hand, as for every component produced, 3D printed objects can also undergo failure, which may be the result of the deterioration of the mechanical properties related to materials use and aging, which affects the integrity of structures and limits the operational lifetime. As a matter of fact, at the moment the tendency in 3D printing consists of using 3D printed objects as disposable once, taking advantage of the fast-printing times and the possibility of on-demand production. This approach is clearly not sustainable, generating materials waste and consuming machines operational times. Repair can be a suitable option, but this seems not trivial in this case. In fact, 3D-printed parts generally have complex architectures with areas hard to repair manually because of access difficulties. Consequently, the

I. Roppolo, M. Caprioli, C. F. Pirri  
 Department of Applied Science and Technology  
 Politecnico di Torino  
 Corso Duca degli Abruzzi 24, Turin 10129, Italy  
 E-mail: ignazio.roppolo@polito.it

I. Roppolo, C. F. Pirri  
 Istituto Italiano di Tecnologia  
 Center for Sustainable Futures @Polito  
 Via Livorno 60, Turin 10144, Italy

M. Caprioli, S. Magdassi  
 Casali Center for Applied Chemistry  
 Institute of Chemistry  
 The Hebrew University of Jerusalem  
 Edmond J. Safra Campus, Jerusalem 9090145, Israel

 The ORCID identification number(s) for the author(s) of this article can be found under <https://doi.org/10.1002/adma.202305537>

© 2023 The Authors. Advanced Materials published by Wiley-VCH GmbH. This is an open access article under the terms of the Creative Commons Attribution License, which permits use, distribution and reproduction in any medium, provided the original work is properly cited.

DOI: 10.1002/adma.202305537

autonomous restoration of the initial performances and properties after damage, also called self-healing (SH), seems to be an appealing approach in 3D printing.<sup>[9]</sup> Although self-healing materials were proposed a long time ago, their integration with 3D printing is relatively new.<sup>[10]</sup> In this context, to achieve structural restoration and function recovery after local mechanical damage without or with limited human intervention, enhancing reliability and extending the useful life of the object, seems particularly attractive.<sup>[11]</sup> Furthermore, thanks to 3D printing may be possible to upscale the self-healing ability from material to structure level, with hopefully selective control of the self-healing functionality in areas that are prone to damage is of high interest. Consequently, in view of the use of SH materials in 3DP, it is necessary to design the polymeric with tailored structure, architecture, and functionality to match requirements of printability while maintaining proper desired final properties, primarily restoration ability. And in this frame, strategies can be multiple.

The aim of this review is to provide a comprehensive overview of the current state-of-the-art 3D printed polymers with intrinsic self-healing ability. We envision that there is still a large margin for progress and improvement in the field, which will expand the potential application of these materials to both structural and functional purposes, also given the rising global attention over resource consumption reduction and performance optimization.

## 2. Self-Healing Mechanisms

Deterioration of mechanical properties is a direct consequence of materials use and aging, resulting in damages and eventually in failures. The most exploited response of modern society to this evidence consists in the development of disposable objects, directly replacing the components when damaged. This approach cannot be sustained in a view of materials and energy saving. As an alternative, materials can be repaired by exploiting different methods: temperature, soldering, material addition, etc. Repair needs continuous monitoring of the mechanical properties, and intervening timely, which is not always possible and may cause undesired failures during operative life. To address this limitation and extend operational performance, materials inherently capable of autonomous repair with limited or no external human intervention must be designed, enabling the so-called self-healing. Self-healing materials are able to partially or fully restore their integrity and mechanical performance after damages, recovering from cracks at the macro or microscale.<sup>[12]</sup>

In general, self-healing materials can be subdivided into two distinct groups, extrinsic and intrinsic, based on the restoration mechanism. In extrinsic self-healing systems, the healing agents, such as unreacted monomers, solvents, or low- $T_g$  polymers, are confined in reservoirs embedded in the polymeric matrix. The healing agents can be arranged in two different configurations: capsule-based or vascular-based.<sup>[13,14]</sup> When mechanical damage occurs, it causes chain cleavage and disentanglement, and ultimately crack formation and propagation. When those cracks reach the reservoirs, the healing agent is released and fills the cracks, to mend the fracture acting as a sealant. The restoring mechanism, based on in situ polymerization, solvent welding, or macromolecular diffusion and entanglement with the matrix, is particularly efficient in restoring large portions of the material.

On the other hand, it is evident that restoration can be achieved only once on the same site.<sup>[11]</sup>

Instead, intrinsic self-healing polymers are based on the restoration of reversible bonds, established by specific functionalities, which in many cases can be different from the pristine macromolecular network. The main advantage of intrinsic self-healing polymers consists in enabling multiple repair processes, usually only for small, localized damage zones but with relevant exceptions.<sup>[9]</sup> Intrinsic self-healing strategies are more versatile, being able to adapt to a lot of matrices and many external conditions. This property can be achieved following two main strategies: by chemical cross-linking through dynamic covalent chemistry or by physical cross-linking through non-covalent supramolecular interactions. However, also their combination can be exploited.

Dynamic bonds are established between latent moieties capable of selective interaction after crack formation. This means that the presence of healing agents is no longer required, preventing problems related to inhomogeneous reservoir distribution and compatibility with the matrix. Polymer structures can be designed to present different binding points depending on the position of the interacting groups, along or within the polymer backbone, and the number of binding sites available, with multifunctional groups that enable the formation of a reversible network with no permanent covalent backbone.<sup>[15]</sup> Newly created surfaces expose many available functional groups that can recombine across fracture interfaces upon re-joining, whose interaction can be supported and amplified by the possibility of diffusion and rearrangement of the macromolecular segments.<sup>[16]</sup> Chain mobility, functional group availability at the surface, and their reactivity could be limiting factors to an efficient healing process, together with external chemical modifications of the useful moieties (e.g., oxidation).

Intrinsic self-healing materials can also be classified into autonomous and non-autonomous systems, depending on whether they have the ability to spontaneously reform bonds within the matrix, which otherwise would require an external stimulus to promote the restoration, such as temperature, light, and pH.<sup>[17]</sup> On the other hand, self-healing can be considered a stimuli-responsive property, since repair is always triggered by the rupture, independently of the constitutive mechanism and the autonomous or externally assisted nature of the healing process.<sup>[6,8]</sup>

Generally, independently from the specific mechanism, before the formation of the reversible bonds, the intrinsic self-healing process is based on an initial macromolecular interdiffusion across the broken surfaces which occurs spontaneously for thermodynamic reasons.<sup>[18]</sup> The restoration is thus mainly governed by polymer chain motion, which depends on the chemical nature and structure of the polymer, its molecular weight, the temperature at which the healing is performed, and eventually by the presence of solvents.<sup>[19]</sup> Therefore, in contrast with their extrinsic counterparts, intrinsic healing materials are generally not fully autonomous and require an external stimulus to activate local mobility.<sup>[20]</sup>

Thermoplastic polymers show molecular interdiffusion between two regions when heated above their  $T_g$ , while diffusion in thermosets is limited to free segments when heated. Soft materials, such as elastomers or hydrogels, are particularly suited to perform intrinsic self-healing since chain mobility in

these systems is particularly high.<sup>[21]</sup> In hydrogels, diffusion is a rapid process even at room temperature thanks to the solvation induced by the water molecules, which enables a large free chain length and segmental motion, resulting in a deeper interpenetration and stronger interactions. However, the reinstatement of reversible bonds is strongly time-dependent and deteriorates with time because of hydrophobic rearrangement of the hydrogel surfaces.<sup>[22,23]</sup> Only freshly cut hydrogel surfaces can undergo efficient healing because after being cut, hydrophilic moieties are initially exposed to the air, but these are rapidly replaced by hydrophobic groups to minimize surface energy at the air-hydrogel interface. This reorganization results in a barrier that prevents the interdiffusion of polymer chains when the severed surfaces are reunited, and this may affect self-healing ability after a considerable separation time. Most self-healing hydrogels do not heal if the delay between separation and rejoining of the surfaces is too long, and this result is also ascribable to solvent loss due to water evaporation. A system modification from hydrogel to organohydrogel or complete organogel via solvent displacement to replace water with an organic solvent improves drying resistance and reduces the loss of healing properties.<sup>[24]</sup>

On the other hand, the chain mobility at room temperature is restricted in glassy or semicrystalline self-healing polymers that require an increase of temperature to facilitate diffusion, which otherwise will reform bonds only at the surface, resulting in a lower healing efficiency.<sup>[25]</sup> Nevertheless, in recent years there has been increasing interest in imparting SH ability to glassy polymers, taking advantage of precisely designed polymeric networks.<sup>[26–28]</sup>

Self-healing in polymeric materials can be achieved by exploiting various chemistries based on many interactions among specific functional groups. A brief overview of the most common chemistries involved is presented in the following paragraphs, more details can be found in other reviews on self-healing mechanisms.<sup>[13,15,18,19,21,29,30]</sup>

## 2.1. Dynamic Covalent Chemistry

The concept of dynamic covalent chemistry (DCC) includes all the covalent bonds able to break and reform under equilibrium control, providing robust materials.<sup>[31]</sup> A specific bonding energy is associated to each type of covalent bond, which defines its stability and therefore the amount of energy required to break /form the bond. These dynamic chemical bonds are usually weaker than other covalent bonds, and thus will be preferentially broken as the crack propagates upon the mechanical stress. Dynamic covalent bonds are generally susceptible to external stimuli such as light, temperature, or pH variations that trigger the activation of the dynamic behavior at the damaged interface, which is mended by the reformation of the bonds upon trigger removal. Dynamic covalent reactions typically have slower kinetics of bond cleavage and formation, and most of them may require the assistance of catalysts to achieve rapid equilibrium.<sup>[32]</sup> Self-healing systems based on dynamic covalent chemistry can be classified according to the type of reaction: condensation, in which the small-molecule by-product is also responsible for the bond disruption and formation of the original moieties; exchange, in which functional groups

recombine among them with specific controlled exchange rates; addition, in which the bond formation and rupture does not involve an additional small molecule.<sup>[15]</sup> Most DCC reactions do not fall into a single class, but the mechanism can be defined by the reaction's kinetic and external conditions, and sometimes different types of DCC bonds are combined to enable multistimuli healing.<sup>[33]</sup> In **Table 1** the dynamic mechanisms that will be described in the following sections are summarized.

### 2.1.1. Imine Bonds

Imine bonds are based on Schiff's base click-chemistry, which involves the formation of a strong carbon-nitrogen double bond by nucleophilic attack of a primary amine to carbonyl groups.<sup>[34]</sup> Aromatic Schiff bases provide higher stability compared to aliphatic species, which in turn provide higher mechanical properties to the system.<sup>[34]</sup> These bonds require long reaction times, are unstable in the presence of water, and are sensitive to many chemical and biological stimuli, such as pH variation or the presence of amino-rich species.<sup>[35]</sup> Most of the self-healing hydrogels relying on this mechanism comprise polysaccharide derivatives, such as oxidized dextran and chitosan, due to the richness of cross-linking sites on these biopolymers, providing greater stability and potential cell-encapsulation ability.<sup>[36]</sup>

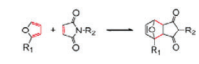
### 2.1.2. Oxime Bonds

Oxime bonds are also based on Schiff base click chemistry, in this case through a condensation reaction between hydroxylamine or alkoxyamines with an aldehyde or ketone. These bonds show higher strength and better stability against hydrolytic cleavage compared to those of imine bonds, resulting in a decrease in the network mobility; this provides better mechanical properties but a lower tendency to self-healing.<sup>[37]</sup> Oxime bond formation, which takes place under mild conditions with high reaction efficiency, is orthogonal to nucleophiles in living systems and biocompatible, posing as a suitable candidate for building adaptable hydrogels for cell encapsulation.<sup>[38]</sup>

### 2.1.3. Acylhydrazone Bonds

Acylhydrazone bonds are formed by a rapid condensation reaction between hydrazine or hydrazide and an aldehyde or ketone. Acylhydrazone bonds are more stable than imine bonds and have been widely used for bioconjugation due to their stimuli-responsive nature and rapid formation under physiological conditions.<sup>[39]</sup> The reversible acylhydrazone reaction can be triggered by either a thermal stimulus or by pH variation, using glacial acetic acid as a catalyst, and the bond formation reaction rate is influenced by the temperature and pH. The bond is stable under mild acidic conditions while the regeneration of the linkage fails under neutral conditions, unless aniline is added as the catalyst to achieve an acylhydrazone exchange reaction.<sup>[40]</sup> Aromatic aldehyde-derived hydrazones show a faster formation rate and hydrolysis compared to those of aliphatic species at neutral pH.<sup>[41]</sup> These bonds are usually combined with other dynamic covalent chemistries because of the strong influence of

**Table 1.** Dynamic reversible covalent reactions pathways. Adapted with permission.<sup>[50]</sup> Copyright 2018, Elsevier.

Dynamic bond	Reversible covalent reactions	Dynamic bond	Reversible covalent reactions
Imine Bond	<p>Reversible formation</p> $R_1-NH_2 + R_2-C(=O)H \rightleftharpoons R_1-N=C(R_2) + H_2O$ <p>Transimination</p> $R_1-NH-C(R_2)=O + R_3-NH-C(R_4)=O \rightleftharpoons R_1-NH-C(R_4)=O + R_3-NH-C(R_2)=O$	Boronic-Ester Bond	<p>Reversible formation</p> $R_1-B(OH)_2 + HO-R_2 \rightleftharpoons R_1-B(O-R_2)(OH) + H_2O$ <p>Dynamic exchange</p> $R_1-B(O-R_2)(OH) + HO-R_3 \rightleftharpoons R_1-B(O-R_3)(OH) + HO-R_2$
Oxime Bond	<p>Reversible formation</p> $R_1-OH + R_2-C(=O)H \rightleftharpoons R_1-O-N=C(R_2) + H_2O$ <p>Transoximization</p> $R_1-O-NH-C(R_2)=O + R_3-O-NH-C(R_4)=O \rightleftharpoons R_1-O-NH-C(R_4)=O + R_3-O-NH-C(R_2)=O$	Disulfide Bond	<p>Reversible formation</p> $R_1-SH + R_2-SH \rightleftharpoons R_1-S-S-R_2$ <p>Disulfide</p> $R_2-S-S-R_1 + R_3-S-S-R_4 \rightleftharpoons R_2-S-S-R_4 + R_1-S-S-R_3$ <p>Exchange</p> $R_1-S-S-R_2 + R_3-SH \rightleftharpoons R_1-S-S-R_3 + R_2-SH$
Acylhydrazone bond	<p>Reversible formation</p> $R_1-NH-C(=O)H + R_2-C(=O)H \rightleftharpoons R_1-NH-C(=O)-C(=O)R_2 + H_2O$ <p>Hydrazone exchange</p> $R_1-NH-C(=O)-C(=O)R_2 + R_3-NH-C(=O)H \rightleftharpoons R_1-NH-C(=O)H + R_3-NH-C(=O)-C(=O)R_2$	Diels-Alder Reaction	<p>DA/rDA reaction</p> 
Urea Bond	<p>Reversible formation</p> $R_1-NH-CO-NH-R_2 + H_2O \rightleftharpoons R_1-NH-CO-NH-R_2 + H_2O$ <p>Dynamic exchange</p> $R_1-NH-CO-NH-R_2 + R_3-NH-CO-NH-R_4 \rightleftharpoons R_1-NH-CO-NH-R_4 + R_3-NH-CO-NH-R_2$	Ester Bond	<p>Reversible formation</p> $R_1-COOH + R_2-OH \rightleftharpoons R_1-COO-R_2 + H_2O$ <p>Transesterification</p> $R_1-COO-R_2 + R_3-COO-R_4 \rightleftharpoons R_1-COO-R_4 + R_3-COO-R_2$

the pH on the bond stability, thus achieving sensitivity to multiple stimuli.<sup>[33]</sup>

#### 2.1.4. Dynamic Urea Bonds

Dynamic urea bonds are established between an isocyanate group and a hindered amine without requiring a catalyst, and they can be conveniently introduced into a single network to yield cross-linked poly(urethane-urea)s.<sup>[42]</sup> These copolymers consist of hard segments, providing strong mechanical properties, and soft sections, which impart the flexibility required for efficient dynamic exchange. In fact, urea linkages can reversibly dissociate into the corresponding isocyanate and hindered amine when attaching bulky substituents to the nitrogen atom of the urea bond. The dynamic behavior can be easily tuned by adjusting the steric hindrance, and the size of the substituents, which determines the kinetics of the exchange. The dynamic urea bond is a strong bond that can be easily broken and reformed under mild conditions, providing good mechanical strength, dimensional rigidity and chemical stability but with sensitivity to humidity.<sup>[43]</sup> These bonds are mainly exploited for welding applications, with the adhesion at the interface strengthened by a hydrogen-bonding established by urea motifs that increase the mechanical strength. Dynamic urea bonds are also mainly used in thermoplastic polyurethanes.<sup>[44]</sup>

#### 2.1.5. Boronate–Ester Complexations

Boronate–ester bonds are obtained by condensation complexation reaction of boronic acid derivatives with 1,2- and 1,3-diols or carboxylic acids in aqueous solution.<sup>[45]</sup> The reversibility of the bond and thus the self-healing behavior can be triggered by various stimuli, such as changes in pH, temperature variation, or the addition of glucose.<sup>[46]</sup> The stability of borate compounds depends largely on the pH: when the pH value is higher than pKa

of both boronic acid and diol, usually under alkaline conditions, the formation of a stable borate ester bond is favored.<sup>[47]</sup> Below the pKa value, the boron atom is susceptible to being attacked by a nucleophilic reagent, for example, water, leading to hydrolysis of borate ester. Therefore, the stability of this bond, and thus the resultant mechanical properties and self-healing efficiency, is highly sensitive to pH changes. The reaction conditions are difficult to control and can be incompatible with the biological neutral environment, but the pKa values can be tuned by selecting the proper substituent of the boronic acid functional group to control the properties and develop cytocompatible hydrogels self-healable at neutral pH.<sup>[48]</sup> The kinetics of boronic ester bond formation can be tuned by many orders of magnitude by changing the neighboring groups.<sup>[49]</sup> Furthermore, phenylboronic acid derivatives have higher stability than aliphatic derivatives, due to the charge conjugation effect of the benzene ring.<sup>[50]</sup> Various strategies have been developed based on different polyols, from natural molecules, such as catechols, inspired by mussel adhesive proteins, or glucose, to nanomaterials such as graphene oxide, to produce self-healing nanocomposites with enhanced mechanical properties.<sup>[51,52]</sup>

#### 2.1.6. Disulfide Bonds

These reversible covalent bonds are based on thiol/disulfide dynamic exchange reactions occurring in the presence of oxidized thiolates in a neutral or alkaline environment. The mechanism relies on the nucleophilic substitution carried out by the S atom in the thiol to cleave a S–S bond to generate a new S–S bond, forming a free thiol group.<sup>[53]</sup> However, thiols are unreactive in the reduced state, and thus reversible crosslinking given by bond dissociation into thiols by reduction and disulfide formation via oxidation instead of bond exchange can be achieved.<sup>[54,55]</sup> The presence of a free thiol group makes the thiol-disulfide exchange faster than the disulfide exchange, but this requires a bland



oxidative environment, such as the presence of oxygen as an oxidation agent, which is sufficient to induce cross-linking.<sup>[56]</sup> Gelation occurs under mild reaction conditions, at a temperature lower than that of other DCCs without catalysts or small molecules, and the dynamic behavior can be triggered by a wide range of stimuli, including pH variation, redox potential, heat, light, or the presence of nucleophiles or external radicals.<sup>[46]</sup> Disulfide chemistry is slow at physiological pH; however, reducing the thiol pK<sub>a</sub> can promote fast gelation kinetics while maintaining cytocompatibility in disulfide-based hydrogels, exploiting naturally existing thiol groups in peptide sequences.<sup>[57]</sup> The bonds formed among thiol side chains of cysteine groups are fundamental for folding, assembly, and stability of some proteins in biological systems.<sup>[58]</sup> The involvement of an oxidation agent can reduce the cytocompatibility of the crosslinking process of hydrogels that rely on these linkages. Limitations to the reversibility can arise from this aspect if the system is under physiological conditions, since proteins may interfere with the dynamic mechanism and the presence of glutathione, which is a reducing agent, in some tissue.<sup>[59]</sup> Nevertheless, thiolate groups are likely to be oxidized into disulfide when exposed to air, leading to the loss of the dynamic and the self-healing features with time, which must be addressed by a protection strategy by capping reactive thiolate groups with Au(I) or Ag(I) ions.<sup>[60]</sup>

Disulfide bonds are some of the most widely used in dynamic covalent chemistry, because of their good simplicity and controllability, even if the healing efficiency is strongly dependent on the extension of the damaged area.<sup>[35]</sup> This self-healing mechanism exhibits obvious advantages in rubbers, such as a full recovery of appearance and mechanical properties at moderate temperatures, since these already contain disulfide links due to the vulcanization process.<sup>[54]</sup> These DCCs are also often implemented in polyurethane-based coatings, to take advantage of the intrinsic shape memory effect to achieve the closure of the crack, while healing is achieved through exchange reactions of the disulfide bonds.<sup>[61]</sup>

### 2.1.7. Diels–Alder Reactions

Diels–Alder (DA) reactions are the most investigated mechanism for achieving self-healing in polymers. In DA reactions, two or more unsaturated precursors react through double bonds, forming a cyclic adduct after heat triggering. [4+2] cycloaddition is a fast “click” type orthogonal reaction without side reactions and by-products that shows high selectivity and yields. It is typically performed without metal catalysts or coupling reagents.<sup>[62]</sup> The bond is formed between an electron-rich diene and an electron-poor dienophile, and the most commonly used functional groups are, respectively, furane derivatives and alkenes or alkynes, typically maleimides, forming furan-maleimide diels-alder (fmDA) adducts.<sup>[63]</sup> The DA linkages show thermoreversibility since they can be cleaved upon heating, resulting in de-cross-linking at elevated temperatures due to the occurrence of retro-DA (rDA) reactions, which leads to increased mobility. Then, upon cooling to a lower temperature, the functional units can reconnect, forming a covalent DA bond to restore the network.<sup>[64,65]</sup> Most rDA reactions require temperatures above 100 °C to be activated, but the reversibility of the DA reaction can be controlled by adjust-

ing the chemical structure. To finely tune the temperature for the healing process, different substituents can be selected because of relatively simple modification techniques and numerous commercially available derivatives.<sup>[66]</sup> Selection of the proper moieties has expanded the application of DA links to biological applications in drug delivery and tissue engineering, due to the ability of the reaction to occur rapidly in an aqueous solution at room temperature and under physiologically compatible conditions.<sup>[67–69]</sup>

In addition to thermally triggered DA reactions, photochemically activated pericyclic reactions have drawn a great deal of attention as an alternative approach to build light-responsive and photoswitchable reversible systems. Bridging among specific chromophores, such as [2+2] cycloaddition for coumarin and cinnamoyl or [4+4] cycloaddition for anthracene, occurs through photodimerization and photocleavage, which proceeds rapidly and at high yields also in the solid state.<sup>[70]</sup> Significant healing can be achieved in these systems by irradiating the broken surfaces with high-energy UV light to further cleave the dimers and then increase the amount of photoreactive moieties available and the polymer chain mobility, while a longer wavelength is used to reform the bonds across the joint interface.<sup>[71]</sup> Photoactivated SH is quite attractive because it can be achieved with UV light or even with sunlight, and the use of light is clean, cost-effective, highly controllable, and selective, causing lower distortions in the material because it is suitable for the repair of specific injured regions without involving the overall material.<sup>[72]</sup> However, sometimes the efficiency of restoration is insufficient because of low light penetration, which results in incomplete healing of the material taking place only on the surface of the material, representing an efficient application in self-healable coatings and films.<sup>[73]</sup>

### 2.1.8. Transesterification

The typical transesterification reaction consists of an exchange between an ester group with an alcohol or a carboxylic acid, but also between epoxy and an anhydride.<sup>[74]</sup> Transesterification requires high temperature, which enables dynamic behavior and determines the time necessary for the reaction to occur, and the presence of a catalyst compatible with the polymer matrix.<sup>[75]</sup> The presence of the catalyst, such as zinc acetate, significantly increases the reversibility and kinetics of the reaction.<sup>[76]</sup> Thermoreversible transesterification is exploited in a particular class of materials, called vitrimers, for topological rearrangement upon external mechanical forces based on ester exchange while maintaining a constant number of dynamic chemical bonds and preserving the integrity of the network.<sup>[77]</sup> Vitrimers behave as a typical thermosetting polymers at operating temperatures while showing a gradual decrease in viscosity with increasing temperature instead of an abrupt drop, in analogy to inorganic glass, which inspired the name of this class of SH materials.<sup>[46]</sup> This behavior combines deformation like thermoplastics and dimensional stability upon heating, similar to thermosets with recovery properties.<sup>[78]</sup> Transesterification exchange reactions also enable recycling and multiple reprocessing of a covalently cross-linked network, which, along with reparability, makes vitrimers environmentally friendly

and sustainable materials, unlike conventional irreversible thermosetting.<sup>[43]</sup>

## 2.2. Non-Covalent Interactions

Under non-covalent interactions different mechanisms are encompassed. Self-healing mechanisms relying on physical bonds are entropy-driven or based on molecular diffusion, and compared to dynamic covalent bond-based systems, those interactions provide soft polymers with generally lower mechanical properties.<sup>[16]</sup> On the other hand, physical interactions involve tunable viscoelastic behavior and well-defined network structures that can be rapidly remodeled, offering faster reversible recovery under ambient conditions.<sup>[79]</sup>

Supramolecular chemistry employs covalently attached moieties to the macromolecule backbone as side chains or chain ends that can establish relatively weak intermolecular and intramolecular interactions between themselves or with small monomer units or molecules.<sup>[80]</sup> Self-healing ability in these systems relies on the cooperative action of numerous non-directional dispersive forces, which are strongly dependent on the moieties' concentration and distribution.<sup>[35]</sup>

Given their nature, most non-covalent self-healing systems can autonomously self-repair without being triggered by external stimuli.<sup>[81]</sup> The range of non-covalent bonds involves several types of interactions, which are sometimes combined with DCC bonds to enable multi-stimuli healing or with irreversible covalent networks to introduce SH into these systems. In **Table 2** the non-covalent mechanisms that will be described in the following sections 2 are reported.

### 2.2.1. Molecular Interdiffusion

Self-healing based on molecular interdiffusion relies on the flowing of a thermoplastic polymer across a severed interface to mend the surfaces by mechanically interlocking them when the system is heated above the  $T_g$  of the linear macromolecules and then cooled down.<sup>[82]</sup> The diffusing chains can entangle with the primary cross-linked network because of their free motion to form a secondary noncovalent network, thus resulting in an interpenetrated network. The healing agent is considered an additive because it is usually made up of a material different from the matrix in which it is located. This kind of restoration, which is a bridge between extrinsic and intrinsic mechanisms depending on the topological arrangement of the healing agent in the matrix, is stored as a separated phase in specific areas such as vesicles and pouches, or homogeneously distributed and mixed within the matrix without visible separation.<sup>[11]</sup> The healing agent is typically a linear polymer with structural simplicity and high chain flexibility to improve diffusivity. Common thermoplastic polymers used in these systems are PCL, PS, and PEG.<sup>[83,84]</sup> Furthermore, when linear poly( $\epsilon$ -caprolactone) (l-PCL) is interpenetrated in a cross-linked poly( $\epsilon$ -caprolactone) (n-PCL) network, the matrix exhibits shape recovery and gradually closes the crack when the temperature increases over the melting point of the PCL, which also activates the diffusion and chain entanglement of l-PCL. This self-healing mechanism is called shape memory-assisted self-healing (SMASH)<sup>[83]</sup>

### 2.2.2. Hydrogen Bonding

Hydrogen bonding plays a critical role in many natural systems, from the pairing of nucleobases in DNA to protein folding and self-assembly in biomaterials.<sup>[85]</sup> A hydrogen atom attached to a highly electronegative atom, a donor such as oxygen or nitrogen, establishes a directional dipole–dipole interaction in proximity to another electronegative atom, called acceptor.<sup>[86]</sup> The single hydrogen bond strength varies depending on the negative charge of the acceptor atom and the pH value of the solvent in which the bonding occurs, but is relatively weak when compared with that of covalent or ionic bonds.<sup>[87]</sup> However, the overall association constant increases sharply when molecules are designed to promote the formation of multiple hydrogen bonds.<sup>[16,88]</sup> This extensive noncovalent secondary interaction can significantly affect bulk viscoelastic properties and establish a rapidly reversible cross-linking useful for imparting self-healing.<sup>[89]</sup>

The hydrogen-bonding strategy requires hydrogen donors and acceptors, usually grafted as side-chain polar groups along the backbone.<sup>[22]</sup> In analogy with nucleobases, typical associative multivalent synthetic moieties are 2,6-diamino triazine (DAT) and ureidopyrimidinone (UPy), which establish triple and quadruple hydrogen bonds per group, respectively.<sup>[90,91]</sup> The complementary H-bonding donor and acceptor motifs assemble into dimers with strong binding affinity, forming clusters that result in phase segregation. Such systems show temperature-dependent dissociation and reassociation processes, leading to repeatable self-healing for both synthetic and natural polymer chains, either in dry systems or hydrogels.<sup>[92–94]</sup> The presence of water typically causes the dissociation of H-bonds among the chains because it interacts with the binding sites, interfering, and replacing their mutual interactions, thus deteriorating the self-healing efficiency. In dry supramolecular polymers, H-bonding competes with air moisture, while in hydrogels, multivalent motifs containing both H-bond donor and acceptor groups must be shielded within pockets by hydrophobic species from the aqueous environment to prevent the competitive effect.<sup>[95–97]</sup> Furthermore, the length of the side chain is a key factor to reduce the impact of steric hindrance: short chains hinder interactions because of the inaccessibility of the functional groups, while long pendants would lead to hydrophobic association shielding of the functional groups.<sup>[18]</sup>

Crystalline polymers also can exhibit rapid self-healing behavior through reversible and dynamic intermolecular interactions established between abundant amide or hydroxyl groups on adjacent chains, as occurs in poly(vinyl alcohol) (PVA).<sup>[98–100]</sup> The recovery efficiency in these systems is strongly related to the polymer backbone rigidity, the ratio between free and crystallized moieties, and the crosslinking density, which must be suitable to provide sufficient mobility to the chains to favor interchain diffusion and aggregation.<sup>[101,102]</sup>

### 2.2.3. Electrostatic Interactions

Electrostatic interactions are formed between two oppositely charged moieties. An ion can interact with either a polar molecule or induce a temporary dipolar character to a nonpolar molecule.<sup>[103,104]</sup> These non-covalent interactions show a lack

**Table 2.** Schematic representations of dynamic non-covalent interactions and relevant examples of functional groups employed.

Non-covalent interaction	General	Example	Non-covalent interaction	General	Example
Molecular interdiffusion			Hydrophobic association		
Hydrogen bonding			Host-guest complexation		
Electrostatic interactions			Self-assembly		
Metal-ligand coordination			Nanocomposite interaction		



of specificity and directionality, and their strength is highly dependent on experimental conditions, such as temperature, electrostatic charge density, and dielectric constant of the solvent in which the binding occurs and may also develop in electrostatic repulsion. The design of the molecules interacting via ionic bonding can vary from small molecules and ionic liquids bearing multiple charges, to polymers containing ionizable groups or side chains. This leads to a wide range of self-healing mechanisms that rely on the strong affinity of ion pairs to reassociate.<sup>[79]</sup>

Ionomers are macromolecules containing a small percentage of monomers showing negatively charged groups, like carboxylate and phosphonate, show thermoactivated self-healing when heated after or by the damage.<sup>[105]</sup> Heat induces interdiffusion of the chains, which is favored by the temperature, elasticity of the chains, and localized interchain repulsion.<sup>[106]</sup> Polyelectrolyte complexes, on the other hand, are neutrally charged neutral because they are composed of oppositely charged macromolecules.<sup>[107]</sup> At last, ionic bonds are strongly sensitive to pH, temperature, solvent nature, and presence of salts.<sup>[108,109]</sup>

When an equal number of anionic and cationic sites are located separately in the same monomer on each chain, thus retaining overall electroneutrality, the polymer is defined zwitterionic.<sup>[110]</sup> Examples of such systems are sulfo- or carboxybetaines with a quaternary ammonium and their copolymers with neutral comonomers.<sup>[111]</sup> The self-healing of these systems at room temperature takes place regardless of the separation time because the cut surface is stabilized by a hydrated layer, and the hydrophilic moieties remain exposed and available without hydrophobic rearrangement.<sup>[112]</sup>

A specific kind of electrostatic interactions is based on  $\pi$ - $\pi$  stacking between  $\pi$  orbitals in aromatic rings or by end-capped  $\pi$  electron-deficient species, such as imide groups or copolyimides, alternated with  $\pi$  electron-rich aromatic backbone molecules or units, such as pyrene.<sup>[113]</sup> The complexes arrange in a secondary structure adopting a chain-folded conformation to maximize the stacking, which can be disrupted upon heating, required to enable chain unfolding, reorientation, and mobility across the fractured surface, which is mended upon reformation of the stacking.<sup>[81]</sup> The Tg of the network can be tuned by adding a flexible spacer which would disengage the interacting moieties and facilitate the chains flow to achieve SH at a wide temperature range.<sup>[17]</sup>

#### 2.2.4. Metal-Ligand Complexation

Metal-ligand coordination complexes are based on the chelation of a positive metal ion by negatively charged ligands via donation of a nonbonding electron pair to one of the empty d orbitals of the metal ion.<sup>[114]</sup> Two or more ligands can be ionically bridged depending on the coordination number of the ion, thus linear chains or networks can be formed.<sup>[115]</sup> The architecture of the backbone where the ligands are bound has a strong effect on the bond robustness, and it differs between linear, branched, and dendritic polymers.<sup>[116]</sup> Binding strength and kinetics can also be fine-tuned by choosing different metal-ligand pairs, thanks to the wide range of available ligands.<sup>[117]</sup> These coordination bonds are highly sensitive to pH, temperature, on which the equilibrium constants depend considerably, and redox potential because it in-

fluences the oxidation state of the metal ion and then the stability of the complexes.

The dynamic nature of the coordination complexes enables rapid and efficient self-healing, because of the migration of the free ions at the cut interface and the mobility of the uncross-linked portions of polymer chains.<sup>[118,119]</sup> Self-healing also depends on the size and type of counterion, which can hinder or suppress restoration if non-coordinating or too big, because of insufficient mobility of the network.<sup>[115]</sup> In this context, there is often a trade-off between mechanical properties and SH, because usually stronger interactions lead to systems with lower dynamics. Nevertheless, some metal-ligand complexation can lead to the formation of fast but thermodynamically stable bonds, achieving outstanding properties.<sup>[119]</sup>

One of the most common self-healing strategies relies on the introduction of ferric ions into a system containing moieties such as carboxylate or catechol groups. This approach found its basis in analogy to the self-healing mechanism of natural mussel adhesive proteins, which is triggered by multivalent cations from seawater.<sup>[120–122]</sup> Particularly interesting are hydrophilic and anionic biopolymers, such as alginate, that are ionically cross-linked in the presence of divalent calcium ions, enabling self-healing. This feature makes them very attractive for tissue engineering and drug delivery, because of their biocompatibility and low toxicity.<sup>[123]</sup>

#### 2.2.5. Hydrophobic Association

In hydrogels, non-polar segment of amphiphilic polymers can aggregate among themselves and be isolated from the bulk aqueous media. Forming a hydrophobic association by physical entanglement is based on dispersive forces and not on directly interacting moieties.<sup>[113,124]</sup> Some authors refrain from calling the hydrophobic association as a type of interaction, as it has nothing to do with the forces between the hydrophobic parts.<sup>[18]</sup> When two micelles come close enough to each other, they tend to aggregate and form a larger and more stable assembly to minimize contact with water, with the subsequent departure of surface-bound water molecules in between.<sup>[36,79]</sup> Hydrophobic interactions can be fine-tuned by controlling various parameters, such as the balance between hydrophobic and hydrophilic segments, the strength of the interaction between hydrophilic units, or the length of the hydrophobic chains.<sup>[30]</sup>

Self-healing dynamic hydrogels formed via supramolecular hydrophobic association are typically obtained by micellar copolymerization between macromolecular amphiphilic chains containing hydrophilic blocks with small amounts of hydrophobic units.<sup>[40]</sup> The presence of a surfactant is thus crucial, because it determines the shape of the micelle and yields reversible dissociation and reassociation of the hydrophobic groups into ordered nanodomains. The repair mechanism can be ascribed to this disengagement and rearrangement.<sup>[125]</sup> Self-healing behavior is lost after extraction of the surfactant from hydrogel networks because the hydrophobic interactions between pure hydrophobic units without micelles are too strong to exhibit reversibility.<sup>[126]</sup> Interestingly, the self-healing ability of the hydrogels improves increasing the length of alkyl non-polar chains until reaching a compromise between free motion and effective association.<sup>[127]</sup>

As stated before, self-healing in hydrogels is typically limited in time by a hydrophobic rearrangement process of the cut surfaces. However, this rearrangement may ensure a time-independent healing of hydrogels on the basis of hydrophobic association. When the freshly cut surface is exposed to air, the micelles dissociate and orient themselves towards the air-gel interface, with the hydrophobic groups arranged in a monolayer on the cut surface.<sup>[128]</sup> This configuration enables the system to be repaired even after long separation times via micelle restoration.<sup>[36]</sup> One important drawback of the above-mentioned self-healable hydrogels is the low water uptake caused by hydrophobic regions within the hydrogel matrix.<sup>[30]</sup>

### 2.2.6. Host–Guest Complexation

Host–guest inclusion complexes are based on a transient spatially targeted association driven by the affinity between a macrocyclic molecule acting as the host and a suitable molecular guest.<sup>[129]</sup> The host's large internal cavity accommodates the selective physical insertion of a variety of appropriate guest molecules, from small molecules to long synthetic polymers or even large biomacromolecules.<sup>[90]</sup> The supramolecular assembly is held together by multiple reversible non-covalent interactions, and this can be exploited to achieve self-healing.<sup>[21]</sup>

Two different strategies have been used to build host-guest-based networks: a threading design and a pendant design.<sup>[130]</sup> Linear polymer chains, such as hydrophobic poly (caprolactone) (PCL), hydrophilic poly(ethylene glycol) (PEG), or amphiphilic poly(urethanes) (PUs), can be threaded within multiple host moieties, yielding a rotaxane structure.<sup>[131–134]</sup> The formation and strength of these complexes largely depend on the relative dimensions of the cavity and the cross-sectional area of the polymer chain, with the possibility of multiple chains inserted in a single cavity producing multiple entanglements. In pendant systems, host and guest moieties are located along the chains as side functional groups through functionalization of polymer backbones or via copolymerization of preformed host-guest inclusion complexes (meth)acrylic or vinyl group-bearing comonomers with comonomers as building blocks, such as (meth)acrylates and (meth)acrylamides.<sup>[135,136]</sup> This configuration confers self-healing ability and shear-thinning properties due to the rapid bond formation and can be easily combined with stronger secondary covalent cross-linking to overcome the intrinsic weak mechanical properties.<sup>[137]</sup>

The host-guest couple must be designed on the basis of the dynamics of the complexations and structural relationship between the moieties, which must be complementary in shape.<sup>[116,138]</sup> The selection of the proper host-guest couple as well as the backbone chains or the copolymerization monomers greatly affects the self-healing mechanics and efficiency.<sup>[129,139]</sup> The number of repeating units determines the cavity size in commonly exploited macrocyclic cavitands, including natural molecules, for example, water-soluble cyclic oligosaccharides such as cyclodextrins (CDs), or synthetic molecules, such as cucurbiturils (CBs), crown ethers, calixarenes (CAs) and pillararenes.<sup>[140]</sup> Although all of these macrocycles show potential for building self-healing gels, mainly cyclodextrins and cucurbit[n]urils have been used so far in the fabrication of self-healing hydrogels, because of their nontoxi-

city and biocompatibility.<sup>[36,136]</sup> Guest molecules range from polar compounds such as alcohols and amino acids to non-polar compounds such as aromatic molecules and steroidal compounds, or in the case of poly(pseudo)rotaxanes, polymeric chains as pendant groups.<sup>[141,142]</sup> Controllable association and dissociation of inclusion complexes is dependent on the specific nature of the guest molecule, which may be inert or stimulate responsive, such as temperature (adamantane (Ad)), light (azobenzene (Az)), pH (phenolphthalein (Ph)), and redox potentials (ferrocene (Fc)).<sup>[135,143–146]</sup>

### 2.2.7. Self-Assembly and Crystallization

The self-assembly of polymer chains can lead to their gelation arranged into regular structures that act as physical cross-links.<sup>[126]</sup> These relatively stable crystals with specific conformations are formed via multiple cooperating noncovalent interactions, such as hydrophobic association, hydrogen bonding, and electrostatic interactions, established among polymer chains.<sup>[130]</sup> The difference with previously mentioned mechanisms is the formation of well-defined architectures to achieve self-healing via incorporation of specific moieties along the polymer chains or exploiting the intrinsic properties of the polymer chain. Such molecular assembly is typical for protein- or peptide-based systems with secondary structures but can also occur in synthetic macromolecules such as poly(caprolactone), with controllable crystallization.<sup>[83,147]</sup>

Self-healing peptide-based systems can be fabricated through the direct engineering of polypeptides or via modification of a long hydrophobic polymer backbone using hydrophilic peptides as pendant groups or copolymers, forming unique peptide sequences that are found in specific protein-binding structural motifs.<sup>[148,149]</sup> These materials have inherent biocompatibility, bioactivity, and biodegradability, and because of their amphiphilic nontoxic nature, they have been studied for controlled drug delivery of hydrophobic drugs in an aqueous environment from stimuli-responsive injectable hydrogel cell scaffolds.<sup>[150,151]</sup> The self-healing efficiency depends on the mobility of the chains to allow hierarchical assembly into specific structures responding to environmental conditions.<sup>[136]</sup> The reversible unfolding and self-assembly of these systems depend on temperature, pH, and ionic strength, enabling triggered self-healing, with conformation-dependent crystallization ( $\alpha$ -helix,  $\beta$ -sheet, or random coil) that provides the system stability at high temperature.<sup>[150,152]</sup> Although they exhibit many advantageous features, drawbacks in peptide-based systems are their high costs, difficult scale-up, and less controllable enzymatic degradation. The mechanical properties of self-assembled polypeptides are low, so cross-linking is usually introduced to increase stability.<sup>[153]</sup>

### 2.2.8. Polymer-Nanocomposite Interactions

Nanocomposites are composed of an inorganic component with nanometric dimensions, such as nanosheets, nanotubes, or nanoparticles, homogeneously dispersed in an organic matrix where it acts as a multifunctional cross-linker.<sup>[154]</sup> Nanomaterial incorporation allows enhancing thermal and mechanical properties thanks to its large surface-to-volume ratio,

which favors strong dispersive interactions but also imparts stimuli-responsiveness, antibiofouling, or introduces electrical conductivity.<sup>[155]</sup> However, drawbacks are their inelasticity and brittleness because these nanofillers may act as stress concentration points, inducing failures in the material.<sup>[156]</sup> This problem can be partially overcome by introducing covalent crosslinking in the matrix, but the exploitation of a reversible noncovalent interaction between functional groups along the polymer chains and the surface of the filler would provide self-healing capability.<sup>[95]</sup>

A wide range of nanomaterials, either inorganic fillers, such as clays, metal oxides, and MXenes, or organic nanomaterials, such as carbon nanotubes, graphene oxide, and nanocrystalline cellulose, have been used to develop self-healing nanocomposite materials.<sup>[152,157]</sup> It is fundamental to achieve a synergy between the supramolecular polymer matrix and its inorganic components to promote chain mobility and dynamic bond restoration to have efficient self-healing. Nanofillers would not provide self-healing unless all components have built-in reversibly interacting segments. Usually, polymer chains physically adsorb onto exfoliated clay surfaces via ionic interactions, while forming hydrogen bonds with organic nanospecies due to the presence of functional moieties like hydroxyl, epoxy, carbonyl, and carboxyl groups.<sup>[158]</sup>

### 3. Assessment of The Self-Healing Efficiency

The assessment of SH efficiency can be performed by applying various strategies, which can be both qualitative and quantitative. However, to describe the restoration of the material, it is fundamental to establish the time scale of healing after damage, which can last from a few seconds to days. This belongs to the dynamics of the macromolecular rearrangements and to the kinetics of the reversible linkages.<sup>[18]</sup> In this context, the common approach in the literature is to define the time after which the property of interest recovers to an acceptable percentage of the initial one. On the other hand, as described below, there are no commonly accepted rules.

The self-healing is demonstrated in most cases by macroscopic visual demonstrations, which is a common and simple test, and particularly useful for complex shapes. Two freshly cut pieces of a specimen are put into contact for a specific period, after which the restoration of the contact interface is observed.<sup>[22]</sup> In some cases, the efficiency of repair is shown using different dyes dispersed in the polymeric matrix, which can diffuse when the network recovers.<sup>[112]</sup> Testing the material's ability to support its own weight after healing without breaking is another common test.<sup>[159]</sup> To have more detailed information, the topography of the restored interface can be evaluated by optical microscopy, while the morphology at a micro/nanoscale can be characterized by scanning electron microscopy (SEM) or atomic force microscopy (AFM).<sup>[160]</sup> Qualitative considerations can be accompanied by quantitative evaluations to determine the effectiveness of recovering the initial mechanical or functional properties.<sup>[20]</sup>

As mentioned above, regarding quantitative evaluation, healing efficiency can be expressed by calculating the percentage of recovery of a specific, measurable property in the pristine specimen and after restoration.<sup>[161]</sup> Recovery of mechanical properties is the most common assessment performed, but the same general approach can be used to determine recovery in several properties, such as electrical or thermal conductivity or optical

transparency.<sup>[161–163]</sup> Among the different techniques used to determine the bulk healing efficiency in mechanical properties, uniaxial tensile strength, and compression strength tests are the most widely employed, from which useful parameters such as Young's modulus, stress and elongation at break, and fracture energy can be obtained and compared.<sup>[128]</sup> Another common experimental method is bending resistance tests to assess healing capacity by comparing the plane strain fracture toughness (KIC) or the strain energy release rate (GIC) of the material both before and after recovery.<sup>[12]</sup> Despite the technique used, these tests are usually performed comparing the values of 3D printed pristine and repaired specimens, while the percentage of recovery is defined as SH ability. The tests can be repeated on the same specimen, to determine the ability to recover after damage/healing cycles.<sup>[164]</sup> The shape of the specimens used usually follows standards, to obtain more reliable results.

Mechanically weak materials such as hydrogels can have the ability to withstand their weight but may not have the structural stability to withstand clamping for uniaxial tensile testing.<sup>[21]</sup> Therefore, their healing efficiencies can be determined using cyclic compression testing, where the hysteresis indicates the decreased number of cross-links and thus reduced structure recovery over many deformation cycles, each one followed by a recovery period.<sup>[148]</sup> Another frequent characterization for SH hydrogels is a step-strain measurement with oscillatory rheology, subjecting the hydrogel to a variable strain periodically alternating high and low strain for damage recovery cycles at constant oscillation frequency to determine the recovery rate of the viscoelastic properties.<sup>[18]</sup>

Ultimately, it is important to point out that the comparison among results from different self-healing systems is often difficult due to inconsistency in healing efficiencies calculated on different parameters arising from different characterization techniques. Furthermore, the outcomes of the characterizations, and thus of the resulting healing efficiency, strongly depend on the testing parameters, such as specimen dimension and geometry, temperature of analysis, as well as the undamaged material properties, the extent of the damaged volume, the time elapsed between breakage and rejoin and the time required for repair to occur, and proper alignment of the joint surfaces.

### 4. 3D Printability Criteria for SH Materials

Several different AM fabrication technologies are available and can be grouped according to the raw material used, and then based on how the layers are created and bonded, determined by the operating principles. According to the American Society for Testing and Materials (ASTM), there are over 50 various AM technologies that can be classified into seven categories: material extrusion, material jetting, binder jetting, sheet lamination, vat photopolymerization, powder bed fusion, and direct energy deposition.<sup>[165]</sup>

Among the aforementioned methods, material extrusion, powder bed fusion, and vat photopolymerization are extensively employed for polymeric materials.<sup>[166]</sup> In particular, 3D-printed self-healing polymers reported in the literature have been fabricated mainly by material extrusion or vat photopolymerization. For this reason, only these two categories will be briefly explained, while the remaining techniques are not included in this work.<sup>[167]</sup>

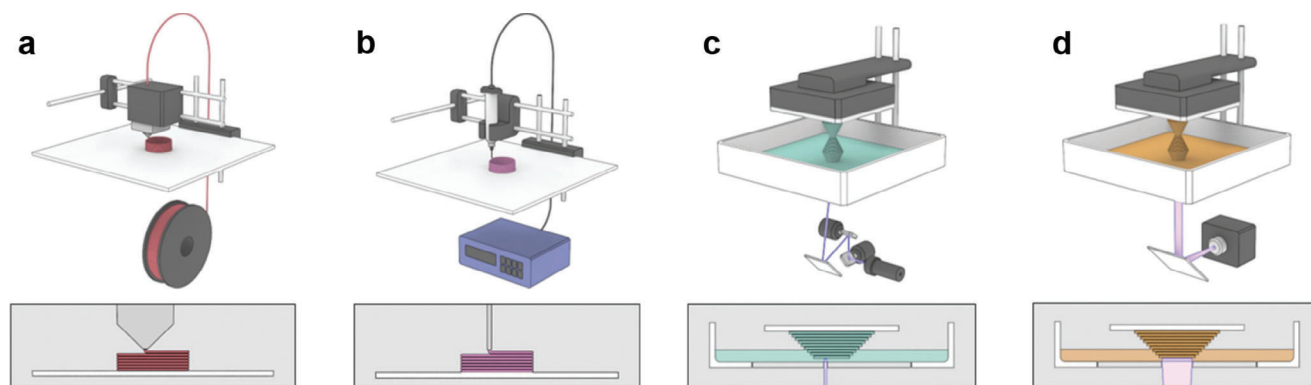


**Figure 1.** Schematic representation of various polymer additive manufacturing technologies. Extrusion-based techniques: a) fused filament fabrication (FFF) and b) direct-ink writing (DIW). Vat photopolymerization: c) stereolithography (SLA) and d) digital light processing (DLP). Adapted with permission.<sup>[8]</sup> Copyright 2019, Elsevier.

#### 4.1. Material Extrusion-Based Printing

3D printing technologies based on material extrusion rely on a controlled layer deposition onto a build platform of one or more materials selectively dispensed through a nozzle or an orifice mounted on a movable print head that follows a predetermined path for each layer.<sup>[168]</sup> This approach forms a 3D object in a line-by-line and then layer-by-layer manner, because the extruded material is shaped into continuous filaments and stacked at precise locations. Extrusion-based printing is the most widely used approach thanks to its versatility and affordability, since it accommodates a wide range of printable polymer materials, from thermoplastic polymers to pastes and polymer solutions, enabling also the fabrication of products based on multiple materials simultaneously.<sup>[169,170]</sup> In this category, the most used methods in the fabrication of self-healing polymer are fused filament fabrication (FFF) and direct ink writing (DIW). In FFF, also known as fused deposition modeling (FDM) (Figure 1a), a continuous filament of thermoplastic polymer is fed as thin strands from a spool into the heated print head, which liquefies the material in a semi-molten state. DIW, also called 3D dispensing or liquid deposition modeling (LDM) (Figure 1b), is an extrusion-based technique that does not necessarily comprise melting the fed material that can lead to degradation but consists in a viscous liquid or flowable slurry stored in a refillable cartridge and extruded through the printhead, usually under ambient conditions.<sup>[171]</sup> The precursor materials, also called inks, can be highly viscous or viscoelastic non-Newtonian fluids that present a shear thinning behavior beyond their yield stress and quickly recover upon removal of the shear stress, to be able to self-support and to prevent ink spreading or structural collapsing.<sup>[172,173]</sup>

A key difference between DIW and FFF is in the solidification of mechanism: while in the first various strategies are exploited, such as pH variation, immersion in a solution, thermal curing, or photopolymerization,<sup>[174]</sup> in the second it occurs only by cooling.

#### 4.2. Vat Photopolymerization

Light-triggered AM techniques rely on spatially controlled light irradiation to selectively induce the hardening of a liquid precursor,

called ink or resin, contained in a reservoir at predetermined locations corresponding to a cross section of the final 3D product.<sup>[175]</sup> The patterned exposure to UV or visible light results in the activation of a light-sensitive compound (photoinitiator), which must be present in the resin.<sup>[176,177]</sup> Photoinitiator absorbs incident radiation and generates reactive species or radicals, promoting the polymerization of the resin to form a solid covalent network.<sup>[178]</sup> Photocurable resins bear single or multiple photoactive groups as side chains or polymer chain ends, enabling the formation of a cross-linked polymeric network.<sup>[179,180]</sup> Vat photopolymerization techniques can be classified into linear, planar, or volumetric building, according to the spatial arrangement of the liquid precursor solidification.<sup>[181]</sup> Stereolithography (SLA) is based on the first configuration, relying on the line-by-line irradiation performed by the spot of a laser (Figure 1c). The second configuration, typical of the projection-based VP techniques, involves the illumination via conventional light sources of a specific area with a bidimensional pattern (Figure 1d). In projection-based VP, also called Digital Light Processing (DLP), the entire cross section of a layer is exposed all-at-once to a selectively masked light source that produces a bidimensional pattern.<sup>[182]</sup> The build time can be further reduced by using a layerless fabrication with continuous liquid interface production (CLIP) in a bottom-up configuration.<sup>[183]</sup> The third approach concerns the projection of holographic patterns into a rotating vat, and it is called volumetric 3D printing. The first two modes are the main ones employed with self-healing polymer-based systems and thus will be discussed in more detail. Volumetric printing has not been used yet in the field, so is beyond the scope of this review, and we refer the reader to other sources for more details.<sup>[184]</sup>

#### 4.3. Printability

Printability is defined as the ability of a material to be three-dimensionally shaped and result in an outcome with specific properties desirable for a given application when subjected to a certain set of printing conditions.<sup>[185]</sup> Therefore, the properties of the material have an impact on various parameters of the printing process, sometimes limiting correct fabrication. Maintaining the proper biological, functional, or mechanical properties while



meeting the manufacturing requirements is challenging and requires the design of polymers with a tailored structure, architecture, and functionality.<sup>[186]</sup>

The integration of SH into materials for 3D printing is a more straightforward approach because it usually does not comprise a modification of the matrix material but the addition of an external healing agent, following an extrinsic SH mechanism.<sup>[13]</sup> Properly shaping intrinsic SH systems in complex 3D shapes could be difficult, especially for soft materials or hydrogels, unless it is performed through AM.<sup>[187]</sup> Intrinsic systems are well suited as inks for 3D printing thanks to their dynamic nature and the absence of additional elements within the structure, such as capsules or vesicles.

Another convenient and common strategy to gather repairability and printability in intrinsic systems is the development of interpenetrated network (IPN) materials, which represents an intermediate approach among the two ways presented before. This solution combines one or more rigid and robust frames made of generally irreversible chemical bonds, generated during 3D fabrication, with at least one much weaker network based on mostly reversible bonds, which imparts SH capability.<sup>[188,189]</sup> IPNs can display tailored features while retaining the characteristics of both constituents simultaneously and matching the requirements for fabrication with different AM techniques.<sup>[173,190]</sup>

The printable material must be specifically adapted to be compatible with the fabrication process, especially in terms of viscosity and solidification mechanism, in accordance with the dynamic and labile nature of the interacting functional groups.<sup>[191]</sup> Monomers and long macromolecules can be tailored in terms of stoichiometry and distribution of reactive groups to match the desired properties together with traditional parameters such as molecular weight, polymer concentration, and cross-linking density. The network adaptability and integrity must be carefully balanced to enable polymer chain mobility for a sufficient timescale of healing and gelation, while still providing appropriate stability to the structure without affecting printing fidelity. Nevertheless, self-healing must be independent of the fabrication process to be preserved and compatible with the target properties for the final application.<sup>[10,192]</sup>

In hydrogels, the presence of water provides high mobility of the chains by increasing the molecular distance, and thus increases the recovery efficiency but reduces the mechanical strength, directly related to the cross-linking density inversely proportional to the self-healing ability.<sup>[21]</sup> In contrast, good mechanical properties are achieved by increasing the number or strengthening the cross-links, but this has a detrimental effect on the effective restoration.<sup>[193]</sup> 3D printing of SH hydrogels has more stringent prerequisites than for conventional fabrication of hydrogels via AM because a balanced compromise should be achieved among competing elements such as water content, crosslinking density, and effectiveness of chain interactions.<sup>[189]</sup> A loose crosslinking would entail a soft hydrogel, beneficial to chain migration but resulting in structures with poor shape fidelity, while the polymer content would favor self-healing if low, but hinder it if excessively low, or support shape retention and abating the restoration capability at the same time when high.<sup>[194]</sup> The simultaneous need for these opposite requirements leads to the definition of a fabrication window determined by the range

of material properties suitable both for efficient self-healing and accurate printability.<sup>[174]</sup>

In details, SH materials relying on intrinsic mechanisms, especially elastomers and hydrogels, are highly suited to be processed by extrusion-based 3D printing techniques because of the dynamic nature of their bonds, which bestow shear-thinning behavior crucial to proper filament flow and gelation after deposition.<sup>[191]</sup> Printability in these techniques refers to two main aspects: extrudability, which is the behavior and shape retention of the filament upon the shear stress imparted by the nozzle of the printer, and shape fidelity, related to the aspect adherence and dimensional accuracy to the computer design by printed object.<sup>[195]</sup> Labile bonds must break down upon extrusion to contribute to the decrease in viscosity, along with the disentanglement and alignments of the polymer chains, and the time required for the restoration of the bonds responsible for self-healing should be compatible with the viscosity recovery time after extrusion to prevent distortions.<sup>[196]</sup> Fast gelation that ensures shape stability combined with a rapid drop in viscosity when the ink is subjected to shear stress is due to highly reversible interactions, which are also favorable for a self-healing occurring in a useful timespan with an almost complete recovery of properties, especially in terms of mechanical strength.<sup>[148]</sup>

The ability to self-heal also contributes to reducing the impact of printing errors because it promotes efficient adhesion between consecutive stacked filaments, with a homogeneous distribution of reversibly interacting moieties that prevents the mechanical anisotropy typical of layered objects with incomplete compliance among the layers.<sup>[197]</sup> Rheological tests such as amplitude or frequency sweep can be carried out to evaluate the printability by detecting the crossover point between storage and loss shear modulus, which must be a good compromise in magnitude between a high value to enable the material to self-withstand when deposited but not too high to not clog the nozzle and hinder the extrusion process.<sup>[198]</sup> Extrudability, as well as self-healing efficiency, can be controlled by tuning the average polymer molecular weight and its dispersity, the type and presence of additives such as plasticizers, and the polymer concentration if a solvent is present in large quantities.<sup>[195]</sup> Some polymers or their solutions do not show a shear thinning behavior; hence, they would not be processable with extrusion-based processes. The addition within the material of interacting functionalities, either establishing dynamic chemical bonds or supramolecular interactions, would overcome the problem, but would also very likely provide a self-healing ability based on the same reversible bonds, thus introducing both printability and repairability.<sup>[192]</sup>

While for extrusion printing the ink can be composed of already polymerized or pre-crosslinked, VP liquid resins are usually based on low molecular weight, reactive multifunctional building blocks. These species are highly versatile and can be functionalized with functional groups able to form dynamic bonds that can be either pendant groups or integrated into the backbone after polymerization.<sup>[199]</sup> Interacting motifs tend to establish reversible dynamic bonds in both the liquid and solid phase before and after printing.<sup>[200,201]</sup> Viscosity in VP is not as crucial as in extrusion printing, but it is still fundamental.<sup>[202]</sup> Similarly to extrusion printing, the viscosity of the ink is determined by the molecular weight and concentration of all elements as well as the presence of solvents and plasticizers, but in this



case, the viscosity must be sufficiently low to process the formulation with sufficient precision and rapid solid-liquid separation during printing.<sup>[203]</sup> A low resin viscosity at processing temperature is beneficial because it can easily flow around the build platform to form new layers upon further exposures by recoating and self-leveling, thus reducing construction times, and it also facilitates the removal of unreacted excess resin from the negative features in the construct before post-curing.<sup>[201]</sup> The curing speed upon light exposure is the most important parameter for successful VP printing, and the interactions in the liquid phase can reduce the mobility of the reacting radicals, hindering the reaction rate speed and thus the printing efficiency and the final shape fidelity.<sup>[204]</sup> SH moieties must not interfere with radical polymerization, but at the same time, the polymerization must not affect the SH properties, with the two sets of bonds that should be orthogonal between them to coexist efficiently. Unlike extrusion printing, VP fabrication relies on generally irreversible reactions that form strong covalent bonds, yielding a dense and rigid chemically cross-linked network, which allows for the simultaneous accurate tuning of the macrostructure and mesostructure.<sup>[205,206]</sup> This necessary cross-linking density, also ascribable to the number of functionalities on the oligomers, would result in short chains generated upon damage which would not be able to migrate sufficiently across the rejoin interface, even being potentially able to establish reversible interactions in the printed objects.<sup>[179,181]</sup> A solution to overcome these issues are hybrid networks in which reversible and nonreversible crosslinks coexists. Self-healing properties can help to retain the final shape by reinforcing the adhesion among layers, already ensured by chemical bonds among them obtained by increasing curing depth within an already printed layer, tuning the extent of light penetration in the ink. Reversible bonds are also beneficial in soft materials, such as hydrogels. These materials can suffer of poor mechanical properties, which in turns can be given by DCC, without losing softness.<sup>[21,207]</sup>

## 5. Self-Healing of 3D-Printed Structures

In this section, various 3D-printed self-healing systems are reported, classifying them according to the printing method used and the self-healing mechanism involved, mainly focusing on the printing step and the healing efficiency achieved. Here it is worth mentioning that we considered only the investigations in which a structure was effectively built, and self-healing evaluated. On the other hand, there are many other studies that involve dynamic chemistry and a printing technique, but self-healing was not evaluated,<sup>[208–214]</sup> or, conversely, in which self-healing was evaluated but injectability or a potential printability has been envisaged but not proven.<sup>[94,215,216]</sup>

### 5.1. Extrusion Printing

#### 5.1.1. Extrinsic Self-Healing

The first self-healing 3D printed materials developed were extrinsic, and fabricated using extrusion-based AM techniques, exploiting microvascular 3D networks embedded within poly-

mer matrices. Sottos and co-workers used a direct ink writing-solvent casting (DIW-SC) method to pattern a sacrificial scaffold with fugitive organic ink.<sup>[217]</sup> The 3D structure was then infiltrated with an epoxy resin and cured to form a composite, from which the fugitive ink was removed by heating aided by mild vacuum. The embedded hollow vascularized structure was then infiltrated with dicyclopentadiene (DCPD) monomer, which provided healing filling of the fracture that reacts under ambient conditions. The concept was then expanded by the same group using a dual interpenetrating network of independent channels containing separate components of a two-component epoxy resin.<sup>[218]</sup> The two components would easily flow to the crack site, curing when in contact and sealing the crack, guaranteeing sufficient self-healing efficiency for localized damages up to 30 damage/repair cycles, with a reduction in efficiency. These vascular systems can autonomously repair multiple damage events, but the extent of restoration is limited to the diffusivity and flowability of the healing agent toward the crack. Furthermore, the network must be designed accurately to be in proximity to areas potentially susceptible to damage without losing its integrity, and once a localized region is depleted of a healing agent, the further repair is prevented.<sup>[14]</sup> This limitation is even more pronounced in capsule-based extrinsic self-healing composites, which are difficult to fabricate with extrusion-based techniques.<sup>[13]</sup>

To avoid these drawbacks many efforts were devoted toward intrinsic self-healing mechanisms, which will be described in the next paragraphs.

### 5.2. Dynamic Covalent Chemistry

#### 5.2.1. Imine Bonds

Wei et al. designed a printable hydrogel based on bifunctional PEG terminated by benzylamine (PEG-BA), deaminated via oxidation to benzaldehyde (PEG-AL) by means of monoamine oxidase B (MAO B) catalyzed by horseradish peroxidase (HRP).<sup>[219]</sup> The obtained bifunctional aldehyde acted as a cross-linker by reacting with primary amines of glycol chitosan (GC) or gelatine (collagen) via an imine bond with Schiff base formation, providing the polysaccharide-based hydrogel dynamic behavior. Self-healing was qualitatively observed by mending two half-discs, stained differently, for 12 h at room temperature without external intervention; it was also demonstrated by the disappearance of a man-made hole in a sample after 6 h. These hydrogels possessed shear thinning properties before gelation occurred, and thus 3D printing was used to print layered simple planar shapes. Furthermore, this system can be employed in biologically relevant environments, because it is biodegradable in the presence of lysine and cells can be mixed in the hydrogel for in situ bioprinting.

Based on the same dynamic chemistry, Nadgorny et al. reported a gel obtained by crosslinking -functionalized poly (2-hydroxyethyl methacrylate) (PHEMA) functionalized with benzaldehyde via carbodiimide coupling reactions, with a bifunctional amine, ethylenediamine (EDA), to form dynamic and reversible imine bonds, which provided fast gelation and fast self-healing.<sup>[220]</sup> The gel could also withstand repeated healing cycles,

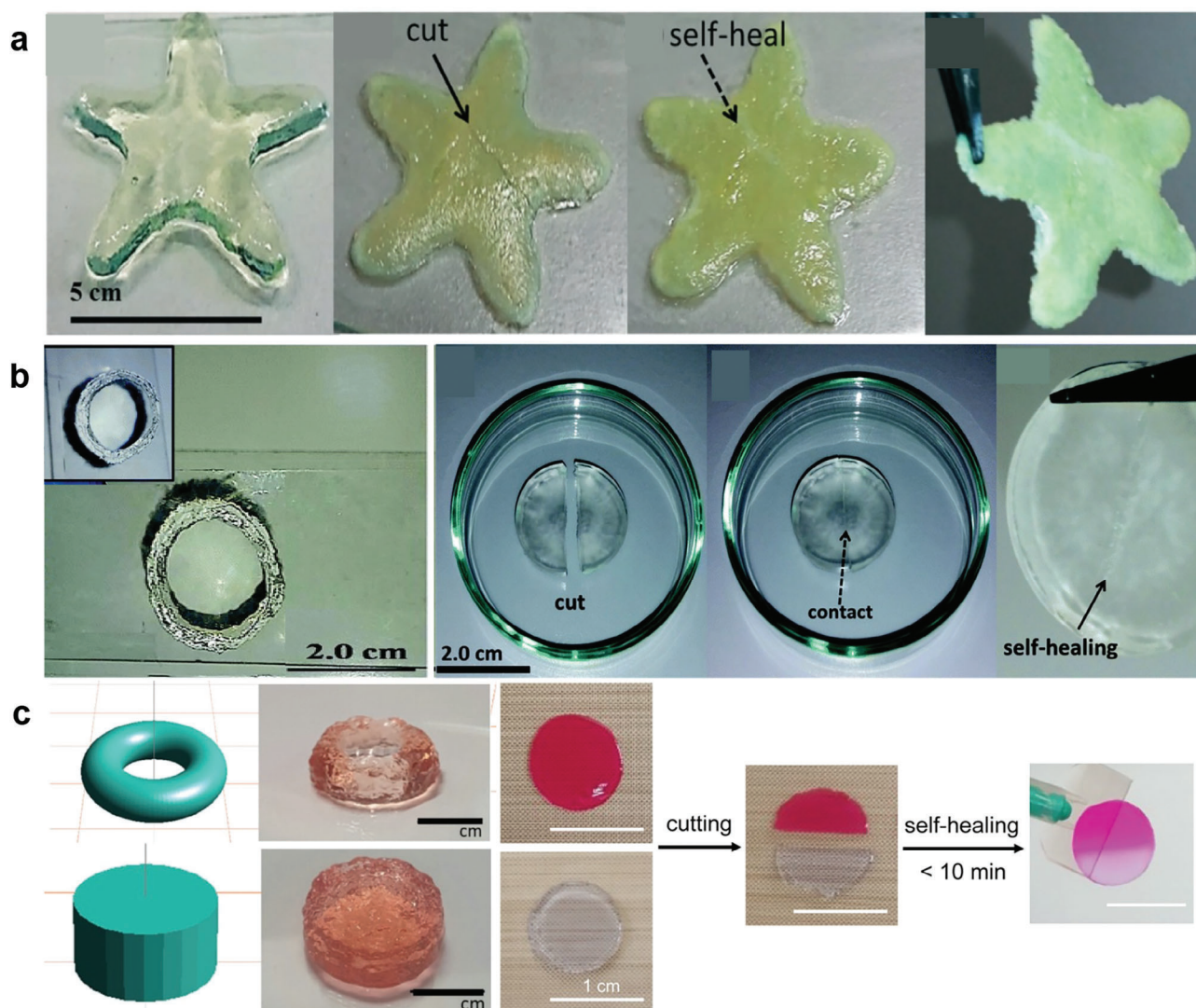


**Figure 2.** Examples of extrusion-based printed systems with dynamic covalent chemistry-based self-healing mechanisms: a) Imine bond. Adapted with permission.<sup>[220]</sup> Copyright 2017, Royal Society of Chemistry. b) Oxime bond. Adapted with permission.<sup>[223]</sup> Copyright 2018, Royal Society of Chemistry. c) Acylhydrazone bond. Adapted with permission.<sup>[226]</sup> Copyright 2019, American Chemical Society.

achieving full recovery every time, although the time required for self-healing gradually increased with an increasing number of subsequent cycles. A time-independent 3D printing of stable and self-supporting macroscopic 3D objects with various simple shapes and dimensions reinforced afterwards with a post-printing step performed via further imine crosslinking with EDA was achieved (Figure 2a).

Chen et al. proposed another approach, developing a time-sharing hydrogel (TSH) bioink through mixing species with different gelation times.<sup>[221]</sup> The imine bonds between aldehyde hyaluronic acid (AHA) and N-carboxymethyl chitosan (CMC) provide both biocompatibility and gelation within minutes at room temperature. The ink was used to print common grid constructs at room temperature with unassisted structural support, but additional post-printing reinforcement by the addition of PEG-SG was still required for shape retention and for cell-laden construct culture. The non-cytotoxic nature of the species and the

high permeability of the hydrogel were favorable for cell viability and proliferation in printed constructs that showed integrity throughout the incubation process. In vitro nerve-like, muscle-like, and cartilage-like constructs were successfully printed where different cells manifested homogeneous growth, as well as biological specificities.

More recently, also Heidarian and Kouzani investigated nanocellulose/gelatine inks in which imine bonds were exploited to enable self-healing.<sup>[222]</sup>

### 5.2.2. Oxime Bonds

Connal research group developed a macroporous hydrogel formed by crosslinking poly(*n*-hydroxyethyl acrylamide-co-methyl vinyl ketone) (PHEAA-co-PMVK) a bifunctional hydroxylamine, tetraethylene glycol bishydroxylamine (TEG-BHA)

in aqueous solution with the formation of oxime linkages with ketone moieties on PMVK.<sup>[223]</sup> The printing process was carried out at 80 °C, to improve the printability, fabricating self-supporting yet simple architectures. A post-printing treatment by a cycled cryogenic thermally induced phase separation (TIPS) facilitated the formation of a secondary supramolecular crosslinking based on strong hydrogen bonds arising from physical interactions among the amide and hydroxyl groups on PHEAA. Cryogels exhibited full and autonomous macroscopic damage restoration observed by cutting a rejoining a printed part (Figure 2b). More recently, oxime-carbamate functionalities were employed by Wang and coworkers to fabricate photo-thermally controlled PU, in which light irradiation was able to trigger SH properties.<sup>[224]</sup>

### 5.2.3. Acylhydrazone Bonds

Wang et al. explored self-healing in hydrogels made of hyaluronic acid (HA) modified with hydrazides (HA-HYD) and HA modified with aldehydes (HA-ALD), exploiting acylhydrazone dynamic chemistry.<sup>[225]</sup> Strain cycling on shear-oscillatory rheometry revealed rapid recovery after stopping hydrogel straining, demonstrating the extrudability and the self-healing capacity of the material. Macroscopic repair was assessed by recombining two halves of differently dyed cylindrical discs that were cut and rejoined and after 10 min of contact they could not be separated by manual stretching. Multilayered lattices were printed, and the filaments were smooth with high shape fidelity and stability to relaxation during printing. These scaffolds were used to encapsulate fibroblasts and showed high cytocompatibility, with 90% cell viability.

Kim et al. developed a biocompatible polysaccharide-based hydrogel bioink prepared from partially oxidized hyaluronate (OHA) and glycol chitosan (GC) in the presence of adipic acid dihydrazide (ADH).<sup>[226]</sup> OHA/GC gels do not exhibit self-healing properties because of the inherent rigidity of the polysaccharide backbone, despite the formation of reversible imine bonds via the Schiff base reaction between the aldehyde of OHA and primary amines on GC. However, the addition of dihydrazide capable of forming acylhydrazone links by condensation with the carbonyl group of OHA imparted them with autonomous healing properties due to competitive reversible covalent bond formation. A high degree of oxidation enables the of the gel in extrusion-based 3D printing. Objects of various basic shapes and sizes were fabricated, exhibiting rapid self-healing (Figure 2c). The same system has been then used to fabricate magnetically responsive self-healing ferrogel, by incorporating super-paramagnetic iron oxide nanoparticles (SPIONs).<sup>[227]</sup> ADH has also been proven to induce self-healing capability while enhancing the flexibility, stretchability, and printability of a hydrazide-modified hyaluronate (hHA)–oxidized hyaluronate (oHA) double network hydrogel.<sup>[228]</sup>

Similarly, Chen et al reported acylhydrazine-terminated three-armed PEG and benzaldehyde-terminated Pluronic F127.<sup>[229]</sup> Those materials, which show SH properties, were 3D printable at 1000 Pa at a temperature of 10 °C.

### 5.2.4. Urea Bonds

In a thermo-plastic polyurethane (TPU), dynamic covalent bonds among polycaprolactone diol (PCL), 4,4-diphenyl-methane diisocyanate (MDI), and N,N'-diisopropyl-1,2-ethanediamine (DE) were exploited to assemble large-sized printed parts fabricated without supporting structures.<sup>[230]</sup> It was also demonstrated that self-healing enhanced interlayer adhesion, providing improved mechanical property. The system showed excellent printability, enabling the possibility to split complex structures such as a chess piece, into parts easier to print with less or no support, which were then fabricated separately and assembled by heating at 80 °C for 30 min (Figure 3a).

### 5.2.5. Boronate Ester

Boronate esters-mediated self-healing was used by Biswas et al. to produce 3D printable dynamic hydrogel hydrogels composed of various phenylboronic acids with guanosine (G).<sup>[231]</sup> G contains cis-1,2-diols capable of forming dynamic bonds with phenylboronic acids, providing thixotropic behavior compatible with extrudability and self-healing properties. A visual observation of the SH properties was performed by joining three separate parts together, which joint in a single piece after 30 min. The gel was non-toxic, and the printing process did not damage the cell viability.

Wu et al. developed a conductive polymer composite ink by reinforcing a polyborosiloxane (PBS) matrix with electrochemically exfoliated graphene nanosheets.<sup>[232]</sup> The synthesized materials showed temperature-dependent and chemical-activated mechanically adaptive properties (MAPs). The presence of the continuous percolative network of graphene provided conductivity, ductility, and higher mechanical properties. Furthermore, the graphene nanosheets contributed to self-healing, which occurs spontaneously at room temperature. This system was used to fabricate a 3D-printed gas sensor to detect various organic vapors such as diethyl ether, hexane, and toluene.

A fully bio-based conductive hydrogel was constructed using cassava starch and natural rubber latex through a simple heating process.<sup>[233]</sup> The healing capability was provided by the addition of boric acid that formed dynamic bonds with the starch, resulting in a healing efficiency of  $\approx 72\%$  in tensile strength recovery after 90 min. 3D printing was performed using a heated syringe and a hot stage, building basic shapes such as a pyramid and a planar mesh-like network (Figure 3b). The thermal process was exploited to impart conductivity via in-situ silver mirror reaction, and the precursor sol was deposited directly onto a glove to fabricate motion sensors, and effective healing was proven by full conductivity recovery.

Recently, Seong and coworkers reported about ionotronic hydrogels for wearable electronic applications.<sup>[234]</sup> In this study, ionogel containing PVA, Pectin, Borax, and tannic were synthesized and investigated, both in terms of printability and electronic properties. Furthermore, SH was guaranteed by a synergistic effect of boronate–ester formation and hydrogen bonding. As a result, the authors demonstrated the possibility of developing flexible electronics.



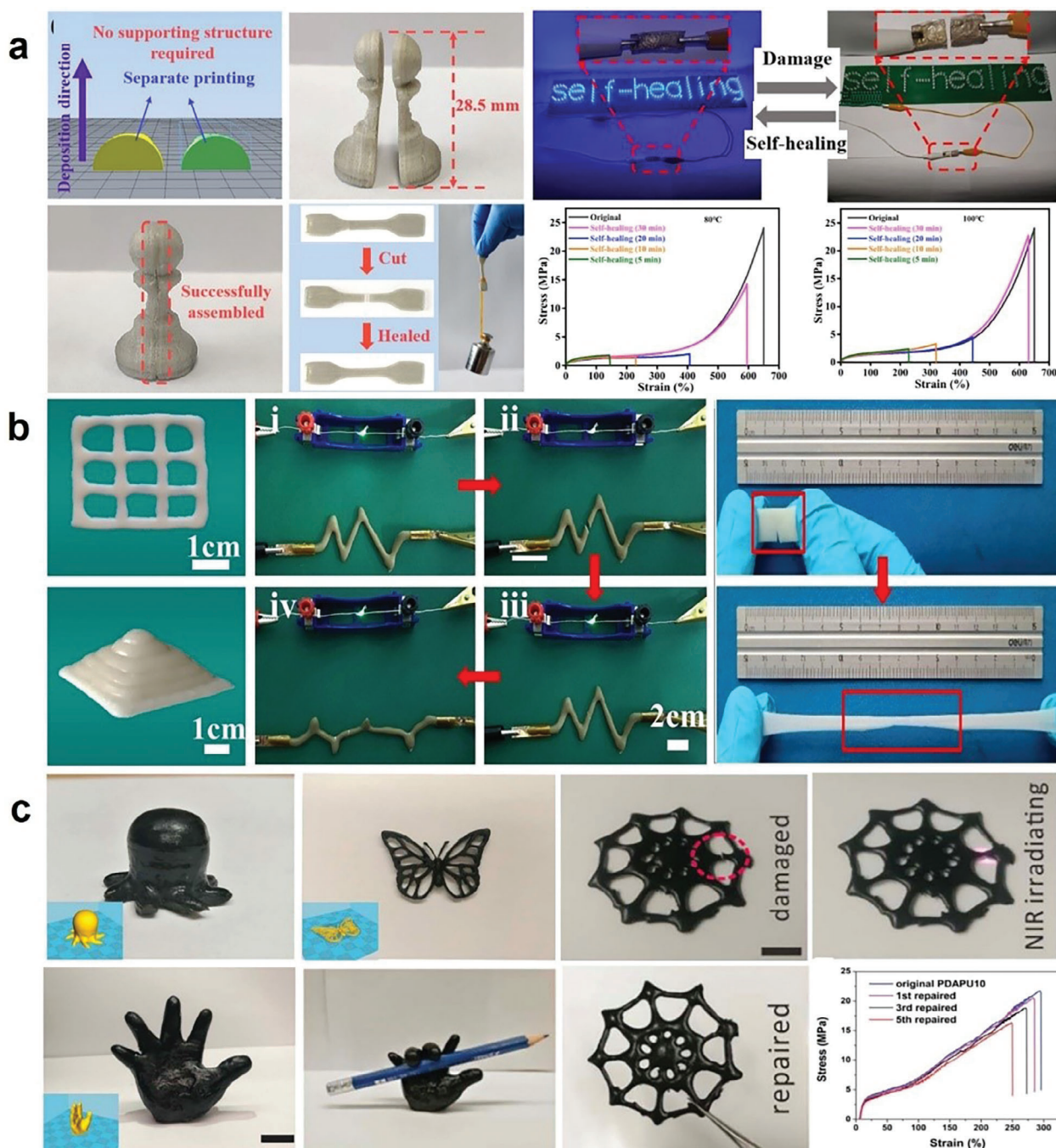


**Figure 3.** Other examples of extrusion-based printed systems with dynamic covalent chemistry-based self-healing mechanisms: a) urea bond. Adapted with permission.<sup>[230]</sup> Copyright 2022, American Chemical Society. b) Boronate-ester bond. Adapted with permission.<sup>[233]</sup> Copyright 2022, Elsevier. c) Diels–Alder reaction. Adapted with permission.<sup>[240]</sup> Copyright 2019, Royal Society of Chemistry.

### 5.2.6. Diels–Alder

Smaldone et al. developed Diels–Alder reversible thermosets (DART) based on lactic acid oligomers functionalized with maleimide chain-ends and multifunctional furan-containing cross-linker.<sup>[235]</sup> This system is dynamic at the temperatures typically used for FFF 3D printing, undergoing depolymerization before extrusion of a retroDA reaction at

temperature higher than 90 °C, thus lowering the molecular weight via de-cross-linking. Repolymerization took place upon cooling at temperatures lower than 60 °C, achieving smooth surface finish and lower anisotropy. However, complex 3D parts could not be printed without the aid of supports, due to the slow formation of the fmDA adducts. To address this drawback, DART were mixed with polylactic acid (PLA) to achieve self-supporting structures.<sup>[236]</sup> The

self-healing efficiency was evaluated through tensile tests on dumbbell-shaped specimens printed along the Z-print direction by comparing the ultimate strength of pristine and healed samples.<sup>[237]</sup>

Yuan et al. developed ink for the fabrication via DIW of a self-healing and high-strength thermoset composed of trifuran epoxy, bis (2-maleimidoethoxy) ethane as monomers, and ethylene glycol (EG) as nonreactive diluent to improve processability.<sup>[238]</sup> Mechanical properties after curing of the resin were comparable to those of engineering-grade epoxies, also due to the low viscosity of the ink, which effectively eliminated voids between the deposited filaments. The printing orientations were also found to be insignificant to the mechanical properties or the healing performance of the polymer due to the isotropic internal structure of the prints, which demonstrated to be also recyclable.

Recently, Guo et al. developed a conductive recyclable composite (PFBC) designed on a dynamic covalently cross-linked elastomer composite for the fabrication of recyclable and degradable electronics.<sup>[239]</sup> Poly (butylene sebacate-co-butylene fumarate) was functionalized with furfurylamine, and then reversibly cross-linked with bismaleimide (BMI) via the DA reaction; furthermore, conductive nanofillers were added to fabricate elastic conductive composites (PFBC). Reversible DA cycloaddition also allowed 3D printed parts recycling over several cycles. The 3D printed was also self-healed by near-infrared light irradiation for 1 min taking advantage of the photoinduced heating of carbon nanotubes (CNTs).

Diels–Alder reactions can also be used to crosslink bis-isocyanate-terminated polyurethanes (NCOPU) by introducing furan alcohol (FA) and high-efficiency photothermal agent aniline trimer (AT), called photothermal DA-reactive PU (PDAPU).<sup>[240]</sup> Introducing AT segments enables intrinsic thermal-related functions, such as shape memory, self-healing, and recyclability. In particular, NIR laser was used to precisely trigger in situ self-healing of the PDAPUs along the damaged interface because AT segments generate large amounts of heat via absorbing NIR light. The localized effect is suited also for complex 3D geometries. Optical confirmation of cutoff specimen healing was given by a 10 s irradiation with a NIR light, the gradual disappearance of deep cracks, while mechanical recovery was tested as 92% effective. Various objects such as a butterfly, octopus, hand, and spider-like structure, were printed by setting the printhead at 130 °C, and localized self-healing and targeted shape memory was proven for remote precise motion control (Figure 3c). Moreover, PDAPUs were recyclable and could be reprinted after crushing without additional additives or reagents while preserving the mechanical properties of the initially printed parts.

### 5.3. Non-Covalent Interactions

#### 5.3.1. Host–Guest

Burdick et al. proposed in 2015 the first example of a 3D printed self-healable hydrogel based on reversible physical crosslinking used as shear thinning ink and a printing support.<sup>[241]</sup> The supramolecular hydrogels used were based on hyaluronic

acid (HA), which was modified with adamantane (Ad) or  $\beta$ -cyclodextrin ( $\beta$ -CD). Printing was performed in a soft matrix that allowed the movement of the print nozzle in all directions without collapses of the printed part, enabling patterning of complex structures at high resolution that showed cell viability superior to 90%. These hydrogels are inherently weak, so HA was partially functionalized with methacrylate moieties to increase its long-term stability via covalent crosslinking upon UV irradiation. The obtained results paved the way for the development of printing processes carried out in hosting media which must possess self-healing ability to effectively support the printed component, which does not necessarily have to show self-healing ability, but only shear-thinning behaviour.<sup>[242]</sup> The same authors' group also studied the use of dual crosslinking HA-based hydrogel filaments for the fabrication of self-resisting layered structures without the need of supporting polymers.<sup>[232,233]</sup>

More recently, Wang et al. proposed a system based on a host-guest supramolecule (HGSM) with three arms, covalently cross-linked with a natural polymer.<sup>[243]</sup> HGSM was obtained by the inclusion reaction between isocyanatoethyl acrylate-modified  $\beta$ -cyclodextrin ( $\beta$ -CD-AOI<sub>2</sub>) and acryloylated tetra-ethylene glycol-modified adamantane (A-TEG-Ad), and it was used as a multifunctional dynamic cross-linker for gelatin methacryloyl (GelMa). The hydrogel showed shear-thinning behavior, but the ink temperature had to be lowered after mixing from 37 to 24 °C to reach a sufficient strength of the extruded filament. Layer-by-layer deposition was performed on a platform kept at 5 °C to induce rapid solidification after dispensing followed by rapid curing by UV irradiation, resulting in the formation of rectangular patterned scaffolds with regular fibers and uniform pores. Self-healing ability was tested at swelling equilibrium on a non-printed gel cut in half and re-joined for 1 hour, after which it could withstand a force applied by tweezers (Figure 4a). The 3D-printed scaffolds presented good biocompatibility, supporting cell attachment and growth in vitro, as well as histocompatibility in vivo when subcutaneously implanted.

#### 5.3.2. Hydrophobic Association

Thermoreversibility in amphiphilic block copolymers can be exploited to achieve heat-triggered self-healing. Poly(isopropyl glycidyl ether)-block-poly(ethylene oxide)-block-poly(isopropyl glycidyl ether) ABA triblock copolymers have lower critical solution temperature (LCST) behavior that enables responsivity to both shear forces and temperature.<sup>[244]</sup> The hydrophobic central blocks can assemble into flower-like micelles and bridged micelles, thus promoting an extended and well-percolated physical network upon heating from 5 °C to room temperature. Rheological studies demonstrated that the gels had a rapid and reversible modulus response to shear stress. Printed high aspect ratio pillars with eight stacked layers maintained adequate structural consistency, envisioning a potential application in tissue engineering. The same approach was recently reported by Hao and coworkers, who studied inks composed of hyaluronic acid and pluronic, in which hydrophobic association of the surfactant was exploited to enable SH.<sup>[245]</sup>



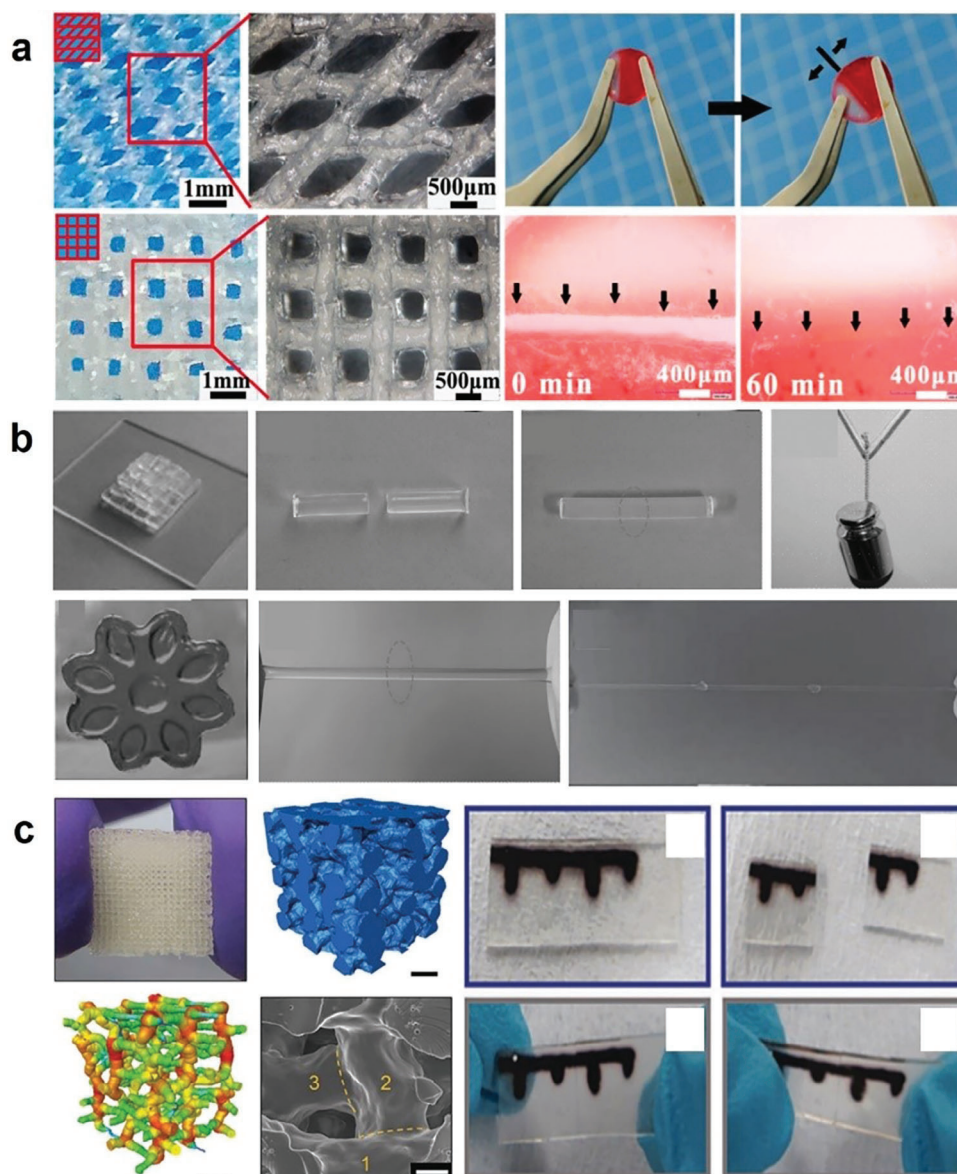


**Figure 4.** Examples of extrusion-based printed systems with non-covalent interaction-based self-healing mechanisms: a) Host–guest inclusion. Adapted with permission.<sup>[243]</sup> Copyright 2019, Royal Society of Chemistry. b) Hydrogen bond. Adapted with permission.<sup>[246]</sup> Copyright 2017, John Wiley and Sons. c) Electrostatic interaction. Adapted with permission.<sup>[253]</sup> Copyright 2018, Royal Society of Chemistry.

### 5.3.3. Hydrogen Bonding

Wang et al. designed mechanically supramolecular hydrogels via copolymerization of N-acryloyl glycinamide (NAGA) and 1-vinyl-1,2,4-triazole (VTZ) without adding any further chemical cross-linker.<sup>[246]</sup> The reversible nature of the hydrogel comes from the multiple hydrogen bonds formed between dual amide motifs in the side chain of NAGA, while introducing VTZ endowed the system with self-repairability, thermoplasticity, and re-processability. Healing capacity was qualitatively evaluated by cutting a cylindrical sample in two parts, then brought into contact with a plastic syringe and immersed in water at 55 °C for 45 min. The thermoreversible sol-gel transition and a facile heat-triggered processing enabled the material to be processed by extrusion-

based 3D printing techniques. The hydrogel was converted to a high-viscosity solution by heating at 80 °C and printed, planar shapes and patterns were then fabricated (Figure 4b). The presence of triazole provided in addition antibacterial, antifungal, antihypertensive, and analgesic activities suitable for implantable medical devices. The same group proposed a different solution based again on NAGA but copolymerized with 2-acrylamide-2-methylpropanesulfonic acid (AMPS) to achieve printability due to dual amide hydrogen bonding that promoted the formation of stable physical gels.<sup>[247]</sup> Heating/cooling cycles induced dynamic breakup and reconstruction of hydrogen bonds, leading to a reversible sol-gel transition and self-healability. Electrical conductivity was attained by doping the hydrogel with poly (3,4-ethylenedioxythiophene)-poly(styrenesulfonate) (PEDOT/PSS),

which had no influence on self-healing properties. The 3D printing process allowed the fabrication of conductive hydrogels with arbitrary planar shapes. Those were used to develop electrodes for supercapacitors with high capacitive performances, by blending activated charcoal powder.

Zhang et al. proposed a self-healable pre-crosslinked hydrogel microparticles (pcHμPs) of photopolymerized chitosan methacrylate (CHMA) and polyvinyl alcohol (PVA) hybrid hydrogels.<sup>[248]</sup> The chemically cross-linked hydrogels did not flow, not resulting suitable for extrusion; therefore, those were fractured into microparticles which show shear-induced reversible gel-fluid transition behavior. The extensive hydrogen bonding between chitosan and PVA chains among different particles provides the typical thixotropic behavior at high shear and rapid self-healing. The proposed hydrogel colloid could be easily extruded with a steady flow into continuous filament, which is 3D printable. Precise tubular structures were printed without requiring any support or post-printing treatments, also showing long-term stability in shape and dimension. The granular hydrogel was also used to fabricate a series of biomimetic and biocompatible constructs with a high aspect ratio and large size, such as a human ear and a rat thighbone. Similarly, a mixture of PVA, Poly(Acrylic Acid) (PAA), and tannic acid was studied to develop flexible bioelectronics.<sup>[249]</sup> In this case, SH was guaranteed by distributed H-bonding, while electrical conductivity was given by adding functionalized CNT.

#### 5.3.4. Electrostatic Interactions

Natural polymers often show shear-thinning behavior and thermally induced self-assembly as a result of electrostatic interactions among the chains. Liu et al. exploited the gelation of gelatin methacryloyl (GelMA) physical gels (GPGs) via the cooling process to develop a cell-laden bioink.<sup>[250]</sup> Self-healing was evaluated only qualitatively. The bioink could be printed into temporally stable constructs that could maintain the pre-designed structures without deformation. Various freeform structures were printed, such as a thin-walled tube or a tilted rhombus-shaped cube. This gel favored cell proliferation, showing potential for applications in tissue engineering.

Egg white (EW) proteins are another mix of low-cost and easily scalable natural polymers that can be used to fabricate hydrogels, incorporating conductive nanomaterials, for example carbon nanotubes.<sup>[251]</sup> SH performances were evaluated by rheological tests via a dynamic strain amplitude cyclic test that showed a complete recovery of the hydrogel network in around 10 seconds. In macroscopic tests, the hydrogel was cut into two parts and then brought together, spontaneously repairing after 30 min in a sealed chamber with 80% humidity at room temperature. Self-healing and printability were preserved after CNT incorporation; DIW was used to fabricate a multilayered cube with an internal well-defined lattice structure, and an ear model. The conductive hydrogel was tested as a body motion sensor and could detect various signals, such as the delicate wrist pulse, distant reflection of index finger flexion, respiration, and vigorous finger bending.

Synthetic polymers can also establish electrostatic interactions, especially when they contain an equal number of positively and negatively charged pendant functional groups. Lei and

Wu have developed a zwitterionic hydrogel composed of units of methacrylic acid (MAA) and 3-dimethyl(methacryloyloxyethyl) ammonium propanesulfonate (DMAPS).<sup>[252]</sup> The proposed hydrogel exhibited tunable thermoresponsivity, turning from an upper critical solution temperature (UCST)-type to an LCST-type hydrogel by increasing the MAA content. Despite the absence of permanent crosslinking in both types of hydrogels, the UCST-type hydrogel is cross-linked by hydrogen bonds and ionic interactions among carboxyl and sulfonic acid groups with the ammonium cations. This resulted in ultra-high stretchability (>10 000% strain) and relatively high strength (>0.1 MPa), while the LCST-type hydrogel, mostly cross-linked by hydrophobic methyl groups, shows enhanced tensile strength (≈0.3 MPa) but lower stretchability. The LCST-type hydrogel shows repetitive autonomous self-healing. On the other hand, the UCST-type hydrogel was suitable for direct ink writing of a grid-like structure with shape retention after extrusion. This hydrogel has been used to develop skin-like soft conductive wearable devices with stimuli sensitivity, optical responsivity, biocompatibility, and antibacterial activity, because DMAPS possess also antimicrobial and anti-fouling properties.

Self-healing developed in 3D printable organic/inorganic hybrid systems. A silica/poly(tetrahydrofuran)/poly( $\epsilon$ -caprolactone) hybrid material (SiO<sub>2</sub>/PTHF/PCL-diCOOH) was prepared exploiting in situ cationic ring-opening polymerization (CROP) and sol-gel chemistry, resulting in an interpenetrated network showing elastomeric behavior.<sup>[253]</sup> The specific combination of various non-covalent bonding interactions between organic components enabled the hybrid materials to display self-healing properties. In particular, the reversible inter-chain intermolecular forces are London forces, dipole-dipole interactions among polymer chains, and hydrogen bonding. The latter are likely to be the strongest forces, because when PCL-diCOOH was not included in the reaction, the elastomer did not show self-healing capacity. The printing of grid-like pattern with aligned 90° layers, with strut and interconnected pore channel, as proven by mCT image analyses, was performed at room temperature (Figure 4c). No interfaces are formed between consecutive chemically bonded layers, and the final properties and shape could be tailored by changing the inorganic/organic ratio. These scaffolds were proposed for the regeneration of articular cartilage, as they closely mimic the compressive behavior of cartilage, favored in vitro chondrogenic differentiation, and were biodegraded safely.

Cao et al. have proposed a bio-inspired, stretchable, and self-healing electronic skin (GLASSES) that combines transparency, stretchability, and self-healing in dry and various aquatic conditions.<sup>[254]</sup> The material is formed of a fluorocarbon amorphous elastomer, poly(vinylidene fluoride-co-hexafluoropropylene) P(VDF-HFP), and a fluorine-rich ionic liquid, 1-ethyl-3-methylimidazolium bis(trifluoromethylsulfonate)imide (EMITFSI), which interacts with polymer chains through highly reversible and strong ion-dipole interactions. Both the fluoro-elastomers and the fluorine-rich ionic liquids have weak interactions with water molecules, because of the high electronegativity. This allows to maintain fast and repeatable electromechanical self-healing properties in wet, acidic, and alkali environments. Autonomous restoration occurs only partially under ambient conditions, but could be enhanced by elevated temperatures, achieving a healing



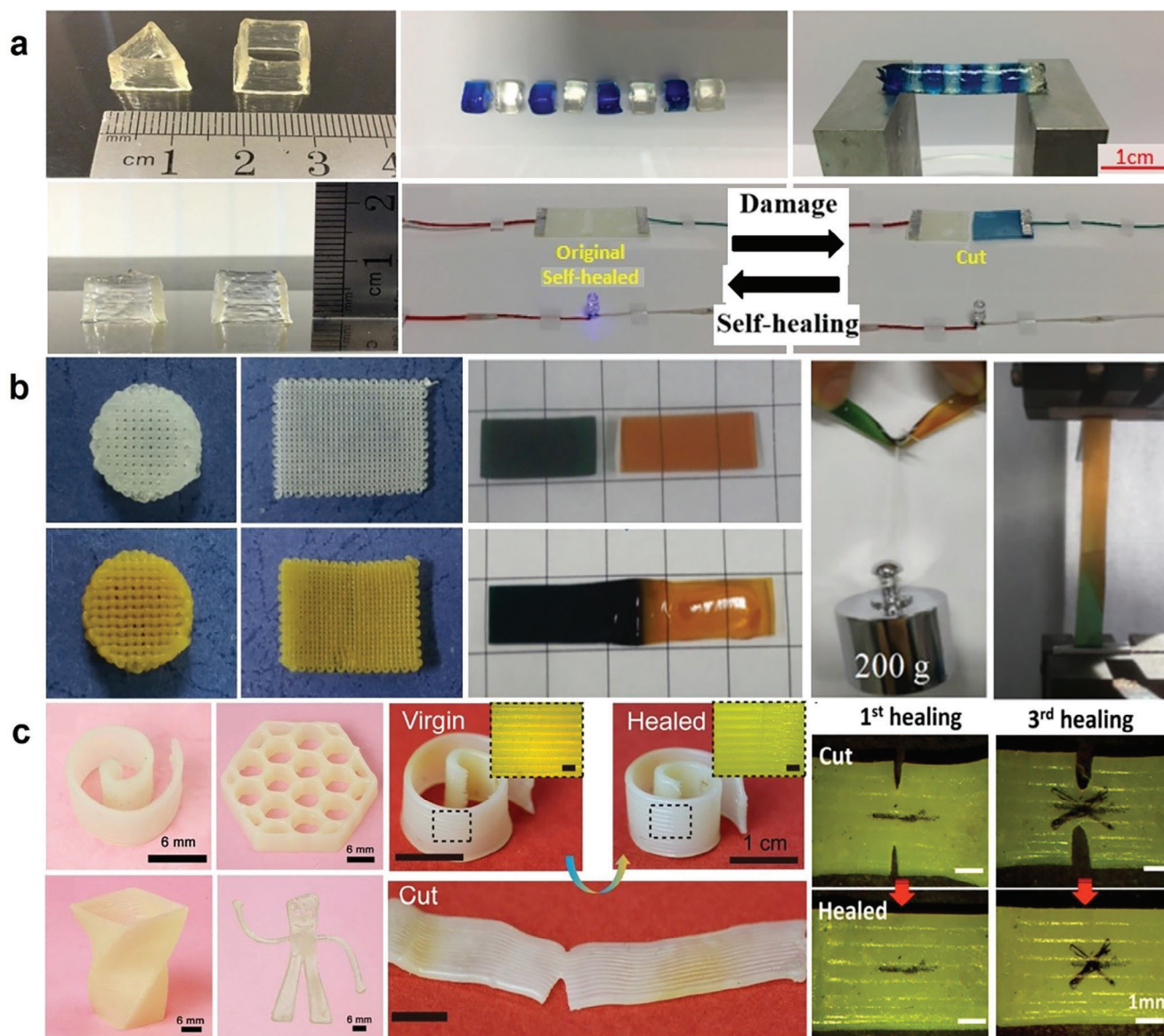


**Figure 5.** Other examples of extrusion-based printed systems with non-covalent interaction-based self-healing mechanisms: a) self-assembly. Adapted with permission.<sup>[255]</sup> Copyright 2017, American Chemical Society. b) metal–ligand complexation. Adapted with permission.<sup>[259]</sup> Copyright 2018, American Chemical Society. c) Linear polymer interdiffusion. Adapted with permission.<sup>[267]</sup> Copyright 2018, American Chemical Society.

efficiency higher than 90. This material was used to fabricate a fully transparent and self-healing soft ionic printed circuit board (PCB).

### 5.3.5. Self-Assembly and Nanocomposite Interactions

Ionic interactions were also exploited to achieve self-healing in hydrogels composed of natural polymers, especially polysaccharides.  $\kappa$ -Carrageenan ( $\kappa$ CA) is a biocompatible linear sulfated polysaccharide derived from red algae that can undergo thermo-reversible and ionic gelation in water.  $\kappa$ CA can be combined with a UV-induced covalently cross-linked polyacrylamide (PAAm) and *N,N'*-methylene bisacrylamide (MBA) network to form a

double network hydrogel (DN).<sup>[255]</sup> The self-healing mechanism is based on the thermal dissociation of carrageenan double helices above the gel-sol transition temperature and reassociation upon cooling mediated by hydrogen bonding, and further enhanced by the addition of potassium ions. A healed sample of this material was demonstrated to stand a weight of 250 g without further failure. Thermoreversible sol-gel transition of  $\kappa$ -CA enabled the extruded ink to maintain the shape before UV irradiation, allowing the printing of 3D structures (Figure 5a). Furthermore, the hydrogel was used as a waveguide for LED light, showing a 99.2% recovery of light transport.

A nanocomposite bioink was developed by incorporating two-dimensional (2D) nanosilicates (nSi) within a  $\kappa$ -CA hydrogel without any covalent double network.<sup>[256]</sup> The introduction of

nSi induced additional hydrogen bonds between nanoparticles surfaces and the hydroxyl groups along  $\kappa$ CA backbone, enhancing the self-healing properties. High-aspect ratio cylinders, nose and ear models, were printed without supports or UV irradiation. These bioinks were used to print cell-laden tissue constructs with non-adherent cells, such as chondrocytes, for regenerative medicine.

SH deriving from self-assembly in combination with shape memory makes it possible to fabricate 4D bio-printed implants. A combination of gelatin, gelatin methacryloyl (GelMA), and biodegradable polyurethane (PU) nanoparticles (PUGG) was used to obtain hydrogels with reversible thermoresponsivity and shape stability.<sup>[257]</sup> The presence of PU enabled also the self-healing, enabling recovery after 24 h at room temperature. The PUGG hydrogel exhibited excellent 3D printability, filament resolution, good stackability (>80 layers) and structural stability after UV crosslinking, being able to be shaped into mesh-like structures and hollow cylinders. The parts were also used as scaffolds for neural stem cells and mesenchymal stem cells in two distinct constructs, showing also cells migration.

### 5.3.6. Metal Ligand Coordination

Metal ion-ligand coordination is among the most common solutions used to tune mechanical properties of hydrogels and to provide other desired properties, including resilience, processability, and dynamic adaptability. Zheng et al. reported a tough yet processable physical hydrogel obtained by swelling in  $\text{FeCl}_3$  aqueous solution a cast film of random copolymer poly(acrylamide-co-acrylic acid) (P(AAm-co-AAc)).<sup>[258]</sup> Supramolecular interactions formed by complexation of  $\text{Fe}^{3+}$  ions with carboxyl groups are influenced by pH, therefore the hydrogel exhibits stimulation-triggered healing ability through reversible sol-gel transition. The fractured gels could be healed only after softening and activation under acidic conditions, followed by re-swelling in  $\text{FeCl}_3$  solution, resulting in a healing efficiency of 73%. The viscous P(AAm-co-AAc) aqueous solutions were directly extruded into gel fibers with different diameters, then 3D printed in bi-dimensional grids, which showed shape-memory properties triggered by pH variation. The addition of sodium alginate (SA) to the same system enabled a dual ionic cross-linking of SA and P(AAm-co-AAc) by a one-step soaking operation in an aqueous  $\text{Fe}(\text{NO}_3)_3$  solution that improved the elongation and toughness of the hydrogels.<sup>[259]</sup> The abundance of carboxyl groups in alginate molecules and the copolymer chains provided multifunctionality and high coordination capacity, allowing the shape memory behavior and healing process. These hydrogels were successfully 3D printed into various complex architectures, such as rectangular or circular lattices and circular ring shapes, with distinct lines clearly visible (Figure 5b).

It is also possible to induce ionic cross-linking by functionalizing the backbone of polymeric chains with specific moieties. For example, hyaluronic acid functionalized with bisphosphonate (HA-BP), which forms reversible dynamic metal ligand coordination with  $\text{Ca}^{2+}$  ions.<sup>[260]</sup> To increase printability, dually functionalized HA derivative with BP and photopolymerizable pendant groups were synthesized. The presence of ions allows at the same time a shear-thinning behavior, which favors printabil-

ity, good mechanical properties, and self-healing, based on dynamic metal-ligand chelating coordination bonds. These bioinks were used to build parts through conventional 3D printing, but also with an alternative technique named 'omnidirectional printing' or 'freeform reversible embedding of suspended hydrogels' (FRESH), developed by the authors. In this second approach, the hydrogel was extruded within a sacrificial gel, which was used as support material. Afterward, UV irradiation was performed, enabling solidification of HA-BP ink, and then the support gel was removed. This allowed the fabrication of more complex and precise parts.

The presence of cations in SH hydrogels allows charge conduction, making those ideal for the fabrication of sensors and artificial skin devices. Park et al. fabricated various devices employing ion-conductive SH hydrogel made of acrylic acid and poly(ethylene glycol) diacrylate, in a ferric solution.<sup>[261]</sup> This material spontaneously heals in 30 min at room temperature, showing as well excellent ion conductivity recovery. The same group also worked in avoiding freezing issues at low temperature by replacing water with ethylene glycol, synthesizing organohydrogels that maintain self-healing and functionality, even in complex 3D structures.<sup>[262]</sup>

Conductive self-healing (CSH) hydrogels can also be designed by enriching a covalent-ionic double-bonded network with the addition of functional conductive species. Polypyrrole (PPy) was grafted onto a double-bond decorated chitosan (DCh) with pendant methacrylate groups. Those were then polymerized with acrylic acid (AAc) and N, N'-methylene bis-acrylamide (MBAA), to form PAAc/DCh-PPy IPN.<sup>[263]</sup> The addition of ferric ions enabled autonomous mechanical and electrical self-healing. CSH exhibited 100% mechanical recovery in 2 min and 90% electrical recovery in 30 s under ambient conditions. The printing was achieved by a two-step solidification process, that exploits the formation of the physical network to retain the shape. Bi-dimensional patterns, such as lattices and regular networks, were printed and used to monitor human motions with a fast resistance response.

Graphene oxide (GO) was also used in CSH, embedded in poly(acrylic acid) (PAA), to synthesize inorganic-organic hybrid composites, produced via a biomimetic mineralization process.<sup>[264]</sup> Chelation of  $\text{Ca}^{2+}$  ions with the carboxylic groups of both GO and PAA provided weak but abundant coordination bonds for fast self-healing. The interface of cut and rejoined samples was completely healed after 50 s at room temperature with no external assistance. These gels were used to fabricate 3D structures, such as triangular shapes and hollow tetrahedrons.

Magnetic nanoparticles were also used to fabricate 3D printed self-healing functional materials, in this case magnetic. Gang et al. embedded  $\text{Fe}_3\text{O}_4$  nanoparticles in a double-network composite hydrogel based on chitosan (CS) interpenetrated with a random terpolymer made of dopamine acrylamide (DAm), acrylic acid (AAc), and acrylamide (Aam).<sup>[265]</sup>  $\text{Fe}_3\text{O}_4$  NPs were treated with HCl solution to improve their dispersion in the matrix, exposing more Fe ions on the surface, which acted as bonding sites with different carboxyl groups/hydroxy groups in the polyolefin matrix. Metal-ion coordination provided self-healing ability for the composites. 3D-printed samples were then fabricated with complex shapes and high vertical aspect ratios. These samples showed magnetic resonance imageability and

magnetogenic effect, promoting cell adhesion and proliferation on anatomical structures for implantation *in vivo*.

At last, poly(dimethylsiloxane) (PDMS) polymers were functionalized with abundant carboxylic acid moieties, and then cross-linked using Zn(II)-carboxylate interactions into a three-dimensional network.<sup>[266]</sup> Zn(II) allows to shape PDMS with sufficient mechanical strength at room temperature, but, upon heating, the coordination equilibrium shifts towards disassociation in non-crosslinked PDMS-COO<sup>-</sup> chains, enabling the material to heal itself when damaged. Almost 100% self-healing efficiency in tensile strength was observed after keeping two cut surfaces in contact for 4 h at 80 °C. Various self-supporting irregular objects, which could also be thermally annealed when damaged, were fabricated with high fidelity. Modular objects were also fabricated, by printing smaller parts and exploiting the self-healing feature to combine them.

### 5.3.7. Molecular Interdiffusion

Poly(caprolactone) (PCL) was used as a mending agent in a semi-interpenetrating polymer network elastomer containing an aliphatic urethane diacrylate and N-butyl acrylate.<sup>[267]</sup> Diffusion and re-entanglement of the linear PCL chains upon heating allow cracks' healing. Furthermore, the system showed thermally triggered shape memory-assisted self-healing (SMASH). UV-light-assisted direct-ink-write printing at 70 °C was used to fabricate well-structured 3D architectures, such as an Archimedean spiral, honeycomb, hollow vase, Gumby toy, and a vascular repair tube, proving the feasibility of the system for potential application in biomedical devices (Figure 5c).

Magnetorheological properties can be exploited by adding magnetic particles in elastomer, e.g., carbonyl iron particles (CIP).<sup>[268]</sup> In this work, a matrix of PCL and TPU was used to host the CIP. Upon heating and under a magnetic field, CIP forms a chain-like structure, parallel to the direction of the magnetic field., which can be then fixed after cooling. Such elastomeric composites showed repeated SH in cyclic uniaxial tensile tests with a disappearance of the boundary between two separated parts after healing and cooling, with good repeatability. The ink was shaped into 2D and 3D structures, such as 2D graphene-like, 2D snow-like, and 3D carbon nanotube-like architectures and used to produce stimuli-sensitive actuators.

## 5.4. Vat Photopolymerization

### 5.4.1. Extrinsic Self-Healing

In vat photopolymerization, the reported studies on extrinsic SH are mainly focused on capsule-based systems, since the vascular systems are not compatible with this technology, due to intrinsic limitations. Sunlight-triggered autonomic self-healing silicone materials were fabricated via photoactivated thiol-ene click reaction between multifunctional mercaptosiloxane (MS) and bifunctional vinylsiloxane (VS).<sup>[269]</sup> Capsules containing low-viscosity unreacted prepolymer resin were incorporated into the composites during printing. When the fracture occurs, those monomers are released, providing rapid SH since polymerization in ambient

sunlight takes less 30 s. This is of particular interest to outdoor applications. This material resulted also in 3D printability, fabricating different objects such as an antagonistic muscle actuator and Kagome tower.

An alternative approach is the incorporation within the matrix of "pockets", containing a solvent compatible with the matrix. In this case, when damage occurs, solvent flows, achieving solvent-welding-based self-healing. Sanders et al. modified a commercial photocurable resin by embedding anisole and PMMA-filled vesicles, encapsulated using *in situ* polymerization of urea-formaldehyde.<sup>[270]</sup> When a crack breaks the capsules, the solvent is released promoting the diffusion of polymers and the formation of entanglements between cracks in the matrix. Despite the presence of microcapsules giving the resin a turbid appearance, no effects on the print quality due to light scattering were observed. This system was envisioned to improve the lifetime expectancy of bone cement due to the low toxicity, high boiling point, and immiscibility of anisole with water.

## 5.5. Dynamic Covalent Chemistry

### 5.5.1. Disulfide Bonds

Yu et al. proposed a photoelastomer ink based on (mercaptopropyl)methylsiloxane-dimethylsiloxane copolymer (MMDS) and vinyl-terminated poly-dimethylsiloxane (V-PDMS) containing both thiol and disulfide groups.<sup>[271]</sup> The former facilitates a thiol-ene photopolymerization during the additive manufacturing process, while the latter enables a disulfide metathesis reaction during the self-healing process. Dumbbell-shaped specimens were printed and cut into two parts and healed at 60 °C for 1 h, showing a total recovery of the original strength that remained above 90% efficiency even after over 10 damage-healing cycles, without requiring any solvent as a plasticizer to induce restoration. Various free-form architectures were printed, such as a circular cone, a pyramid, a cup, and an octet truss lattice. Multi-material structures composed of a non-healable stiff plastic phase and a healable soft elastomer phase with relatively strong interfacial bonding between the two phases were also fabricated, to be employed as soft actuators, multiphase composites, and architected electronics.

The same group exploited disulfide-based self-healing mechanisms in transformable lattice structures enabled by fracture and shape-memory-assisted autonomous healing.<sup>[272]</sup> The polymer network was constructed by an aromatic diisocyanate (isophorone diisocyanate (IPDI)) and a diol (polytetramethylene ether glycol, PTMEG) via urethane links, onto which dynamic disulfide bonds were incorporated by linking a diol-terminated disulfide. Printability via photocuring was enabled by embedding hydroxyl-ended acrylate groups onto the polymer backbone, and thus, the ink was made of disulfide-linked urethane-acrylate oligomers. The healed strip sample can sustain a weight of 50 g after being brought into contact at 80 °C for 6 h, resulting in a 90% recovery in tensile strength compared to the original samples. The authors also demonstrated the possibility to combine SH and shape memory, repairing objects after shape changes, and recovering initial properties (Figure 6a).



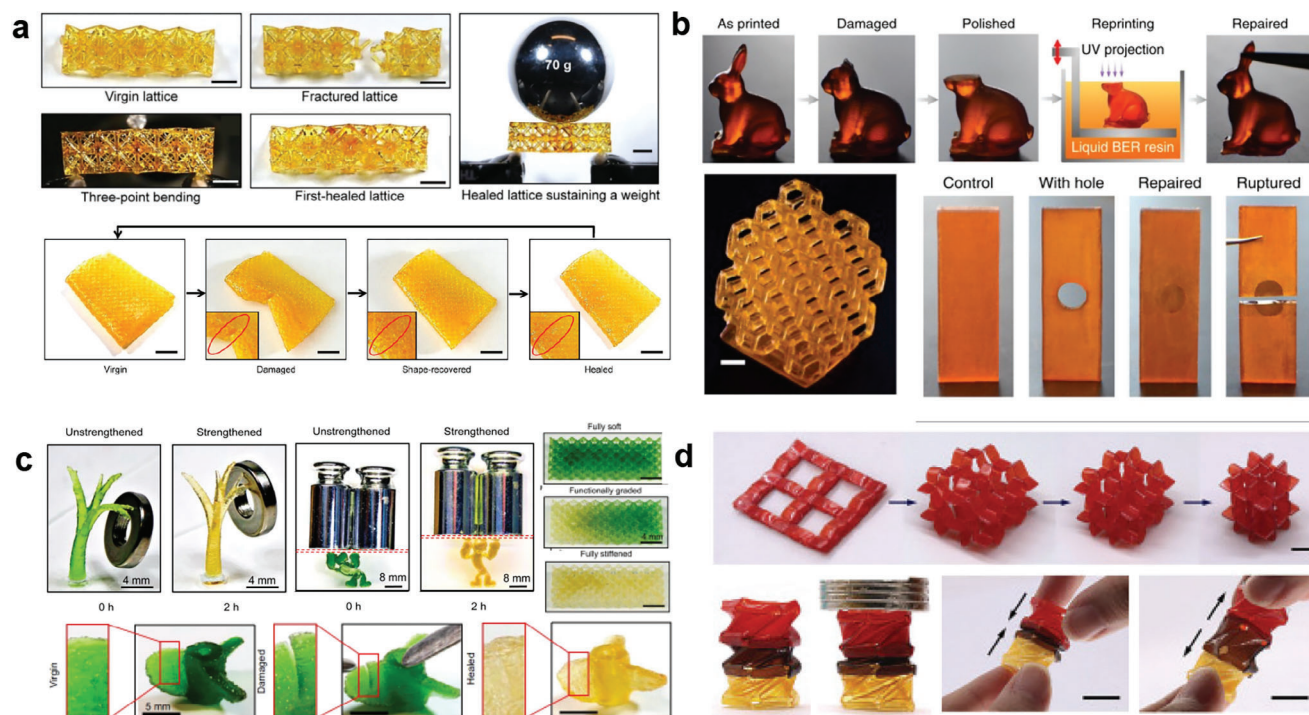


**Figure 6.** Examples of vat photopolymerization-based printed systems with dynamic covalent chemistry-based self-healing mechanisms: a) disulfide bond. Adapted with permission.<sup>[272]</sup> Copyright 2020, Springer Nature. b) Transesterification. Adapted with permission.<sup>[242]</sup> Copyright 2020, Springer Nature. c) Urethane bond. Adapted with permission.<sup>[279]</sup> Copyright 2021, National Academy of Sciences of the United States of America (NAS). d) Urea bond. Adapted with permission.<sup>[280]</sup> Copyright 2020, Elsevier.

Another polyurethane (PU)-based elastomer healable via the metathesis of disulfide bonds was proposed for applications in applications in flexible electronics, soft robotics, and sensors. In this case, the material was based on polyurethane chains functionalized with both acrylic and disulfide functional units, using hydroxyethyl acrylate as a reactive diluent.<sup>[273]</sup> Multiple healing was demonstrated on dumbbell-shaped specimens cut from UV-cured sheets. Self-healing was also visually proven by cutting small cylinders of different colors, connecting and healing them to form a healed cylinder that could lift a weight of 100 g and be stretched to a large deformation. Complex structures with high shape-retention, such as a honeycomb, a hollow cube, a Maya Pyramid, and a circular cone, were printed and showed self-healing ability.

### 5.5.2. Transesterification

Ge et al. proposed a reprocessable thermoset system made of commercially available chemicals, including 2-hydroxy-3-phenoxypropyl acrylate and bisphenol A glycerolate (1 glycerol/phenol) diacrylate, able to be reshaped, repaired, or recycled due to the presence of zinc acetylacetonate hydrate as a catalyst to accelerate transesterification reactions.<sup>[274]</sup> The heat-triggered bond exchange reactions (BERs) involved hydroxyl functional groups and adjacent ester functional groups capable of simultaneously breaking and reconnecting across the two damaged surfaces. Self-healing was obtained by deposition of virgin material in the damaged area followed by heating at 180 °C for a few

hours, resulting in 100% recovery of stiffness and 93% recovery of strength. A printed rabbit with broken ears was repaired by polishing the damage site to achieve a flat surface and then performing a new 3D printing to rebuild the missing part (Figure 6b).

The transesterification of exchangeable  $\beta$ -hydroxyl esters integrated in the oligomer can be combined with hydrogen bonds into an acrylate-based vitrimer composed of a diacrylate prepolymer synthesized by the chemical reaction between glycidyl methacrylate (GMA) and suberic acid (SA) mixed with acrylamide (AM) and tetrahydrofurfuryl acrylate (THFA).<sup>[275]</sup> The network rearrangement proceeds upon heating, with the gradual disappearance of hydrogen bonds at increasing temperatures. A tensile lap shear test at room temperature was used to check the welding of two pieces of fractured vitrimers by partial overlap followed by pressing at 180 °C for 1 h, resulting in an efficiency of 73%. Objects with various complex structures such as a set of gears and a honeycomb, were printed, and then remolded after dissolution in ethylene glycol.

Schlögl et al. presented a new transesterification catalyst based on a soluble monofunctional methacrylate phosphate that does not compromise cure rate and pot life and is covalently incorporated into a network obtained by click reactions of thiol-acrylate between hydroxy-2-phenoxypropyl acrylate, glycerol 1,3-diglycerolate diacrylate and trimethylolpropane tri(3-mercaptopropionate).<sup>[276]</sup> The liquid catalyst is able to catalyze esterifications and transesterifications in the solid polymer network, which rapidly undergoes thermoactivated rearrangements of its topology, because functional thiols act as chain transfer agents in the exchange reactions with hydroxyl groups present.

Healing efficiency was determined by printing uniaxial tensile tests with circular-shaped holes in the center fitted by a circular-shaped counterpart and healed by thermal treatment at 180 °C for 4 h, resulting in a total recovery of the original tensile strength compared to a defect-free bar. 3D objects with simple planar shapes and various substructures with different dimensions were printed, demonstrating triple shape memory upon heating.

Alternatively, materials extracted from bioresources can be used for developing these 3D printable vitrimers.<sup>[277]</sup> In this context, recently Liguori and coworkers reported on the use of resins based on vanillin for DLP 3D printing. The fabricated objects present good printability and precision, while repair was thermally enabled.

Changing type of chemistry employed, Kuenstler and coworkers recently proposed transesterification of thio–thioester photocurable resins as a suitable strategy to fabricate SH and recyclable 3D printed structures.<sup>[278]</sup>

### 5.5.3. Urethane Bonds

Photosynthesis-assisted healing was recently proposed as self-healing solution. Hybrid synthetic living materials can remodel their microstructures or recover mechanical properties by photosynthesis of embedded living chloroplasts extracted from spinach leaves, to generate glucose capable of forming urethane strong linkages (–NH–CO–O–) with isocyanate distal groups (NCO) incorporated onto a poly (tetrahydrofuran)-based polymer.<sup>[279]</sup> Samples are endowed with matrix strengthening and crack healing when exposed to white light, which induces the formation of stiff regions with artificial polysaccharides. 3D printed dumbbell-shaped samples with free NCO groups and embedded chloroplasts were cut, re-joined, and then subjected to 4 h illumination and 4 h darkness, resulting in a smooth healing interface with a healing strength ratio of 70% ± 7%. Various architectures could be printed, such as treelike, Popeye-like structures, and octet lattices, all of which showed tunable stiffness and healing ability that enabled mechanical properties recovery, as demonstrated by the healing of a boat propeller (Figure 6c).

### 5.5.4. Dynamic Urea Bonds

Modular 4D printing enables the fabrication of shapes by assembling multilayered complex structures and integrating multiple materials. Building blocks can be connected through hindered urea bonds, since these do not require a catalyst, and their dynamic characteristic can be tunable by simply adjusting the steric hindrance.<sup>[280]</sup> In this work, the photocurable formulation was based on a diacrylate cross-linker containing polycaprolactone (PCL) and dynamic hindered urea linkages, synthesized with ditin butyl dilaurate (DBTDL), isophorone diisocyanate (IPDI), *N,N'*-diisopropylethylenediamine (DPEA) and 2-isocyanatoethyl acrylate (ICA). The precursor was poured into a reaction cell and subjected to double-side irradiation with a commercial projector, to develop the 2D film. Those were then assembled in a layered fashion by interfacial bond exchange. Complex multilayered structures were assembled, including a 3D Miura-patterned structure with zero Poisson ratio and a Kresling-patterned cylin-

drical structure, and these devices also showed shape memory behaviour (Figure 6d). Similarly, Peng and coworkers reported on photocurable flexible polyurethanes to fabricate wearable sensors.<sup>[281]</sup>

### 5.5.5. Imine Bonds

Recently, Cortes-Guzman and co-workers studied a series of DLP-printable resins based on vanilline. In particular, the authors reported of a report five biobased, formulations that consist of an optimized mixture of vanillin methacrylate-functionalized Jeffamines and vanillin acrylate.<sup>[282]</sup> Thanks to the presence of imine moieties, SH was also provided. All the resins show high printability and possibility of recycling, demonstrating to be interesting for sustainable production.

## 5.6. Non-Covalent Interactions

### 5.6.1. Hydrogen Bonding

Invernizzi et al. developed SH in shape memory objects fabricated by vat photopolymerization using poly(caprolactone) dimethacrylate (PCLDMA) and methacrylated 2-ureido-4[1H]-pyrimidinone (UPyMA) units.<sup>[283]</sup> The material showed restoration after 1 h at 80 °C, with a healing efficiency of 54%. An L-shaped layered structure was printed to mimic the index finger and the thumb, which was partially cut and then repaired to prove that shape memory functionalities are still preserved after healing, making these printed actuators suitable for soft robotics.

*N*-acryloylmorpholine (ACMO) is another species capable of establishing abundant intermolecular hydrogen bonds and it was used with carboxyl multi-walled carbon nanotubes (c-CNTs).<sup>[284]</sup> Self-healing can be attributed to the interactions between carboxyl groups of c-CNTs and carbonyl/amino groups of poly (ACMO), activated by a water-uptake process when two pieces are brought together for a few hours in a humidity chamber. Mechanical self-healing efficiency was measured as 96% after the first cut-healing cycle, but gradually decreased with increasing healing times and cycles. Printability of complex structures such as a ladder pyramid, a conical gear, a bolt, and a set of spikes, was proved (Figure 7a), but no SH was shown on printed objects, which were used as strain sensors for the detection of human activities.

A ternary polymerizable deep eutectic solvent (PDESs) based on natural tannic acid (TA), choline chloride (ChCl), and hydroxyethyl methacrylate (HEMA), showed extensive secondary interactions.<sup>[285]</sup> These extensive interaction forces determined high self-healing efficiency, about 74% recovery in tensile stress after 12 h at 80 °C. Other than contributing to the healing process, natural TA improves mechanical strength thanks to its rigid aromatic structure and serves as an antibacterial agent, inhibitor, and already embedded UV-light absorber. Various complex structures, such as a logo, chinese knotting, and Doraemon, were fabricated with fast printing speed and high resolution.

Hydrogen bonding was also exploited to fabricate self-healing elastomers (SHEs) based on acrylic acid (AAc) with alkyl acrylates, with various chain lengths and stiffness.<sup>[286]</sup> PAA alone exhibited a typical elastic behavior above its *T<sub>g</sub>*, but no self-healing.

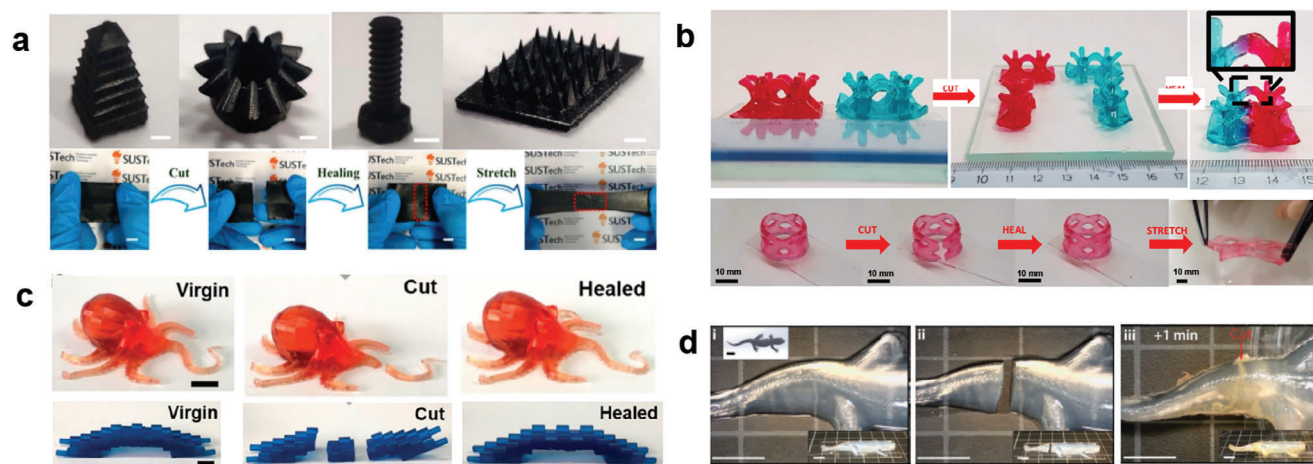


**Figure 7.** Examples of vat photopolymerization-based printed systems with non-covalent interaction-based self-healing mechanisms: a) hydrogen bonding in an elastomer. Adapted with permission.<sup>[284]</sup> Copyright 2020, Informa UK Limited, trading as Taylor & Francis Group. b) Hydrogen bonding in a hydrogel. Adapted with permission.<sup>[287]</sup> Copyright 2021, Springer Nature. c) Metal–ligand complexation in a dry system. Adapted with permission.<sup>[289]</sup> Copyright 2021, American Chemical Society. d) Metal–ligand complexation in a hydrogel. Adapted with permission.<sup>[290]</sup> Copyright 2019, Royal Society of Chemistry.

AA was then copolymerized with butyl acrylate (BA), and the newly obtained elastomers exhibited self-healing behavior, proving that the self-healing behavior can be related to the interactions between the ester carbonyl group of BA units and the carboxyl group of AA units. After damage, complete recovery of the mechanical properties was obtained after 12 h at room temperature. Various specimens such as a gear, the model of an ear and a hand, a honeycomb lattice, and a gecko, were printed, with the latter used to prove effective self-healing by replanting its tail after cutting. Given the absence of a chemical crosslinker, the copolymer elastomers were soluble in various solvents, and therefore, they were reprocessed by the solvent-casting method. The introduction of carboxylic ionic liquid led to the formation of a non-leaking and attachable ionogel by 3D printing for the detection of various human gestures.

Intrinsic SH in vat photopolymerized hydrogels was reported for the first time in a system designed as a semi-IPN by embedding a linear uncross-linked polymer, poly(vinyl alcohol) (PVA), into a chemical covalent network made of commercial photocurable species, acrylic acid (AAc), and poly(ethylene glycol) diacrylate (PEGDA), starting from a waterborne formulation.<sup>[287]</sup> PVA provided extensive hydrogen bonding due to the considerable amount of hydroxyl groups located along the polymer backbone, which enabled them to overcome the hindrance caused by the presence of water molecules. The self-healing ability occurred in a sealed container at room temperature without any stimuli because hydroxyl groups became available on freshly cut surfaces, and PVA migrated across the ruptured interface because of the presence of large volumes of water. Healed dumbbell-shaped samples could immediately bear bending deformation without failing, and SH efficiency was quantified to be 72% of the uncut uniaxial tensile strength after 12 hours in contact. The self-supporting body-centered cubic lattice with overhanging features and the axisymmetric structure with a central pillar were successfully printed and SH was also shown in these complex structures (Figure 7b).

### 5.6.2. Ionic Interactions

Self-healing in silicone elastomer was obtained employing amino-modified silicone oil (PDMS-NH<sub>2</sub>) and carboxyl-modified silicone oil (PDMS-COOH), in the presence of thiol-modified silicone oil (PDMS-SH), and vinyl-terminated polysiloxane (PDMS-Vi).<sup>[288]</sup> Thiol-ene photopolymerization between the thiol and vinyl functionalities enabled a rapid formation of the primary covalent cross-linked network by VP, while thermoinduced ionic association between carboxyl and amido moieties formed a secondary reversible network. Self-healing was achieved by heating the system at 120 °C and then cooling it to room temperature, activating the dissociation and reassociation of ionic bonds. Repeatable healing tests were performed on printed dumbbell samples, showing a recovery of 92%. Thick planar-layered architectures with no complex features were printed, such as gears and a half moon, and efficient self-healing was proven by healing and deforming cut samples without immediate failure.

### 5.6.3. Metal Ligand Coordination

Recyclable and self-healable structures can be printed using a resin comprising urethane monoacrylate (UMA) and acrylic acid (AAc), and zinc dimethacrylate (ZDMA) as cross-linker.<sup>[289]</sup> Monomers were crosslinked by ionic bonding between Zn<sup>2+</sup> and –COO– and hydrogen bonding between –NH or –OH and –C=O that can be dissociated when heated and while the bonded state is restored upon cooling. Mechanical tests were carried out on printed specimens, which exhibited a healing efficiency greater than 75% after healing at 90 °C for 12 h, which decreases for shorter healing times or lower temperature. By varying the monomer ratio (UMA/AA), soft elastomers to rigid plastics could be selectively printed into complex architectures, such as a soft octopus or rigid bridge, showing healing ability (Figure 7c). Soft and rigid parts were assembled into more complex structures,



including a thin-wall structure reshaped at high temperature into a cylindrical structure and a modular snowman model.

Modular 4D printing can also be obtained by exploiting ions introduced later in the structure, by soaking. Self-adhesive hydrogel building blocks made of covalently cross-linked poly(ethylene glycol) diacrylate (PEGDA) in the presence of dispersed anionic high-molecular-weight poly(acrylic acid) (PAA) could be printed and connected via ion-mediated adhesion.<sup>[290]</sup> Trivalent ferric cations bridged between PAA polymer chains on adjacent surfaces, and this coordination bond can be reversed using ethylenediaminetetraacetic acid (EDTA) to chelate ferric ions. Self-healing was assessed by cutting a cylindrical specimen, and then both halves were brought back in contact in a ferric ions' solution. After 60 min, the structure was able to support itself and was tested using a three-point flexural test that showed a flexural modulus similar to ionically cross-linked uncut samples, but lower displacement. Cylinders and a salamander were printed to prove effective self-adhesion, whereas LEGO-like hydrogel blocks with internal channels and external mechanical connectors were fabricated to be stacked into complex microfluidic devices and multilevel architectures (Figure 7d).

Hydrogels can be also obtained after hydration of 3D-printed dry networks. A dry-gel made of *N*-acrylomorpholine (ACMO) and Acrylic acid (AAc) was first printed with good fidelity and then swelled in an aqueous solution containing iron or aluminum ions, capable of coordinating with carboxyl groups.<sup>[291]</sup> The printed objects were fabricated without cross-linker, but were insoluble in water thanks to the strong metal ion-crosslink. Furthermore, they showed excellent weldability, nearly 90%. Similarly, Huand and coworkers reported on the development of composite resins for DLP based on 4-acryloylmorpholine (ACMO), monofunctional urethane (MUA), and Zinc methacrylate (ZMA).<sup>[292]</sup> In this case, the authors reported precise printing together with SH properties and recyclability.

Following a similar route, an interpenetrated network hydrogel based on poly(acrylic acid) (AAc)-*N*-vinyl-2-pyrrolidone (NVP) and carboxymethylcellulose (CMC) was printed without the use of a cross-linker.<sup>[293]</sup> A dual physical interaction occurs between the CMC and poly(NVP-AA) based on  $Zn^{2+}$  ligand coordination and hydrogen bonding, imparting toughness and self-healing ability to the gel. Self-healing efficiency was assessed by cutting and self-healing printed dumbbell-shaped hydrogels at room temperature for 24 h, showing that the healed samples regained 81% and 91% of the original stress and strain. Custom objects for wearable human motion sensing were printed with high resolution and tested in real time.

#### 5.6.4. Molecular Interdiffusion

PCL can be used as a mending agent for autonomous self-healing, also in VP-printed objects, by incorporating the linear polymer into a covalent network made of poly(ethylene glycol) dimethacrylate (PEGDMA) and benzyl methacrylate (BMA).<sup>[294]</sup> The SH process is based on thermally triggered PCL semicrystalline domains melting, diffusion across the boundary, and bonding of two damaged surfaces by entangling upon cooling. Mechanical properties of a damaged structure could be recovered to more than 90% after healing for 20 min at 80 °C. The print-

ing solution was obtained by increasing the temperature above the melting temperature of the healing agent ( $\approx 60$  °C). A chess piece, a Kelvin foam, a closed gripper, and a cardiovascular stent were fabricated, then damaged and healed at 80 °C for 5 min to show recovery of mechanical properties and shape memory ability to restore correct functionality.

At last, PEG-based gels were successfully 3D printed by DLP by Wang et al.<sup>[295]</sup> In this work, the authors combined interdiffusion properties of PEG 400 with H-bonding of photocurable hydroxy ethyl methacrylate (HEMA) and acrylic acid (AAc). In this case, the mechanical properties were almost completely recovered after 1 min and totally recovered after 1 hour. Furthermore, these materials demonstrated self-repairing also after scratching or punches.

## 6. Applications of SH 3D Printed Materials

In this review article, we sorted the different SH approaches by 3D printing technology, to give an overview of the possible strategies according to the available technologies. Obviously, it is possible to classify the reported literature from a different point of view, considering primarily the final applications. In Tables 3–6, methods, strategies, and final applications of the articles reported in this survey are summarized, together with the peculiarities of each system. For the sake of clarity, in this section those are summarized across the printing methods, to highlight the most important technological fields in which SH 3D printed structures are employed.

Furthermore, the SH mechanism utilized in the specific applications is important in selecting the materials and consequently critical for designing the printing composition system, according to the printing technology. For example, a critical property is the viscosity of the ink system; for extrusion-based printing, highly viscous materials are required to achieve rapid fixation, whereas for most light-based printing such as DLP, the viscosity should not exceed a certain range. So, for SH based on polymer chains, most likely the preferred printing system would be extrusion, while if starting from small molecules or dilute solutions, DLP will be more suitable. In this respect, it should be mentioned that printing of low viscosity ink system by extrusion is possible by providing a proper rapid fixation mechanism, such as combining extrusion with photopolymerization.<sup>[296]</sup> Another example is self-healing based on filler particles; in extrusion, a limiting factor would be clogging of the nozzle if too large particles are used, while in low viscosity DLP inks, too rapid sedimentation of the particles may occur. Below are reported examples of potential applications in which combining SH and 3D printing will bring a unique added value.

### 6.1. Biomedical Field

Certainly, the most explored field of applications for SH 3D printable materials is the biomedical field. As previously mentioned, the mimicking of biological tissues is based on soft materials, with some self-repairing properties and complex geometries, which are exactly 3D printed structures with SH ability. This resulted in a large number of investigations that report the fabrication of scaffolds,<sup>[213,215,219–222,225,237,242,244,247,250,251,254,261]</sup> whose

**Table 3.** Healing mechanism characteristics, system characteristics, printing condition and results, and application of extrusion-based printed systems with dynamic covalent chemistry-based self-healing mechanisms.

Material	Healing mechanism	Healing procedure	Self-healing efficiency	System configuration	Printing conditions	Geometrical dimensions	Complex structure healing [Y/N]	Application	Refs.
PEG benzylamine-terminated (PEG-BA), PEG benzaldehyde-terminated (PEG-AL), glycol chitosan (GC) or gelatine (collagen)	Imine bond	12 h @ RT	100% recovery amplitude oscillatory sweep test Visual observation	Hydrogel, chemically crosslinked single network	37 °C syringe	2D	N	Bioscaffold	[213]
Benzaldehyde-functionalized poly(2-hydroxyethyl methacrylate) (PHEMA), ethylenediamine (EDA)	Imine bond	1 h @ RT	100% recovery amplitude oscillatory sweep test Visual observation	Dynamic chemically crosslinked single network	Piston pressure 0.6 bar, temperature 25 °C, 0.36 mm layer height.	2D	N	Self-rolling objects	[214]
Aldehyde hyaluronic acid (AHA), N-carboxymethyl chitosan (CMC), gelatin (GEL), 4-arm poly(ethylene glycol) succinimidyl glutarate (PEG-SG)	Imine bond	4 h @ 37 °C, sealed environment	100% recovery amplitude oscillatory sweep test Visual observation	Hydrogel, double physical network	Immersion in EDA in DMF solution for 20 min after printing 0.07 mL min <sup>-1</sup> extrusion speed, temperature 25 °C, 0.26 mm layer height, RT, immersion in PEG-SG solution for 3 min after printing	2.5D	N	Bioscaffold	[215]
n-Hydroxyethyl acrylamide (HEAA), methyl vinyl ketone (PMVK), tetraethylene glycol bis(hydroxylamine) (TEG-BHA)	Oxime bond	3 h @ RT	100% recovery amplitude oscillatory sweep test Visual observation	Hydrogel, single dynamic chemical covalent network	Temperature 25 °C, 0.4 mm layer height, freezing/thawing cycles after printing	2D	N	—	[217]
Hydrazide-modified hyaluronic acid (HA-HYD), aldehyde-modified hyaluronic acid (HA-ALD), norbornene-modified hyaluronic acid (Nor-HA), pentaerythritol tetramercaptoacetate (PETMA)	Acylhydrazide bond	10 min in air or PBS	100% recovery amplitude oscillatory sweep test Visual observation	Hydrogel, double chemical network	18 G / 25 G needles, 0.5/1 mL h <sup>-1</sup> , 10 min UV curing after printing	2.5D	N	Bioscaffold	[219]
Oxidized hyaluronate (oHA), glycol chitosan (GC), adipic acid dihydrazide (ADH)	Acylhydrazide bond	10 min @ RT	100% recovery amplitude oscillatory sweep test Visual observation	Hydrogel, double chemical network	—	2D	N	Bioscaffold, bioprinting	[220–221]
Oxidized hyaluronate (oHA), Hydrazide-modified hyaluronate (hHA), adipic acid dihydrazide (ADH)	Acylhydrazide bond	10 min @ RT	100% recovery amplitude oscillatory sweep test Visual observation	Hydrogel, double chemical network	25 G needle, 2.5 mL h <sup>-1</sup>	2.5D	N	Bioscaffold, bioprinting	[222]

(Continued)



**Table 3.** (Continued).

Material	Healing mechanism	Healing procedure	Self-healing efficiency	System configuration	Printing conditions	Geometrical dimensions	Complex structure healing [Y/N]	Application	Refs.
Diisocyanate-modified polycaprolactone diol (DI-PCL), N,N'-diisopropyl-1,2-ethanediamine (DE)	Urea bond	30 min @ 100 °C	> 90% (tensile stress)	Elastomer	2 mm layer height, 140 °C	2.5D	Y	—	[224]
Phenyl boronic acid (PBA), 4-nitrophenyl boronic acid (4-NPBA), 4-methoxyphenyl boronic acid (4-MPBA) with guanosine (G)	Boronate-ester bond	30 min @ RT	100% recovery amplitude oscillatory sweep test Visual observation	Hydrogel, guanosine-quadruplex structures self-assembled in nanofibrils	0.25 mm layer height, RT	2D	N	Bioscaffold	[225]
Polyborosiloxane (PBS), electrochemically exfoliated multilayer graphene (G5)	Boronate-ester bond	—	99.4% (conductivity)	Composite elastomer	Methanol-activated mechanism, 0.41 mm layer height, RT	2D	N	Gas sensor	[226]
Starch, boric acid, natural rubber	Boronate-ester bond	90 min @ RT	≈71.8% (tensile stress)	Elastomer, physical-chemical dual network	64 °C syringe, 95 °C stage	2.5D	N	Wearable sensor	[227]
Multifuran monomers (Furan-modified trimethylolpropane triacrylate (3F), furan-modified tris[2-(acryloyloxy)-ethyl] isocyanurate (ICN3F), furan-modified pentaerythritol tetraacrylate (4F), bismaleimide (2M)	Diels-Alder reaction	—	—	Dynamic chemically crosslinked single network	0.5 mm layer height, 130–138 °C, air cooling, cold storage for 8–12 h	2D	N	—	[229]
Poly(lactic acid), furan-modified p-phenylenediamine (2F), furan-modified tris(2-aminoethyl)amine, bismaleimide (2M)	Diels-Alder reaction	—	—	Semi-interpenetrated network, uncrosslinked polymer within dynamic chemically crosslinked network	0.5 mm layer height, 190–205 °C, stage 48–60 °C	2D	N	—	[230]
Furan-modified p-phenylenediamine (2F), furan-modified tris(2-aminoethyl)amine (3F), bismaleimide (2M)	Diels-Alder reaction	5s @ 120 °C, then 15 min @ 65 °C	≈77% (tensile stress)	Dynamic chemically crosslinked single network	0.5 mm layer height, 200–205 °C, stage 50–60 °C	2D	N	—	[231]
Trifuran epoxy (TE), 1,2-bis(2-maleimidoethoxy) ethane (BMIO)	Diels-Alder reaction	2h @ 120 °C, then overnight @ 80 °C	≈85% (tensile stress)	Dynamic chemically crosslinked single network	120 °C, 18 G syringe, 1mm layer height, 22G syringe, 0.5 mm layer height, 80 °C post curing overnight	2D	N	Remoldability	[232]

(Continued)

**Table 3.** (Continued).

Material	Healing mechanism	Healing procedure	Self-healing efficiency	System configuration	Printing conditions	Geometrical dimensions	Complex structure healing [Y/N]	Application	Refs.
Furan-modified poly(butylene sebacate-co-butylene fumarate) (PBSF), bismaleimide (BMI), carbon nanotubes (CNTs), silver nano-flakes (AgNF), carbon black (CB)	Diels-Alder reaction	IR irradiation for 1 min (808 nm, 0.35 W cm <sup>-2</sup> )	Visual confirmation of conductivity restoration	Composite, elastomer	132–142 °C, 0.4 mm layer height	2D	N	Remoldability, wearable sensors	[233]
Furan-terminated polycaprolactone-based polyurethane (FPU), aniline trimer-terminated polycaprolactone-based polyurethane (APU), bismaleimide (BMI)	Diels-Alder reaction	IR irradiation for 10s (808 nm, 0.8 W cm <sup>-2</sup> )	≈92% (tensile stress)	Dynamic chemically crosslinked single network	0.8 mm layer height, 130 °C, stage 20 °C, 72h rest	3D	Y	Shape memory, remoldability	[234]

properties depend on the chemical structure of the polymers used. Beyond this application, the use of 3D-printable SH materials is reported as artificial skin,<sup>[246]</sup> as devices for controlled drug release<sup>[259]</sup>, and as supporting gel material for embedded printing.<sup>[235]</sup>

## 6.2. Robotics and Soft Robotics

Other important fields of application are robotics and soft robotics. In this field, 3D printing is exploited to fabricate complex structures, where SH is useful to extend the usage time of the components. Furthermore, to induce SH ability to a polymer network means sometimes to also induce shape memory properties, i.e., the ability of a material/structure to have autonomous movements after programming.<sup>[297]</sup> Consequently, those two characteristics are exploited to fabricate actuators<sup>[234,251–253,258,261,262,265,266,270,277,288]</sup> which can be used either in soft robotics or in robotics, according to the mechanical characteristics of the polymer used and the requirements of the application. Interestingly, while most of the structures in the biomedical field are fabricated by extrusion-based 3D printing, in robotics and especially soft robotics light-induced 3D printing is mostly used. This could be related to the requirements of fabricating objects with high structural complexity, for example in pneumatic grippers that contain internal channels.<sup>[298,299]</sup>

## 6.3. Sensors and Electronics

Another relevant field of applications is related to the functional properties of the materials, such as providing an electrical or optical sensor that should be restored after structural failure. Here,, the important aspect is that SH enables not only restoring the mechanical properties but also the functional properties, such as electrical and optical continuity, enabling the reusing of a device after being healed. Applications of sensors are important in soft robotics, as presented in a recent review,<sup>[300]</sup> thus providing an interesting future field of applications. Interestingly, often functional properties are recovered faster than mechanical ones, making those materials even more appealing.<sup>[301]</sup> In this frame, SH 3D printed constructs were exploited to fabricate reusable<sup>[226,227,251,255–257,278,280,287]</sup> and wearable<sup>[233,245,249]</sup> sensors, as well as other devices such as supercapacitors<sup>[241]</sup> or other energy storage systems<sup>[258]</sup>, electronic skins<sup>[248]</sup> or, in general, devices able to transport electrical charges.<sup>[260,265]</sup>

## 6.4. Other Applications

Finally, we envisage a last field of interest, which is more conventional for 3D printing, i.e. rapid prototyping. In this case, 3D printing is required to rapidly fabricate complex structures, to be used for their mechanical properties. SH can be employed to assemble complex devices, by creating chemical bonds between different parts.<sup>[274,283–285]</sup> On the other hand, in most cases the 3D printed parts are disposable, and once the object ends its use or is damaged, it's thrown away, without considering reuse. In this frame, SH can extend the usage time, but also be exploited to recycle the object, enabling remolding,<sup>[232–234]</sup> in some cases even employing different 3D printing techniques.<sup>[268,269,280,282,283]</sup>

**Table 4.** Healing mechanism characteristics, system characteristics, printing condition and results, and application of extrusion-based printed systems with non-covalent interaction-based self-healing mechanisms.

Material	Healing mechanism	Healing procedure	Self-healing efficiency	System configuration	Printing conditions	Geometrical dimensions	Complex structure healing [Y/N]	Application	Ref.
$\beta$ -cyclodextrin-modified hyaluronic acid (CD-HA), adamantane-modified hyaluronic acid (Ad-HA)	Host-guest interaction	—	100% recovery amplitude oscillatory sweep test Visual observation	Hydrogel, physical network	—	3D	N	Support gel for embedded printing, bioscaffold	[235]
Ad-modified acryloylated tetra-ethylene glycol (A-TEG-Ad), $\beta$ -cyclodextrin-dually coniugated 2-isocyanatoethyl acrylate ( $\beta$ -CD-AOI2), gelatin methacryloyl (GelMA)	Host-guest interaction	1 h @ RT	≈80% (tensile stress)	Hydrogel, double chemical physical network	22G syringe, 0.8 mm layer height, 24 °C, stage 5 °C, UV curing after printing	3D	N	Bioscaffold	[237]
Poly(isopropyl glycidyl ether)-block-poly(ethylene glycol)-block-poly(isopropyl glycidyl ether) (PIPrGE-b-PEG-b-PIPrGE)	Hydrophobic association	—	—	Hydrogel, physical network	5 °C, 0.1 mm layer height	2D	N	—	[238]
N-acryloyl glycinamide (NAGA), 1-vinyl-1,2,4-triazole (VTZ)	Hydrogen bonding	in contact in a glass syringe, immersed in water, 45 min @ 55 °C	≈90% (tensile stress)	Hydrogel, physical network	80 °C syringe, RT stage, 1 mm layer height	2.5D	N	—	[240]
N-acryloyl glycinamide (NAGA), 2-acrylamide-2-methylpropanesulfonic (AMPS), PEDOT/PSS, activated charcoal powder	Hydrogen bonding	in contact in a plastic syringe, immersed in water, 3 h @ 90 °C	≈80% (tensile stress)	Hydrogel, physical network	80 °C syringe, RT stage, 1 mm layer height	2D	N	Supercapacitor	[241]
chitosan methacrylate (CHMA), polyvinyl alcohol (PVA)	Hydrogen bonding	—	100% recovery amplitude oscillatory sweep test	Hydrogel, microparticles, double chemical physical network	30G syringe, 0.35 mm layer height, 0.2 Mpa pressure, freezing/thawing cycles after printing	2D	N	Bioscaffold	[242]
Gelatin methacryloyl (GelMA)	Electrostatic interaction	—	100% recovery amplitude oscillatory sweep test	Hydrogel, chemically crosslinked single network	21 °C, 0.5 mm layer height, UV curing after printing	2D	N	Bioscaffold, bioprinting	[244]
Egg white, carbon nanotubes (CNTs)	Electrostatic interaction	30 min @ RT, 80% humidity	100% recovery amplitude oscillatory sweep test Visual observation	Hydrogel, physical network	27G syringe, 0.4 mm layer height, immersion in Dulbecco's Modified Eagle Medium (DMEM) or after printing	2.5D	N	Wearable sensor	[245]

(Continued)

**Table 4.** (Continued).

Material	Healing mechanism	Healing procedure	Self-healing efficiency	System configuration	Printing conditions	Geometrical dimensions	Complex structure healing [Y/N]	Application	Ref.
Methacrylic acid (MAA), 3-dimethyl (methacryloyloxyethyl) ammonium propanesulfonate (DMAPS)	Electrostatic interaction	12 h @ RT	≈75% (tensile stress) ≈98% (tensile strain)	Hydrogel, physical network	60 °C syringe, 0.6 mm layer height, 0.45 Mpa pressure, stage 20 °C	2D	N	Artificial skin, bioscaffold	[246]
Poly(tetrahydrofuran) (PTHF) poly( $\epsilon$ -caprolactone) (PCL-dicOOH), silica (SiO <sub>2</sub> )	Electrostatic interaction	24 h @ RT, 50% humidity	≈31% (tensile stress) ≈36% (tensile strain)	Hybrid material, triple network, organic-inorganic	RT, 3 days ageing @ 40 °C, 7 days drying @ 40 °C	3D	N	Bioscaffold	[247]
Vinylidenefluoride (VDF), hexafluoropropylene (HFP), 1-ethyl-3-methylimidazolium bis(trifluoromethylsulfonyl) imide (EMITFSI)	Electrostatic interaction	24 h @ 50 °C	≈91% (conductivity) ≈99% (toughness)	Elastomer, amorphous with ionic liquid	—	2D	N	Electronic skin for aquatic environments	[248]
$\kappa$ -carrageenan ( $\kappa$ -CA), acrylamide (AAm), N,N'-methylene bisacrylamide (MBA)	Self-assembly	in contact in a plastic syringe, sealed in a plastic bag, immersed in water, 40 min @ 90 °C	≈99% (conductivity)	Hydrogel, double chemical physical network	40–70 °C syringe, 0.1–5 bars pressure, 0.3 mm layer height, UV curing after printing	2D	N	Wearable sensor	[249]
$\kappa$ -carrageenan ( $\kappa$ -CA), nano Laportite XLS (nSi)	Self-assembly and nanocomposite interactions	—	100% recovery amplitude oscillatory sweep test	Hydrogel, physical organic-inorganic network	40 °C 23G syringe, 0.35 mm layer height, 0.3mL h <sup>-1</sup> flow rate, immersion in salt solution after printing	2.5D	N	Bioscaffold	[250]
polycaprolactone diol (PCL), poly(D,L-lactide) diol (PDLLA), isophorone diisocyanate (IPDI), gelatin methacryloyl (GelMA)	Self-assembly	24 h @ 25 °C	100% recovery amplitude oscillatory sweep test Visual observation	Hydrogel, double chemical network	25 °C, 0.45 Mpa pressure, 4 °C stage, UV curing after printing	2.5D	Y	Shape memory, sensor, actuator, bioscaffold	[251]
Acrylic acid (AAc), acrylamide (AAm), iron chloride (III)	Metal-ligand coordination	10 min 1 M HCl solution at the interface. Swelling in 0.1 M FeCl <sub>3</sub> solution for 2 h and pure water for 12 h	≈73% (tensile stress)	Hydrogel, physical network	—	2D	N	Shape memory	[252]

(Continued)

**Table 4.** (Continued).

Material	Healing mechanism	Healing procedure	Self-healing efficiency	System configuration	Printing conditions	Geometrical dimensions	Complex structure healing [Y/N]	Application	Ref.
Sodium alginate (SA), acrylic acid (AAc), acrylamide (AAm), iron chloride (III)	Metal-ligand coordination	pH 14 solution at the interface. 24 h in sealed bag, then soaking in 0.1 M FeCl <sub>3</sub> solution for 2 h and pure water for 24 h	≈56% (tensile stress) ≈17% (tensile strain)	Hydrogel, double chemical physical network	UV curing after printing, followed by soaking in iron chloride solution and then soaking in water	3D	N	Shape memory	[253]
Bisphosphonate-functionalized hyaluronic acid (HA-BP), calcium chloride	Metal-ligand coordination	—	100% recovery amplitude oscillatory sweep test Visual observation	Hydrogel, physical network	Required functionalization for printing, UV curing after printing	2D	N	Bioscaffold	[254]
Acrylic Acid (AAc), iron chloride (III), poly(ethylene glycol) diacrylate (PEGDA), ethylene glycol (EG)	Metal-ligand coordination	30 min @ RT	100% recovery amplitude oscillatory sweep test Visual observation	Hydrogel, chemically physically crosslinked single network	RT, 0.6 mm layer height, 0.3 Mpa	2.5D	N	Sensors	[255,256]
Acrylic acid (AAc), methacrylic anhydride (MA), iron chloride (III), N,N'-methylenebis-acrylamide (MBAA), chitosan (Ch), pyrrole (Py)	Metal-ligand coordination	2 min @ RT	100% recovery amplitude oscillatory sweep test Visual observation	Hydrogel, double chemical physical network	RT, 0.3 mm layer height, 0.28 Mpa	2D	N	Sensors	[257]
Graphene oxide (GO), poly(acrylic acid) (PAA), amorphous calcium carbonate (ACC)	Metal-ligand coordination	1 min @ RT	Visual observation (conductivity)	Swellable composite, dually crosslinked physical network	—	2D	N	Energy-storage, actuators	[258]
Chitosan (CS), dopamine acrylamide (DAAm), acrylic acid (AA), acrylamide (AAm), iron chloride (III)	Metal-ligand coordination	12 h @ 70 °C sealed container	Visual observation	Hydrogel, double chemical physical network	RT, 0.25 mm layer height, 0.1 Mpa	3D	N	Treatment of tumors, controlled release of drugs	[259]
Carboxylated poly(dimethylsiloxane) (PDMS-COOH), Zinc Chloride (II), graphene	Metal-ligand coordination	4 h @ 80 °C	≈99% (flexural stress)	Physical network	130 °C, 0.4 mm layer height, 0.4 Mpa	2.5D	N	Adhesive, conductor	[260]
Aliphatic urethane diacrylate (AUD), Isobornyl acrylate (IBOA), N-butyl acrylate (BA), polycaprolactone (PCL)	Molecular interdiffusion	20 min @ 80 °C	< 30% (tensile strain)	Elastomer, semi-interpenetrated network	70 °C, 0.6 mm layer height, 0.1 Mpa UV curing after printing	2.5D	N	Shape memory, bioscaffold	[261]
Polycaprolactone (PCL), thermoplastic polyurethane 108SA (TPU), carbonyl iron particles (CIP)	Molecular interdiffusion	3 min @ 80 °C	≈91.1% (tensile modulus) ≈74.2% (residual tensile strain)	Plastomer, physical network	200 °C, 1.7 mm layer height	3D	N	Shape memory, actuator	[262]



**Table 5.** Healing mechanism characteristics, system characteristics, printing condition and results, and application of vat photopolymerization-based printed systems with dynamic covalent chemistry-based self-healing mechanisms.

Material	Healing mechanism	Healing procedure	Self-healing efficiency	System configuration	Printing conditions	Geometrical dimensions	Complex structure healing [Y/N]	Application	Ref.
Vinyl-terminated polydimethylsiloxanes (V-PDMS) [4–6% (mercaptopropyl)methylsiloxane]-dimethylsiloxane (MMDS), iodobenzene diacetate (IBDA), 1,6-hexanediol diacrylate (HDDA)	Disulfide bond	2 h @ 60 °C	≈100% (tensile modulus)	Elastomer, containing dynamic covalent bonds	25 μm s <sup>-1</sup> curing coefficient, 405 nm UV light	3D	N	Actuator, composite, conductor	[265]
Polytetramethylene ether glycol (PTMEG), isophorone diisocyanate (IPDI), dimethylacetamide (DMAc), dibutyltin dilaurate (DBTDL), 2-hydroxyethyl disulfide (HEDS), 2-hydroxyethyl methacrylate (HEMA)	Disulfide bond	8–18 h @ 60 °C	≈100% (tensile modulus)	Covalent network containing crystalline domains and dynamic covalent bonds	0.2 μm s <sup>-1</sup> curing coefficient, 405 nm UV light	3D	Y	Shape memory, actuator	[266]
Polyethylene glycol (PEG), isophorone diisocyanate (IPDI), hydroxyethyl acrylate (HEA), bis(2-hydroxyethyl) disulfide (HEDS)	Disulfide bond	12 h @ 80 °C	≈95% (tensile stress)	Elastomer, containing dynamic covalent bonds	200 μm layers, 10–120 s exposure per layer 405 nm UV light, 29 mW cm <sup>-2</sup>	3D	N	—	[267]
2-Hydroxy-3-phenoxypropyl acrylate (HPPA), (zinc acetylacetonate hydrate, (Zn(acac) <sub>2</sub> ), bisphenol A glycerolate (1 glycerol/phenol) diacrylate (BAGPDA)	Transesterification	4 h @ 180 °C	≈100% (tensile modulus) ≈93% (tensile stress)	Covalent network containing dynamic covalent bonds	50 μm layers, 2 s exposure per layer	3D	Y	Remoldability	[268]
Glycidyl methacrylate (GMA), suberic acid (SA), 1,5,7-triazabicyclo[4.4.0]dec-5-ene (TBD), tetrahydro-furfuryl acrylate (THFA), acrylamide (AM)	Transesterification	2 h @ 180 °C	≈100% (shear stress)	Covalent network containing dynamic covalent bonds	—	2.5D	N	Remoldability	[269]
2-Hydroxy-2-phenoxypropyl acrylate (HPPA), glycerol 1,3-diglycerolate diacrylate (GDGDA), Miramer A99, trimethylolpropane tris(3-mercaptopropionate) (TMPTP)	Transesterification	4 h @ 180 °C	≈100% (tensile stress)	Covalent network containing dynamic covalent bonds	50 μm layers, 8 s exposure per layer 405 nm UV light	2.5D	N	Shape memory, actuator	[270]

(Continued)

**Table 5.** (Continued).

Material	Healing mechanism	Healing procedure	Self-healing efficiency	System configuration	Printing conditions	Geometrical dimensions	Complex structure healing [Y/N]	Application	Ref.
Living chloroplasts, glucose, isophorone diisocyanate (IPDI), dimethylacetamide (DMAc)	Urethane bond	4h illumination + 4 h darkness white light 69.3 mW cm <sup>-2</sup>	≈70% (tensile stress)	Hydrogel, hybrid composite, chemical network with chloroplast embedded for glucose release	75–400 μm s <sup>-1</sup> curing coefficient, 405 nm UV light	3D	Y	Self-remodeling	[273]
Polycaprolactone diol (PCL-D), N,N'-diisopropylethylenediamine (DPEA), 2-isocyanatoethyl acrylate (ICA), isophorone diisocyanate (IPDI) 2-phenoxyethyl acrylate (PEA), isobornyl acrylate (IBOA)	Urea bond	2 h @ 160 °C	≈99% (tensile modulus) ≈89% (tensile strain)	Covalent network containing dynamic covalent bonds	180 s irradiation white light 50 mW cm <sup>-2</sup>	3D	Y	Modular tunable devices	[274]

## 7. Conclusions and Future Perspectives

In the past decade, additive manufacturing technologies have quickly evolved from prototyping or hobby into advanced manufacturing systems for the fabrication of highly complex structures. Nowadays, 3D printing is an effective tool to prompt innovative research directions in many fields that are not achievable with conventional manufacturing methods. However, objects fabricated via AM have a limited lifetime, and their geometrically intricate structures complicate their repair by external intervention after a failure, forcing a complete replacement of the object. Therefore, materials able to autonomously reestablish the connection in the structure interrupted by the damage are fundamental for the evolution of this technology. Self-healing materials were first developed as planar coating materials, thus not directly influencing bulk properties, and when formed into massive components, their shape was limited to simple geometries, given their incompatibility with subtractive techniques. The combination between AM and SH enables further expansion of the potential applications, because the fine control over material position allows tuning the properties locally, especially where there is a higher probability of failure. Among the possible mechanisms, materials with intrinsic SH are more suitable to be used in 3D printing than with extrinsic SH because they can adapt to numerous matrices and many conditions. At the same time, they greatly benefit from AM because of their adaptable nature, which enables high chain mobility for efficient restoration but low mechanical strength. Polymer systems must be designed accurately to allow both printability and repairability, which is not trivial, as outlined in this review. The interdependent relationship between these requirements is fundamental for a successful fabrication and for achieving suitable SH performances in the printed part. Self-healing is also beneficial for the printing process itself because it helps to reduce the impact of printing errors and defects created after fabrication, as well as to reduce the mechanical anisotropy by increasing layers adhesion.

The presented review shows that a large variety of self-healable polymers, elastomers, and hydrogels have been obtained mainly by extrusion-based 3D printing and vat photopolymerization, which are highly versatile techniques that enable the fabrication of a wide variety of materials. Extrusion-based printing allows preformed materials to be processed with shear thinning behavior, while vat photopolymerization relies on liquid precursors, permitting precise printed constructs with intricate structures and self-standing architectures. Several SH chemistries have been successfully exploited, some of which were proven to be compatible with distinct printing techniques. However, it is challenging to compare restoration performances among various systems due to the different geometries of the tested specimen and the different testing procedures adopted to assess SH.

Tables 3–6 summarize characteristics of the systems here reviewed, including details regarding the healing mechanism and assessment, the system configuration and printing conditions, whether or not self-healing has been shown on printed samples with complex structure and the final applications, if demonstrated.

The most explored group of 3D printable SH materials are hydrogels, which find wide application in the biomedical field, especially in regenerative medicine.<sup>[187,302]</sup> These materials enable

**Table 6.** Healing mechanism characteristics, system characteristics, printing condition and results, and application of vat photopolymerization-based printed systems with non-covalent interactions-based self-healing mechanisms.

Material	Healing mechanism	Healing procedure	Self-healing efficiency	System configuration	Printing Conditions	Geometrical dimensions	Complex structure healing [Y/N]	Application	Ref.
Poly( $\epsilon$ -caprolactone) dimethacrylate (PCLDMA), methacrylated 2-ureido-4[1H]-pyrimidinone (UPyMA)	Hydrogen Bonding	1 h @ 80 °C	$\approx 51.7 - 53.6\%$ (tensile stress)	Covalent network containing crystalline domain	45 °C, 100 $\mu\text{m}$ layers, 20 s exposure per layer 260–410 nm broad UV light 0.8 mW $\text{cm}^{-2}$	2D	N	Shape memory	[277]
N-Acryloylmorpholine (ACMO), Carboxyl Multi-Walled Carbon Nanotubes (c-CNTs), BYK	Hydrogen Bonding	10 min @ RT contact under mild pressure ( $\sim 14$ Kpa)	$\approx 96.5\%$ (tensile modulus)	Composite, elastomer	25 $\mu\text{m}$ layers, 405 nm UV light, 450 mJ $\text{cm}^{-2}$	3D	N	Sensors	[278]
Tannic acid (TA), choline chloride (ChCl), hydroxyethyl methacrylate (HEMA)	Hydrogen Bonding	12 h @ 80 °C	$\approx 73.6\%$ (tensile stress) $\approx 85.2\%$ (tensile modulus)	Deep eutectic solvent	50 $\mu\text{m}$ layers, 15 s exposure per layer 405 nm UV light, 3 mW $\text{cm}^{-2}$	3D	N	—	[279]
Acrylic Acid (AAc), butyl acrylate (BA)	Hydrogen Bonding	12 h @ RT	$\approx 99\%$ (tensile stress) $\approx 99\%$ (tensile strain)	Elastomer	90 s exposure per layer	3D	Y	Remoldability, sensors	[280]
Acrylic Acid (AAc), poly(ethylene glycol) diacrylate (PEGDA), poly(vinyl alcohol) (PVA)	Hydrogen Bonding	12 h @ RT sealed environment	$\approx 72\%$ (tensile stress)	Hydrogel, semi-interpenetrated network	200 $\mu\text{m}$ layers, 5 s exposure per layer 385 nm UV light, 2.1 mW $\text{cm}^{-2}$	3D	Y	—	[281]
Amino-modified polysiloxane (PDMS-NH <sub>2</sub> ) and carboxyl-modified polysiloxane (PDMS-COOH), thiol-modified polysiloxane (PDMS-SH), vinyl-terminated polysiloxane (PDMS-VI)	Hydrogen Bonding	24 h @ 100 °C	$\approx 98\%$ (tensile stress)	Elastomer, physical-chemical dual network	495 nm 250 mW laser	2D	N	Remoldability	[282]
Urethane monoacrylate (UMA), acrylic acid (AAc), zinc dimethacrylate (ZDMA)	Metal-ligand coordination	12 h @ 90 °C	$\approx 100\%$ (tensile stress)	Tailorable physical network	100 $\mu\text{m}$ layers, 10–20 s exposure per layer 445 nm UV light, 10 mW $\text{cm}^{-2}$	3D	Y	Remoldability, modular tunable devices, substrate for functional devices	[283]

(Continued)

**Table 6.** (Continued).

Material	Healing mechanism	Healing procedure	Self-healing efficiency	System configuration	Printing Conditions	Geometrical dimensions	Complex structure healing [Y/N]	Application	Ref.
Poly(ethylene glycol) diacrylate (PEGDA), poly(acrylic acid) (PAA), Iron (II) Chloride	Metal-ligand coordination	immersion in 0.1 M FeCl <sub>3</sub> in 1x PBS for 60 min	≈80% (tensile stress)	Hydrogel, semi-interpenetrated network	350 μm layers, 355 nm 60 W laser, 46 mJ cm <sup>-2</sup>	3D	Y	Modular devices, microfluidics	[284]
4-acryloylmorpholine (ACMO), acrylic acid (AAc), Iron (III) chloride, aluminum sulfate octadecahydrate	Metal-ligand coordination	30 s 0.1 M Al <sub>2</sub> (SO <sub>4</sub> ) <sub>3</sub> solution at the interface. Swelling in 0.1 M Al <sub>2</sub> (SO <sub>4</sub> ) <sub>3</sub> solution for 24h	≈90% (tensile stress)	Swollen drygel, physical network	100 μm layers, 8 s exposure per layer broad white light, 3 mW cm <sup>-2</sup>	2.5D	N	Modular swellable devices	[285]
Acrylic acid (AAc)-N-vinyl-2-pyrrolidone (NVP) and carboxymethylcellulose (CMC)	Metal-ligand coordination	24 h @ 25 °C	≈81% (tensile stress) ≈91% (tensile strain)	Hydrogel, interpenetrated physical networks	50 μm layers, 15 s exposure per layer 405 nm UV light, 40 W	3D	N	Sensors	[287]
Poly(caprolactone) PCL, poly(ethylene glycol) dimethacrylate (PEGDMA) and benzyl methacrylate (BMA)	Molecular interdiffusion	30 min @ 80 °C	> 90% (shear stress)	Semi-interpenetrated network	50 μm layers, 35 s exposure per layer 120 lumen	3D	Y	Shape memory, actuator	[288]



to attain constructs similar to natural tissues intended to be replaced or modeled thanks to their ability to become scaffolds for cell encapsulation, capable of mimicking living tissues features and properties, and reproduce the hierarchical organization and heterogeneity of organs.<sup>[174]</sup> This is a rapidly growing multidisciplinary field called bioprinting, aimed at combining engineering principles and life sciences to develop on-demand products highly customized for the patient.<sup>[194]</sup> This technology can go beyond this envisioned role by providing advantages in therapeutic delivery, surgical planning, implant design, and organ modeling for simulation purposes.<sup>[303]</sup> SH could further boost these studies, mimicking living tissues, enabling more complex in vitro studies, and ultimately advancing prostheses.

SH 3D-printed materials have also attracted growing interest in outside healthcare thanks to the potential application of both soft and rigid materials in a wide range of technologies, from sensors to robotics and energy harvesting.<sup>[304–308]</sup> In this context, adaptation of novel chemistries can be interesting, as for instance the recently reported use of photo-RAFT.<sup>[309]</sup> Alternatively, the use of suitable fillers can induce electronic properties and SH, helping in the control of polymerization times and 3D printing resolution.<sup>[310,311]</sup> A further improvement in the field could arise from the combination between SH and shape memory ability.<sup>[312]</sup> In fact, the ability not only to restore the initial properties, but also the initial shape after damage and/or as a response to a controlled stimulus would be key achievement for a completely autonomous restoration.<sup>[313]</sup> These materials can be combined with on-purpose design for a predictable response to achieve 4D printing, which enables the fabrication of dynamic adjustable architectures consisting of programmable parts.<sup>[171]</sup> To the best of our knowledge, there are currently no special AM techniques for 4D printing, which must be properly designed to best exploit the characteristics of smart materials.<sup>[314]</sup> Therefore, as the field of SH 3D-printed materials moves towards other dimensional scales by expanding to other printing techniques, from volumetric printing and material jetting to microstereolithography or two-photon polymerization, materials and technologies should be co-designed to provide new strategies with higher performance.<sup>[315,316]</sup>

Eventually, since the main advantage of SH is to extend the lifetime of printed parts, further considerations can be made to prolong the life of materials well beyond the end-of-life of the object, given the intrinsic limitations posed by thermosetting materials that are irreversibly cross-linked.<sup>[317]</sup> In this frame, it would be of particular interest to implement 3D printing of commodity polymers, modified to add SH ability, which can be fully exploited in extrusion 3D printing.<sup>[27,28]</sup> Furthermore, there is a growing effort to apply the knowledge developed on synthetic materials to natural-based ones. Natural source, self-healing, recyclability, and degradability by design are key concepts to meet the recent demand to realize a sustainable society because these functions would reduce waste and produce less hazardous residuals able to be reused or easily disposed.<sup>[318,319]</sup> The transition towards polymerization mechanisms totally based on dynamic chemistries that could intrinsically provide printability and repairability would address some of the environmental issues arising from unprocessed thermosets produced by the already established 3D printing, increasing the sustainability of these technologies.<sup>[320,321]</sup>

## Acknowledgements

This work was supported by Compagnia di San Paolo through the funding scheme “Joint Project with Top Universities”, by the National Research Foundation, Prime Minister’s Office, Singapore, under its Campus of Research Excellence and Technological Enterprise (CREATE), SGSR program, and within MICS (Made in Italy – Circular and Sustainable) Extended Partnership and received funding from the European Union Next-GenerationEU (PIANO NAZIONALE DI RIPRESA E RESILIENZA (PNRR) – MISSIONE 4 COMPONENTE 2, INVESTIMENTO 1.3 – D.D. 1551.11-10-2022, PE00000004). This manuscript reflects only the authors’ views and opinions, neither the European Union nor the European Commission can be considered responsible for them.

Open access funding provided by Università degli Studi di Bologna within the CRUI-CARE Agreement.

## Conflict of Interest

The authors declare no conflict of interest.

## Keywords

3D printing, dynamic bonds, polymer, self-healing

Received: June 9, 2023

Revised: September 11, 2023

Published online: December 7, 2023

- [1] N. Jones, *Nature* **2012**, *487*, 22.
- [2] W. Gao, Y. Zhang, D. Ramanujan, K. Ramani, Y. Chen, C. B. Williams, C. C. L. Wang, Y. C. Shin, S. Zhang, P. D. Zavattieri, *CAD Computer Aided Design* **2015**, *69*, 65.
- [3] A. Bhatia, A. K. Sehgal, *Mater. Today Proc.* **2021**, *81*, 1060.
- [4] B. Berman, *Bus Horiz* **2012**, *55*, 155.
- [5] S. C. Ligon, R. Liska, J. Stampfl, M. Gurr, R. Mülhaupt, *Chem. Rev.* **2017**, *117*, 10212.
- [6] A. J. Boydston, B. Cao, A. Nelson, R. J. Ono, A. Saha, J. J. Schwartz, C. J. Thrasher, *J. Mater. Chem. A Mater.* **2018**, *6*, 20621.
- [7] S. Tibbitts, *Architectural Design* **2014**, *84*, 116.
- [8] R. T. Shafraanek, S. C. Millik, P. T. Smith, C.-U. Lee, A. J. Boydston, A. Nelson, *Prog. Polym. Sci.* **2019**, *93*, 36.
- [9] A. J. R. Amaral, G. Pasparakis, *Polym. Chem.* **2017**, *8*, 6464.
- [10] M. Nadgorny, A. Ameli, *ACS Appl. Mater. Interfaces* **2018**, *10*, 17489.
- [11] B. J. Blaiszik, S. L. B. Kramer, S. C. Olugebefola, J. S. Moore, N. R. Sottos, S. R. White, *Annu. Rev. Mater. Res.* **2010**, *40*, 179.
- [12] E. B. Murphy, F. Wudl, *Progress in Polymer Science (Oxford)* **2010**, *35*, 223.
- [13] S. Utrera-Barrios, R. Verdejo, M. A. López-Manchado, M. Hernández Santana, *Mater. Horiz.* **2020**, *7*, 2882.
- [14] I. P. S. Qamar, N. R. Sottos, R. S. Trask, *Multifunctional Materials* **2019**, *3*, 013001.
- [15] J. Dahlke, S. Zechel, M. D. Hager, U. S. Schubert, *Adv. Mater. Interfaces* **2018**, *5*, 1800051.
- [16] A. Campanella, D. Döhler, W. H. Binder, *Macromol. Rapid Commun.* **2018**, *39*, 1700739.
- [17] S. Y. An, D. Arunbabu, S. M. Noh, Y. K. Song, J. K. Oh, *Chem. Commun.* **2015**, *51*, 13058.
- [18] B. Gyarmati, B. Á. Szilágyi, A. Szilágyi, *Eur. Polym. J.* **2017**, *93*, 642.
- [19] K. Urdl, A. Kandelbauer, W. Kern, U. Müller, M. Thebault, E. Zikulnig-Rusch, *Prog. Org. Coat.* **2017**, *104*, 232.

- [20] N. Zhong, W. Post, *Compos Part A Appl. Sci. Manuf.* **2015**, 69, 226.
- [21] D. L. Taylor, M. In Het Panhuis, M. in het Panhuis, *Adv. Mater.* **2016**, 28, 9060.
- [22] A. Phadke, C. Zhang, B. Arman, C.-C. Hsu, R. A. Mashelkar, A. K. Lele, M. J. Tauber, G. Arya, S. Varghese, *Proc. Natl. Acad. Sci. U S A* **2012**, 109, 4383.
- [23] Y. Bai, Q. Zhang, J. Sun, K. Lv, X. Shang, C. Liu, R. Cheng, F. Wang, *J. Nat. Gas. Sci. Eng.* **2021**, 96, 104250.
- [24] Z. Wang, L. Scheres, H. Xia, H. Zuillhof, *Adv. Funct. Mater.* **2020**, 30, 1908098.
- [25] F. Herbst, D. Döhler, P. Michael, W. H. Binder, *Macromol. Rapid Commun.* **2013**, 34, 203.
- [26] M. Röttger, T. Domenech, R. Van Der Weegen, A. Breuillac, R. Nicolaÿ, L. Leibler, *Science (1979)* **2017**, 356, 62.
- [27] H. Wang, H. Liu, Z. Cao, W. Li, X. Huang, Y. Zhu, F. Ling, H. Xu, Q. Wu, Y. Peng, B. Yang, R. Zhang, O. Kessler, G. Huang, J. Wu, *Proc. Natl. Acad. Sci. U S A* **2020**, 117, 11299.
- [28] J. Xu, J. Chen, Y. Zhang, T. Liu, J. Fu, *Angewandte Chemie – International Edition* **2021**, 60, 7947.
- [29] S. Wang, M. W. Urban, *Nat. Rev. Mater.* **2020**, 5, 562.
- [30] S. Talebian, M. Mehrali, N. Taebnia, C. P. Pennisi, F. B. Kadumudi, J. Foroughi, M. Hasany, M. Nikkiah, M. Akbari, G. Orive, A. Dolatshahi-Pirouz, *Adv. Sci.* **2019**, 6, 1801664.
- [31] M. K. McBride, B. T. Worrell, T. Brown, L. M. Cox, N. Sowan, C. Wang, M. Podgorski, A. M. Martinez, C. N. Bowman, *Annu. Rev. Chem. Biomol. Eng.* **2019**, 10, 175.
- [32] H. Wang, H. Wang, Z. Wang, L. Tang, G. Zeng, P. Xu, M. Chen, T. Xiong, C. Zhou, X. Li, D. Huang, Y. Zhu, Z. Wang, J. Tang, *Chem. Soc. Rev.* **2020**, 49, 4135.
- [33] G. Deng, F. Li, H. Yu, F. Liu, C. Liu, W. Sun, H. Jiang, Y. Chen, *ACS Macro Lett.* **2012**, 1, 275.
- [34] J. Xu, Y. Liu, S.-H. Hsu, *Molecules* **2019**, 24, 3005.
- [35] Z. Wei, J. H. Yang, J. Zhou, F. Xu, M. Zrinyi, P. H. Dussault, Y. Osada, Y. M. Chen, *Chem. Soc. Rev.* **2014**, 43, 8114.
- [36] H. Wang, S. C. Heilshorn, *Adv. Mater.* **2015**, 27, 3717.
- [37] N. Kuhl, M. Abend, S. Bode, U. S. Schubert, M. D. Hager, *J. Appl. Polym. Sci.* **2016**, 133, 44168.
- [38] G. N. Grover, J. Lam, T. H. Nguyen, T. Segura, H. D. Maynard, *Biomacromolecules* **2012**, 13, 3013.
- [39] A. Dirksen, S. Yegneswaran, P. E. Dawson, *Angewandte Chemie – International Edition* **2010**, 49, 2023.
- [40] Y. Tu, N. Chen, C. Li, H. Liu, R. Zhu, S. Chen, Q. Xiao, J. Liu, S. Ramakrishna, L. He, *Acta Biomater.* **2019**, 90, 1.
- [41] D. D. McKinnon, D. W. Dommelle, J. N. Cha, K. S. Anseth, *Chem. Mater.* **2014**, 26, 2382.
- [42] H. Ying, Y. Zhang, J. Cheng, *Nat. Commun.* **2014**, 5, 3218.
- [43] N. Zheng, Y. Xu, Q. Zhao, T. Xie, *Chem. Rev.* **2021**, 121, 1716.
- [44] Y. Zhang, H. Ying, K. R. Hart, Y. Wu, A. J. Hsu, A. M. Coppola, T. A. Kim, K. Yang, N. R. Sottos, S. R. White, J. Cheng, *Adv. Mater.* **2016**, 28, 7646.
- [45] J. P. M. António, R. Russo, C. P. Carvalho, P. M. S. D. Cal, P. M. P. Gois, *Chem. Soc. Rev.* **2019**, 48, 3513.
- [46] M. Zhu, J. Liu, L. Gan, M. Long, *Eur. Polym. J.* **2020**, 129, 109651.
- [47] J. Yan, G. Springsteen, S. Deeter, B. Wang, *Tetrahedron* **2004**, 60, 11205.
- [48] V. Yesilyurt, M. J. Webber, E. A. Appel, C. Godwin, R. Langer, D. G. Anderson, *Adv. Mater.* **2016**, 28, 86.
- [49] O. R. Cromwell, J. Chung, Z. Guan, *J. Am. Chem. Soc.* **2015**, 137, 6492.
- [50] Z. P. Zhang, M. Z. Rong, M. Q. Zhang, *Prog. Polym. Sci.* **2018**, 80, 39.
- [51] B. Wang, Y. S. Jeon, H. S. Park, J.-H. Kim, *Materials Science and Engineering C* **2016**, 69, 160.
- [52] Y. Dong, W. Wang, O. Veisoh, E. A. Appel, K. Xue, M. J. Webber, B. C. Tang, X.-W. Yang, G. C. Weir, R. Langer, D. G. Anderson, *Langmuir* **2016**, 32, 8743.
- [53] P. A. Fernandes, M. J. Ramos, *Chemistry* **2004**, 10, 257.
- [54] J. Canadell, H. Goossens, B. Klumperman, *Macromolecules* **2011**, 44, 2536.
- [55] M. Pepels, I. Filot, B. Klumperman, H. Goossens, *Polym. Chem.* **2013**, 4, 4955.
- [56] Y. Sun, Y. Huang, *J. Mater. Chem. B* **2016**, 4, 2768.
- [57] D. Bermejo-Velasco, A. Azémar, O. P. Oommen, J. Hilborn, O. P. Varghese, *Biomacromolecules* **2019**, 20, 1412.
- [58] B. Mandal, B. Basu, *RSC Adv.* **2014**, 4, 13854.
- [59] M. Patenaude, N. M. B. Smeets, T. Hoare, *Macromol. Rapid Commun.* **2014**, 35, 598.
- [60] P. Casuso, I. Odriozola, A. Pérez-San Vicente, I. Loinaz, G. Cabañero, H.-J. Grande, D. Dupin, *Biomacromolecules* **2015**, 16, 3552.
- [61] K. Chang, H. Jia, S.-Y. Gu, *Eur. Polym. J.* **2019**, 112, 822.
- [62] H. Nandivada, X. Jiang, J. Lahann, *Adv. Mater.* **2007**, 19, 2197.
- [63] S. Otto, J. B. F. N. Engberts, *Pure Appl. Chem.* **2000**, 72, 1365.
- [64] G. Scheltjens, M. M. Diaz, J. Brancart, G. Van Assche, B. Van Mele, *React. Funct. Polym.* **2013**, 73, 413.
- [65] Y.-L. Liu, T.-W. Chuo, *Polym. Chem.* **2013**, 4, 2194.
- [66] N. Roy, B. Bruchmann, J.-M. Lehn, *Chem. Soc. Rev.* **2015**, 44, 3786.
- [67] K. C. Koehler, D. L. Alge, K. S. Anseth, C. N. Bowman, *Biomaterials* **2013**, 34, 4150.
- [68] Z. Wei, J. H. Yang, X. J. Du, F. Xu, M. Zrinyi, Y. Osada, F. Li, Y. M. Chen, *Macromol. Rapid Commun.* **2013**, 34, 1464.
- [69] S. Kirchhof, F. P. Brandl, N. Hammer, A. M. Goepferich, *J. Mater. Chem. B* **2013**, 1, 4855.
- [70] C. Cardenas-Daw, A. Kroeger, W. Schaertl, P. Froimowicz, K. Landfester, *Macromol. Chem. Phys.* **2012**, 213, 144.
- [71] D. Habault, H. Zhang, Y. Zhao, *Chem. Soc. Rev.* **2013**, 42, 7244.
- [72] C. A. Murphy, K. S. Lim, T. B. F. Woodfield, *Adv. Mater.* **2022**, 34, 2107759.
- [73] J. Ling, M. Z. Rong, M. Q. Zhang, *Polymer (Guildf)* **2012**, 53, 2691.
- [74] Y. Jin, C. Yu, R. J. Denman, W. Zhang, *Chem. Soc. Rev.* **2013**, 42, 6634.
- [75] W. Zou, J. Dong, Y. Luo, Q. Zhao, T. Xie, *Adv. Mater.* **2017**, 29, 1606100.
- [76] D. Montarnal, M. Capelot, F. Tournilhac, L. Leibler, *Science (1979)* **2011**, 334, 965.
- [77] N. J. Van Zee, R. Nicolaÿ, *Prog. Polym. Sci.* **2020**, 104, 101233.
- [78] W. Denissen, J. M. Winne, F. E. Du Prez, *Chem. Sci.* **2016**, 7, 30.
- [79] Y. Yang, M. W. Urban, *Adv. Mater. Interfaces* **2018**, 5, 1800384.
- [80] S. Seiffert, J. Sprakel, *Chem. Soc. Rev.* **2012**, 41, 909.
- [81] L. M. De Espinosa, G. L. Fiore, C. Weder, E. Johan Foster, Y. C. Simon, *Prog. Polym. Sci.* **2015**, 49-50, 60.
- [82] D. G. Bekas, K. Tsirka, D. Baltzis, A. S. Paipetis, *Compos B Eng.* **2016**, 87, 92.
- [83] E. D. Rodriguez, X. Luo, P. T. Mather, *ACS Appl. Mater. Interfaces* **2011**, 3, 152.
- [84] K. Chen, Y. Feng, Y. Zhang, L. Yu, X. Hao, F. Shao, Z. Dou, C. An, Z. Zhuang, Y. Luo, Y. Wang, J. Wu, P. Ji, T. Chen, H. Wang, *ACS Appl. Mater. Interfaces* **2019**, 11, 36458.
- [85] X. Huang, S. Nakagawa, H. Houjou, N. Yoshie, *Macromolecules* **2021**, 54, 4070.
- [86] T. Steiner, *Acta Crystallogr. B* **2001**, 57, 103.
- [87] G. R. Desiraju, *Acc. Chem. Res.* **2002**, 35, 565.
- [88] P. Michael, D. Döhler, W. H. Binder, *Polymer (Guildf)* **2015**, 69, 216.
- [89] T. Steinel, J. B. Asbury, J. Zheng, M. D. Fayer, *J. Phys. Chem. A* **2004**, 108, 10957.
- [90] E. A. Appel, J. Del Barrio, X. J. Loh, O. A. Scherman, *Chem. Soc. Rev.* **2012**, 41, 6195.
- [91] F. Herbst, D. Döhler, P. Michael, W. H. Binder, *Macromol. Rapid Commun.* **2013**, 34, 203.

- [92] Y. Lin, G. Li, *J. Mater. Chem. B* **2014**, 2, 6878.
- [93] J. Cui, A. del Campo, *Chem. Commun.* **2012**, 48, 9302.
- [94] S. Hou, X. Wang, S. Park, X. Jin, P. X. Ma, *Adv. Healthcare Mater.* **2015**, 4, 1491.
- [95] I. Jeon, J. Cui, W. R. K. Illeperuma, J. Aizenberg, J. J. Vlassak, *Adv. Mater.* **2016**, 28, 4678.
- [96] J. Y. Sun, X. Zhao, W. R. K. Illeperuma, O. Chaudhuri, K. H. Oh, D. J. Mooney, J. J. Vlassak, Z. Suo, *Nature* **2012**, 489, 133.
- [97] M. Guo, L. M. Pitet, H. M. Wyss, M. Vos, P. Y. W. Dankers, E. W. Meijer, *J. Am. Chem. Soc.* **2014**, 136, 6969.
- [98] H. Zhang, H. Xia, Y. Zhao, *ACS Macro Lett.* **2012**, 1, 1233.
- [99] Z. Gong, G. Zhang, X. Zeng, J. Li, G. Li, W. Huang, R. Sun, C. Wong, *ACS Appl. Mater. Interfaces* **2016**, 8, 24030.
- [100] Y. Yan, S. Xu, H. Liu, X. Cui, J. Shao, P. Yao, J. Huang, X. Qiu, C. Huang, *Colloids Surf A Physicochem. Eng. Asp.* **2020**, 593, 124622.
- [101] G. Li, Q. Yan, H. Xia, Y. Zhao, *ACS Appl. Mater. Interfaces* **2015**, 7, 12067.
- [102] G. Li, H. Zhang, D. Fortin, H. Xia, Y. Zhao, *Langmuir* **2015**, 31, 11709.
- [103] X. Lin, M. W. Grinstaff, *Isr. J. Chem.* **2013**, 53, 498.
- [104] M. J. Webber, E. A. Appel, E. W. Meijer, R. Langer, *Nat. Mater.* **2015**, 15, 13.
- [105] S. J. Kalista, T. C. Ward, *J. R. Soc. Interface* **2007**, 4, 405.
- [106] S. J. Kalista, J. R. Pflug, R. J. Varley, *Polym. Chem.* **2013**, 4, 4910.
- [107] N. Y. Abu-Thabit, A. S. Hamdy, *Surf. Coat. Technol.* **2016**, 303, 406.
- [108] T. L. Sun, T. Kurokawa, S. Kuroda, A. bin Ihsan, T. Akasaki, K. Sato, M. A. Haque, T. Nakajima, J. P. Gong, *Nat. Mater.* **2013**, 12, 932.
- [109] X. Fang, J. Sun, *ACS Macro Lett.* **2019**, 8, 500.
- [110] A. B. Lowe, C. L. McCormick, *Chem. Rev.* **2002**, 102, 4177.
- [111] A. Laschewsky, *Polymers (Basel)* **2014**, 6, 1544.
- [112] T. Bai, S. Liu, F. Sun, A. Sinclair, L. Zhang, Q. Shao, S. Jiang, *Biomaterials* **2014**, 35, 3926.
- [113] S. Otto, J. B. F. N. Engberts, *Org. Biomol. Chem.* **2003**, 1, 2809.
- [114] J. R. Khusnutdinova, D. Milstein, *Angewandte Chemie – International Edition* **2015**, 54, 12236.
- [115] L. Shi, P. Ding, Y. Wang, Y. Zhang, D. Ossipov, J. Hilborn, *Macromol. Rapid Commun.* **2019**, 40, 1800837.
- [116] Y. Yang, X. Ding, M. W. Urban, *Prog. Polym. Sci.* **2015**, 49–50, 34.
- [117] A. J. McConnell, C. S. Wood, P. P. Neelakandan, J. R. Nitschke, *Chem. Rev.* **2015**, 115, 7729.
- [118] Q. Li, C. Liu, J. Wen, Y. Wu, Y. Shan, J. Liao, *Chin. Chem. Lett.* **2017**, 28, 1857.
- [119] J.-C. Lai, X.-Y. Jia, D.-P. Wang, Y.-B. Deng, P. Zheng, C.-H. Li, J.-L. Zuo, Z. Bao, *Nat. Commun.* **2019**, 10, 1164.
- [120] M. J. Harrington, A. Masic, N. Holten-Andersen, J. H. Waite, P. Fratzl, *Science (1979)* **2010**, 328, 216.
- [121] P. S. Yavvari, A. Srivastava, *J. Mater. Chem. B* **2015**, 3, 899.
- [122] Z. Wei, J. He, T. Liang, H. Oh, J. Athas, Z. Tong, C. Wang, Z. Nie, *Polym. Chem.* **2013**, 4, 4601.
- [123] Q. Zheng, L. Zhao, J. Wang, S. Wang, Y. Liu, X. Liu, *Colloids Surf A Physicochem. Eng. Asp.* **2020**, 589, 124402.
- [124] H. Jiang, L. Duan, X. Ren, G. Gao, *Eur. Polym. J.* **2019**, 112, 660.
- [125] D. C. Tuncaboylu, M. Sari, W. Oppermann, O. Okay, *Macromolecules* **2011**, 44, 4997.
- [126] O. Okay, *J. Mater. Chem. B* **2019**, 7, 1581.
- [127] D. C. Tuncaboylu, A. Argun, M. Sahin, M. Sari, O. Okay, *Polymer (Guildf)* **2012**, 53, 5513.
- [128] O. Okay, in *Advances in Polymer Science*, Springer, Cham **2020**, pp. 21–62.
- [129] J. Jin, L. Cai, Y. G. Jia, S. Liu, Y. Chen, L. Ren, *J. Mater. Chem. B* **2019**, 7, 1637.
- [130] M. Diba, S. Spaans, K. Ning, B. D. Ippel, F. Yang, B. Loomans, P. Y. W. Dankers, S. C. G. Leeuwenburgh, *Adv. Mater. Interfaces* **2018**, 5, 1.
- [131] J. Li, A. Harada, M. Kamachi, *Polym. J.* **1994**, 26, 1019.
- [132] A. Harada, M. Okada, J. Li, M. Kamachi, *Macromolecules* **1995**, 28, 8406.
- [133] A. Harada, Y. Kawaguchi, T. Nishiyama, M. Kamachi, *Macromol. Rapid Commun.* **1997**, 18, 535.
- [134] D.-E. Liu, Q. Chen, Y.-B. Long, J. Ma, H. Gao, *Polym. Chem.* **2018**, 9, 228.
- [135] B. V. K. J. Schmidt, C. Barner-Kowollik, *Angewandte Chemie – International Edition* **2017**, 56, 8350.
- [136] S. Strandman, X. X. Zhu, *Gels* **2016**, 2, 16.
- [137] C. B. Rodell, J. W. Macarthur, S. M. Dorsey, R. J. Wade, L. L. Wang, Y. J. Woo, J. A. Burdick, *Adv. Funct. Mater.* **2015**, 25, 636.
- [138] H.-J. Schneider, A. K. Yatsimirsky, *Chem. Soc. Rev.* **2008**, 37, 263.
- [139] M. Nakahata, Y. Takashima, A. Harada, *Macromol. Rapid Commun.* **2016**, 37, 86.
- [140] X. Yang, H. Yu, L. Wang, R. Tong, M. Akram, Y. Chen, X. Zhai, *Soft Matter* **2015**, 11, 1242.
- [141] K. L. Liu, Z. Zhang, J. Li, *Soft Matter* **2011**, 7, 11290.
- [142] G. Yu, K. Jie, F. Huang, *Chem. Rev.* **2015**, 115, 7240.
- [143] Z. Wang, Y. Ren, Y. Zhu, L. Hao, Y. Chen, G. An, H. Wu, X. Shi, C. Mao, *Angewandte Chemie – International Edition* **2018**, 57, 9008.
- [144] C. Xiong, L. Zhang, M. Xie, R. Sun, *Macromol. Rapid Commun.* **2018**, 39, 1800018.
- [145] M. Hetzer, C. Fleischmann, B. V. K. J. Schmidt, C. Barner-Kowollik, H. Ritter, *Polymer (Guildf)* **2013**, 54, 5141.
- [146] M. Nakahata, Y. Takashima, H. Yamaguchi, A. Harada, *Nat. Commun.* **2011**, 2, 511.
- [147] L. Cai, S. Liu, J. Guo, Y.-G. Jia, *Acta Biomater.* **2020**, 113, 84.
- [148] S. Uman, A. Dhand, J. A. Burdick, *J. Appl. Polym. Sci.* **2020**, 137, 48668.
- [149] G. Fichman, E. Gazit, *Acta Biomater.* **2014**, 10, 1671.
- [150] A. P. Nowak, V. Breedveld, L. Pakstis, B. Ozbaz, D. J. Pine, D. Pochan, T. J. Deming, *Nature* **2002**, 417, 424.
- [151] M. Ikeda, T. Tanida, T. Yoshii, K. Kurotani, S. Onogi, K. Urayama, I. Hamachi, *Nat. Chem.* **2014**, 6, 511.
- [152] M. D. Golinska, M. K. Włodarczyk-Biegun, M. W. T. Werten, M. A. C. Stuart, F. A. De Wolf, R. De Vries, *Biomacromolecules* **2014**, 15, 699.
- [153] D. E. Clarke, E. T. Pashuck, S. Bertazzo, J. V. M. Weaver, M. M. Stevens, *J. Am. Chem. Soc.* **2017**, 139, 7250.
- [154] A. K. Gaharwar, N. A. Peppas, A. Khademhosseini, *Biotechnol. Bioeng.* **2014**, 111, 441.
- [155] N. Y. Kostina, S. Sharifi, A. De Los Santos Pereira, J. Michálek, D. W. Grijpma, C. Rodriguez-Emmenegger, *J. Mater. Chem. B* **2013**, 1, 5644.
- [156] V. K. Thakur, M. R. Kessler, *Polymer (Guildf)* **2015**, 69, 369.
- [157] Y.-Z. Zhang, K. H. Lee, D. H. Anjum, R. Sougrat, Q. Jiang, H. Kim, H. N. Alshareef, *Sci. Adv.* **2018**, 4, eaat0098.
- [158] G. Thangavel, M. W. M. Tan, P. S. Lee, *Nano Converge* **2019**, 6, 29.
- [159] L. J. Macdougall, M. M. Pérez-Madrigal, J. E. Shaw, M. Inam, J. A. Hoyland, R. O'reilly, S. M. Richardson, A. P. Dove, *Biomater. Sci.* **2018**, 6, 2932.
- [160] J. Brancart, G. Scheltjens, T. Muselle, B. Van Mele, H. Terryn, G. Van Assche, *Intell. Mater. Syst. Struct.* **2014**, 25, 40.
- [161] S. Pati, B. P. Singh, S. R. Dhakate, in *Smart Polymer Nanocomposites* (Eds.: D. Ponnamm, K. K. Sadasivuni, J.-J. Cabibihan, M. A.-A. Al-Maadeed), Springer International Publishing, Cham, **2017**, pp. 119–152.
- [162] K. Haraguchi, K. Uyama, H. Tanimoto, *Macromol. Rapid Commun.* **2011**, 32, 1253.
- [163] K. Parida, G. Thangavel, G. Cai, X. Zhou, S. Park, J. Xiong, P. S. Lee, *Nat. Commun.* **2019**, 10, 2158.
- [164] M. Gharakhloo, M. Karbarz, *Eur. Polym. J.* **2022**, 165, 111004.
- [165] Z.-X. Low, Y. T. Chua, B. M. Ray, D. Mattia, I. S. Metcalfe, D. A. Patterson, *J. Memb. Sci.* **2017**, 523, 596.
- [166] J.-Y. Lee, J. An, C. K. Chua, *Appl. Mater. Today* **2017**, 7, 120.



- [167] Y. Dong, S. Wang, Y. Ke, L. Ding, X. Zeng, S. Magdassi, Y. Long, *Adv. Mater. Technol.* **2020**, 5, 1.
- [168] S. Pollack, C. Venkatesh, M. Neff, A. V. Healy, G. Hu, E. A. Fuenmayor, J. G. Lyons, I. Major, D. M. Devine, in *Polymer-Based Additive Manufacturing*, Springer International Publishing, Cham, **2019**, pp. 1-22.
- [169] M. Rafiee, R. D. Farahani, D. Therriault, *Adv. Sci.* **2020**, 7, 1902307.
- [170] D. Han, H. Lee, *Curr. Opin. Chem. Eng.* **2020**, 28, 158.
- [171] C. M. González-Henríquez, M. A. Sarabia-Vallejos, J. Rodríguez-Hernández, *Prog. Polym. Sci.* **2019**, 94, 57.
- [172] L.-Y. Zhou, J. Fu, Y. He, *Adv. Funct. Mater.* **2020**, 30, 2000187.
- [173] M. L. Bedell, A. M. Navara, Y. Du, S. Zhang, A. G. Mikos, *Chem. Rev.* **2020**, 120, 10744.
- [174] A. Schwab, R. Levato, M. D'este, S. Piluso, D. Eglín, J. Malda, *Chem. Rev.* **2020**, 120, 11028.
- [175] K. Jung, N. Corrigan, M. Ciftci, J. Xu, S. E. Seo, C. J. Hawker, C. Boyer, *Adv. Mater.* **2020**, 32, 1.
- [176] Y. Bao, *Macromol. Rapid Commun.* **2022**, 43, 2200202.
- [177] W. Tomal, J. Ortyl, *Polymers (Basel)* **2020**, 12, 1.
- [178] G. A. Appuhamillage, N. Chartrain, V. Meenakshisundaram, K. D. Feller, C. B. Williams, T. E. Long, *Ind. Eng. Chem. Res.* **2019**, 58, 15109.
- [179] A. Bagheri, J. Jin, *ACS Appl. Polym. Mater.* **2019**, 1, 593.
- [180] S. C. Ligon-Auer, M. Schwentenwein, C. Gorsche, J. Stampfl, R. Liska, *Polym. Chem.* **2016**, 7, 257.
- [181] C. Yu, J. Schimelman, P. Wang, K. L. Miller, X. Ma, S. You, J. Guan, B. Sun, W. Zhu, S. Chen, *Chem. Rev.* **2020**, 120, 10695.
- [182] M. Pagac, J. Hajnys, Q.-P. Ma, L. Jancar, J. Jansa, P. Stefek, J. Mesicek, *Polymers (Basel)* **2021**, 13, 598.
- [183] J. R. Tumbleston, D. Shirvanyants, N. Ermoshkin, R. Januszewicz, A. R. Johnson, D. Kelly, K. Chen, R. Pinschmidt, J. P. Rolland, A. Ermoshkin, E. T. Samulski, J. M. Desimone, *Science (1979)* **2015**, 347, 1349.
- [184] B. E. Kelly, I. Bhattacharya, H. Heidari, M. Shusteff, C. M. Spadaccini, H. K. Taylor, *Science (1979)* **2019**, 363, 1075.
- [185] G. Gillispie, P. Prim, J. Copus, J. Fisher, A. G. Mikos, J. J. Yoo, A. Atala, S. J. Lee, *Biofabrication* **2020**, 12, 022003.
- [186] A. M. Pekkanen, R. J. Mondschein, C. B. Williams, T. E. Long, *Biomacromolecules* **2017**, 18, 2669.
- [187] R. L. Truby, J. A. Lewis, *Nature* **2016**, 540, 371.
- [188] E. S. Dragan, *Chem. Eng. J.* **2014**, 243, 572.
- [189] D. Chimene, R. Kaunas, A. K. Gaharwar, *Adv. Mater.* **2020**, 32, 1902026.
- [190] J. Li, C. Wu, P. K. Chu, M. Gelinsky, *Materials Science and Engineering R: Reports* **2020**, 140, 100543.
- [191] T. Jungst, W. Smolan, K. Schacht, T. Scheibel, J. Groll, *Chem. Rev.* **2016**, 116, 1496.
- [192] P. Heidarian, A. Z. Kouzani, A. Kaynak, M. Paulino, B. Nasri-Nasrabadi, *ACS Biomater. Sci. Eng.* **2019**, 5, 2688.
- [193] X. Zhao, *Soft Matter* **2014**, 10, 672.
- [194] R. Levato, T. Jungst, R. G. Scheuring, T. Blunk, J. Groll, J. Malda, *Adv. Mater.* **2020**, 32, 1906423.
- [195] M. Champeau, D. A. Heinze, T. N. Viana, E. R. De Souza, A. C. Chinellato, S. Titotto, *Adv. Funct. Mater.* **2020**, 30, 1910606.
- [196] J. H. Kim, J. J. Yoo, S. J. Lee, *Tissue Eng. Regen. Med.* **2016**, 13, 647.
- [197] M. Lee, R. Rizzo, F. Surman, M. Zenobi-Wong, *Chem. Rev.* **2020**, 120, 10950.
- [198] S. Kyle, Z. M. Jessop, A. Al-Sabah, I. S. Whitaker, *Adv. Healthcare Mater.* **2017**, 6, 1700264.
- [199] J. J. Cash, T. Kubo, A. P. Bapat, B. S. Sumerlin, *Macromolecules* **2015**, 48, 2098.
- [200] L. J. Tan, W. Zhu, K. Zhou, *Adv. Funct. Mater.* **2020**, 30, 1.
- [201] R. J. Mondschein, A. Kanitkar, C. B. Williams, S. S. Verbridge, T. E. Long, *Biomaterials* **2017**, 140, 170.
- [202] E. M. Wilts, A. M. Pekkanen, B. T. White, V. Meenakshisundaram, D. C. Aduba, C. B. Williams, T. E. Long, *Polym. Chem.* **2019**, 10, 1442.
- [203] K. S. Lim, J. H. Galarraga, X. Cui, G. C. J. Lindberg, J. A. Burdick, T. B. F. Woodfield, *Chem. Rev.* **2020**, 120, 10662.
- [204] L. Valot, J. Martinez, A. Mehdi, G. Subra, *Chem. Soc. Rev.* **2019**, 48, 4049.
- [205] H. Yao, J. Wang, S. Mi, *Polymers (Basel)* **2017**, 10, 11.
- [206] N. A. Chartrain, C. B. Williams, A. R. Whittington, *Acta Biomater.* **2018**, 74, 90.
- [207] D. C. Tuncaboylu, A. Argun, M. P. Algi, O. Okay, *Polymer (Guildf)* **2013**, 54, 6381.
- [208] S. Hong, D. Sycks, H. F. Chan, S. Lin, G. P. Lopez, F. Guilak, K. W. Seong, X. Zhao, *Adv. Mater.* **2015**, 27, 4035.
- [209] Q. Liu, Q. Li, S. Xu, Q. Zheng, X. Cao, *Polymers (Basel)* **2018**, 10, 664.
- [210] T. Zehnder, B. Sarker, A. R. Boccaccini, R. Detsch, *Biofabrication* **2015**, 7, 025001.
- [211] C. P. Kabb, C. S. O'bryan, C. C. Deng, T. E. Angelini, B. S. Sumerlin, *ACS Appl. Mater. Interfaces* **2018**, 10, 16793.
- [212] J.-H. Shim, K.-M. Jang, S. K. Hahn, J. Y. Park, H. Jung, K. Oh, K. M. Park, J. Yeom, S. H. Park, S. W. Kim, J. H. Wang, K. Kim, D.-W. Cho, *Biofabrication* **2016**, 8, 014102.
- [213] F. Zhu, L. Cheng, J. Yin, Z. L. Wu, J. Qian, J. Fu, Q. Zheng, *ACS Appl. Mater. Interfaces* **2016**, 8, 31304.
- [214] T. Zhao, R. Yu, S. Li, X. Li, Y. Zhang, X. Yang, X. Zhao, C. Wang, Z. Liu, R. Dou, W. Huang, *ACS Appl. Mater. Interfaces* **2019**, 11, 14391.
- [215] F. Luo, T. L. Sun, T. Nakajima, T. Kurokawa, A. B. Ihsan, X. Li, H. Guo, J. P. Gong, *ACS Macro Lett.* **2015**, 4, 961.
- [216] A. Trejo-Machin, L. Puchot, P. Verge, *Polym. Chem.* **2020**, 11, 7026.
- [217] K. S. Toohey, N. R. Sottos, J. A. Lewis, J. S. Moore, S. R. White, *Nat. Mater.* **2007**, 6, 581.
- [218] C. J. Hansen, W. Wu, K. S. Toohey, N. R. Sottos, S. R. White, J. A. Lewis, *Adv. Mater.* **2009**, 21, 4143.
- [219] Q. Wei, W. Xu, Q. Zhang, S. Zhang, L. Cheng, Q. Wang, *J. Mater. Chem. B* **2017**, 5, 5092.
- [220] M. Nadgorny, Z. Xiao, L. A. Connal, *Mol. Syst. Des. Eng.* **2017**, 2, 283.
- [221] H. Chen, F. Fei, X. Li, Z. Nie, D. Zhou, L. Liu, J. Zhang, H. Zhang, Z. Fei, T. Xu, *Bioact. Mater.* **2021**, 6, 3580.
- [222] P. Heidarian, A. Z. Kouzani, *Carbohydr. Polym.* **2023**, 313, 120879.
- [223] M. Nadgorny, J. Collins, Z. Xiao, P. J. Scales, L. A. Connal, *Polym. Chem.* **2018**, 9, 1684.
- [224] J. Wang, X. Lin, R. Wang, Y. Lu, L. Zhang, *Adv. Funct. Mater.* **2023**, 33, 2211579.
- [225] L. L. Wang, C. B. Highley, Y.-C. Yeh, J. H. Galarraga, S. Uman, J. A. Burdick, *J. Biomed. Mater. Res. A* **2018**, 106, 865.
- [226] S. W. Kim, D. Y. Kim, H. H. Roh, H. S. Kim, J. W. Lee, K. Y. Lee, *Biomacromolecules* **2019**, 20, 1860.
- [227] Y. Choi, C. Kim, H. S. Kim, C. Moon, K. Y. Lee, *Colloids Surf. B Biointerfaces* **2021**, 208, 112108.
- [228] H. S. Kim, K. Y. Lee, *Carbohydr. Polym.* **2022**, 295, 119846.
- [229] H. Chen, P. Wang, C. Zheng, L. Zhang, *ACS Appl. Polym. Mater.* **2022**, 4, 6312.
- [230] J. Wang, S. Hu, B. Yang, G. Jin, X. Zhou, X. Lin, R. Wang, Y. Lu, L. Zhang, *ACS Appl. Mater. Interfaces* **2022**, 14, 1994.
- [231] A. Biswas, S. Malferrari, D. M. Kalaskar, A. K. Das, *Chem. Commun.* **2018**, 54, 1778.
- [232] T. Wu, E. Gray, B. Chen, *J. Mater. Chem. C Mater.* **2018**, 6, 6200.
- [233] W. Zhao, B. Huang, L. Zhu, X. Feng, J. Xu, H. Zhang, S. Yan, *Int. J. Biol. Macromol.* **2022**, 218, 580.
- [234] M. Seong, S. Kondaveeti, G. Choi, S. Kim, J. Kim, M. Kang, H. E. Jeong, *ACS Appl. Mater. Interfaces* **2023**, 15, 11042.
- [235] K. Yang, J. C. Grant, P. Lamey, A. Joshi-Imre, B. R. Lund, R. A. Smaldone, W. Voit, W. Voit, *Adv. Funct. Mater.* **2017**, 27, 1700318.
- [236] J. R. Davidson, G. A. Appuhamillage, C. M. Thompson, W. Voit, R. A. Smaldone, *ACS Appl. Mater. Interfaces* **2016**, 8, 16961.



- [237] G. A. Appuhamillage, J. C. Reagan, S. Khorsandi, J. R. Davidson, W. Voit, R. A. Smaldone, *Polym. Chem.* **2017**, *8*, 2087.
- [238] T. Yuan, L. Zhang, T. Li, R. Tu, H. A. Sodano, *Polym. Chem.* **2020**, *11*, 6441.
- [239] Y. Guo, S. Chen, L. Sun, L. Yang, L. Zhang, J. Lou, Z. You, *Adv. Funct. Mater.* **2021**, *31*, 2009799.
- [240] Y. Zhang, X.-Y. Yin, M. Zheng, C. Moorlag, J. Yang, Z. L. Wang, *J. Mater. Chem. A Mater.* **2019**, *7*, 6972.
- [241] C. B. Highley, C. B. Rodell, J. A. Burdick, *Adv. Mater.* **2015**, *27*, 5075.
- [242] J. Zhao, N. He, *J. Mater. Chem. B* **2020**, *8*, 10474.
- [243] Z. Wang, G. An, Y. Zhu, X. Liu, Y. Chen, H. Wu, Y. Wang, X. Shi, C. Mao, *Mater. Horiz.* **2019**, *6*, 733.
- [244] M. Zhang, A. Vora, W. Han, R. J. Wojtecki, H. Maune, A. B. A. Le, L. E. Thompson, G. M. McClelland, F. Ribet, A. C. Engler, A. Nelson, *Macromolecules* **2015**, *48*, 6482.
- [245] L. Hao, X. Tao, M. Feng, K. Zhou, Y. He, J. Yang, H. Mao, Z. Gu, *ACS Appl. Mater. Interfaces* **2023**, *15*, 24034.
- [246] H. Wang, H. Zhu, W. Fu, Y. Zhang, B. Xu, F. Gao, Z. Cao, W. Liu, *Macromol. Rapid Commun.* **2017**, *38*, 1600695.
- [247] Q. Wu, J. Wei, B. Xu, X. Liu, H. Wang, W. Wang, Q. Wang, W. Liu, *Sci. Rep.* **2017**, *7*, 1.
- [248] H. Zhang, Y. Cong, A. R. Osi, Y. Zhou, F. Huang, R. P. Zaccaria, J. Chen, R. Wang, J. Fu, *Adv. Funct. Mater.* **2020**, *30*, 1910573.
- [249] J. Park, J. Y. Kim, J. H. Heo, Y. Kim, S. A. Kim, K. Park, Y. Lee, Y. Jin, S. R. Shin, D. W. Kim, J. Seo, J. Seo, *Adv. Sci.* **2023**, *10*, 2207237.
- [250] W. Liu, M. A. Heinrich, Y. Zhou, A. Akpek, N. Hu, X. Liu, X. Guan, Z. Zhong, X. Jin, A. Khademhosseini, Y. S. Zhang, *Adv. Healthcare Mater.* **2017**, *6*, 1601451.
- [251] Q. Chang, M. A. Darabi, Y. Liu, Y. He, W. Zhong, K. Mequanin, B. Li, F. Lu, M. M. Q. Xing, *J. Mater. Chem. A Mater.* **2019**, *7*, 24626.
- [252] Z. Lei, P. Wu, *ACS Nano* **2018**, *12*, 12860.
- [253] F. Tallia, L. Russo, S. Li, A. L. H. Orrin, X. Shi, S. Chen, J. A. M. Steele, S. Meille, J. Chevalier, P. D. Lee, M. M. Stevens, L. Cipolla, J. R. Jones, *Mater. Horiz.* **2018**, *5*, 849.
- [254] Y. Cao, Y. J. Tan, S. Li, W. W. Lee, H. Guo, Y. Cai, C. Wang, B. C.-K. Tee, *Nat. Electron.* **2019**, *2*, 75.
- [255] S. Liu, L. Li, *ACS Appl. Mater. Interfaces* **2017**, *9*, 26429.
- [256] S. A. Wilson, L. M. Cross, C. W. Peak, A. K. Gaharwar, *ACS Appl. Mater. Interfaces* **2017**, *9*, 43449.
- [257] S.-D. Wu, S.-H. Hsu, *Biofabrication* **2021**, *13*, 045029.
- [258] S. Y. Zheng, H. Ding, J. Qian, J. Yin, Z. L. Wu, Y. Song, Q. Zheng, *Macromolecules* **2016**, *49*, 9637.
- [259] X. Li, H. Wang, D. Li, S. Long, G. Zhang, Z. Wu, *ACS Appl. Mater. Interfaces* **2018**, *10*, 31198.
- [260] L. Shi, H. Carstensen, K. Hölzl, M. Lunzer, H. Li, J. Hilborn, A. Ovsianikov, D. A. Ossipov, *Chem. Mater.* **2017**, *29*, 5816.
- [261] S. Park, B.-G. Shin, S. Jang, K. Chung, *ACS Appl. Mater. Interfaces* **2020**, *12*, 3953.
- [262] W. Shin, J. S. Kim, H. J. Choi, H. Kim, S. Park, H. J. Lee, M. K. Choi, K. Chung, *Macromol. Rapid Commun.* **2021**, *42*, 2100011.
- [263] M. A. Darabi, A. Khosrozadeh, R. Mbeleck, Y. Liu, Q. Chang, J. Jiang, J. Cai, Q. Wang, G. Luo, M. Xing, *Adv. Mater.* **2017**, *29*, 1700533.
- [264] S. Lin, Y. Zhong, X. Zhao, T. Sawada, X. Li, W. Lei, M. Wang, T. Serizawa, H. Zhu, *Adv. Mater.* **2018**, *30*, 1803004.
- [265] F. Gang, H. Yan, C. Ma, L. Jiang, Y. Gu, Z. Liu, L. Zhao, X. Wang, J. Zhang, X. Sun, *Chem. Commun.* **2019**, *55*, 9801.
- [266] J.-C. Lai, L. Li, D.-P. Wang, M.-H. Zhang, S.-R. Mo, X. Wang, K.-Y. Zeng, C.-H. Li, Q. Jiang, X.-Z. You, J.-L. Zuo, *Nat. Commun.* **2018**, *9*, 2725.
- [267] X. Kuang, K. Chen, C. K. Dunn, J. Wu, V. C. F. Li, H. J. Qi, *ACS Appl. Mater. Interfaces* **2018**, *10*, 7381.
- [268] S. Qi, J. Fu, Y. Xie, Y. Li, R. Gan, M. Yu, *Compos. Sci. Technol.* **2019**, *183*, 107817.
- [269] T. J. Wallin, J. H. Pikul, S. Bodkhe, B. N. Peele, B. C. Mac Murray, D. Theriault, B. W. Mcenerney, R. P. Dillon, E. P. Giannelis, R. F. Shepherd, *J. Mater. Chem. B* **2017**, *5*, 6249.
- [270] P. Sanders, A. J. Young, Y. Qin, K. S. Fancey, M. R. Reithofer, R. Guillet-Nicolas, F. Kleitz, N. Pamme, J. M. Chin, *Sci. Rep.* **2019**, *9*, 388.
- [271] K. Yu, A. Xin, H. Du, Y. Li, Q. Wang, *NPG Asia Mater* **2019**, *11*, 7.
- [272] K. Yu, H. Du, A. Xin, K. H. Lee, Z. Feng, S. F. Masri, Y. Chen, G. Huang, Q. Wang, *NPG Asia Mater* **2020**, *12*, 26.
- [273] X. Li, R. Yu, Y. He, Y. Zhang, X. Yang, X. Zhao, W. Huang, *ACS Macro Lett.* **2019**, *8*, 1511.
- [274] B. Zhang, K. Kowsari, A. Serjouei, M. L. Dunn, Q. Ge, *Nat. Commun.* **2018**, *9*, 1831.
- [275] H. Gao, Y. Sun, M. Wang, Z. Wang, G. Han, L. Jin, P. Lin, Y. Xia, K. Zhang, *ACS Appl. Mater. Interfaces* **2021**, *13*, 1581.
- [276] E. Rossegger, R. Höller, D. Reisinger, J. Strasser, M. Fleisch, T. Griesser, S. Schlögl, *Polym. Chem.* **2021**, *12*, 638.
- [277] A. Liguori, S. Subramaniyan, J. G. Yao, M. Hakkarainen, *Eur. Polym. J.* **2022**, *178*, 111489.
- [278] A. S. Kuenstler, J. J. Hernandez, M. Trujillo-Lemon, A. Osterbaan, C. N. Bowman, *ACS Appl. Mater. Interfaces* **2023**, *15*, 11111.
- [279] K. Yu, Z. Feng, H. Du, A. Xin, K. H. Lee, K. Li, Y. Su, Q. Wang, N. X. Fang, C. Daraio, *Proc. Natl. Acad. Sci. U S A* **2021**, *118*, 1.
- [280] Z. Fang, H. Song, Y. Zhang, B. Jin, J. Wu, Q. Zhao, T. Xie, *Matter* **2020**, *2*, 1187.
- [281] S. Peng, N. Thirunavukkarasu, J. Chen, X. Zheng, C. Long, X. Huang, Z. Weng, L. Zheng, H. Wang, X. Peng, L. Wu, *Chem. Eng. J.* **2023**, *463*, 142312.
- [282] K. P. Cortés-Guzmán, A. R. Parikh, M. L. Sparacin, A. K. Remy, L. Adegoke, C. Chitrakar, M. Ecker, W. E. Voit, R. A. Smaldone, *ACS Sustain Chem. Eng.* **2022**, *10*, 13091.
- [283] M. Invernizzi, S. Turri, M. Levi, R. Suriano, *Eur. Polym. J.* **2018**, *101*, 169.
- [284] B. Guo, X. Ji, X. Chen, G. Li, Y. Lu, J. Bai, *Virtual Model. Rapid Manuf.: Adv. Res. Virtual Rapid Prototyping, Proc. Int. Conf. Adv. Res. Rapid Prototyping, 2nd* **2020**, *15*, 520.
- [285] G. Zhu, J. Zhang, J. Huang, X. Yu, J. Cheng, Q. Shang, Y. Hu, C. Liu, M. Zhang, L. Hu, Y. Zhou, *ACS Sustain Chem. Eng.* **2022**, *10*, 7954.
- [286] H. Chen, P. Ge, Z. Yan, M. Chen, X. Dai, H. Zhuo, S. Chen, L.-B. Huang, T. Zhang, *Chem. Eng. J.* **2021**, *430*, 133111.
- [287] M. Caprioli, I. Roppolo, A. Chiappone, L. Larush, C. F. Pirri, S. Magdassi, *Nat. Commun.* **2021**, *12*, 2462.
- [288] Z. Liu, P. Hong, Z. Huang, T. Zhang, R. Xu, L. Chen, H. Xiang, X. Liu, *Chem. Eng. J.* **2020**, *387*, 124142.
- [289] G. Zhu, Y. Hou, J. Xiang, J. Xu, N. Zhao, *ACS Appl. Mater. Interfaces* **2021**, *13*, 34954.
- [290] T. M. Valentin, E. M. Dubois, C. E. Machnicki, D. Bhaskar, F. R. Cui, I. Y. Wong, *Polym. Chem.* **2019**, *10*, 2015.
- [291] Z. Sun, Y. Lu, Q. Zhao, J. Wu, *Addit. Manuf.* **2022**, *50*, 102563.
- [292] W. Huang, J. Zhang, V. Singh, L. Xu, P. Kabi, E. Bele, M. K. Tiwari, *Addit. Manuf.* **2023**, *103343*, 103343.
- [293] Y. Wu, Y. Zeng, Y. Chen, C. Li, R. Qiu, W. Liu, *Adv. Funct. Mater.* **2021**, *31*, 2107202.
- [294] B. Zhang, W. Zhang, Z. Zhang, Y.-F. Zhang, H. Hingorani, Z. Liu, J. Liu, Q. Ge, *ACS Appl. Mater. Interfaces* **2019**, *11*, 10328.
- [295] Z. Wang, H. Cui, M. Liu, S. L. Grage, M. Hoffmann, E. Sedghamiz, W. Wenzel, P. A. Levkin, *Adv. Mater.* **2022**, *34*, 2107791.
- [296] D. Kam, A. Braner, A. Abouzglo, L. Larush, A. Chiappone, O. Shoseyov, S. Magdassi, *Langmuir* **2021**, *37*, 6451.
- [297] M. Gastaldi, C. A. Spiegel, C. Vazquez-Martel, C. Barolo, I. Roppolo, E. Blasco, *Mol. Syst. Des. Eng.* **2022**, *8*, 323.
- [298] O. Bliash, S. Joe, R. Reinberg, A. B. Nardin, L. Beccai, S. Magdassi, *Mater. Horiz.* **2023**, *10*, 4976.
- [299] S. Joe, O. Bliash, S. Magdassi, L. Beccai, *Adv. Sci.* **2023**, *10*, 2302080.

- [300] C. Hegde, J. Su, J. M. R. Tan, K. He, X. Chen, S. Magdassi, *ACS Nano* **2023**, 17, 15277.
- [301] G. Ge, Q. Wang, Y.-Z. Zhang, H. N. Alshareef, X. Dong, *Adv. Funct. Mater.* **2021**, 31, 2107437.
- [302] Y.-Z. Zhang, J. K. El-Demellawi, Q. Jiang, G. Ge, H. Liang, K. Lee, X. Dong, H. N. Alshareef, *Chem. Soc. Rev.* **2020**, 49, 7229.
- [303] P. Ahangar, M. E. Cooke, M. H. Weber, D. H. Rosenzweig, *Applied Sciences (Switzerland)* **2019**, 9, 1713.
- [304] M. Shahbazi, H. Jäger, *ACS Appl. Bio. Mater.* **2021**, 4, 325.
- [305] T. J. Wallin, J. Pikul, R. F. Shepherd, *Nat. Rev. Mater.* **2018**, 3, 84.
- [306] D. Chen, D. Wang, Y. Yang, Q. Huang, S. Zhu, Z. Zheng, *Adv. Energy Mater.* **2017**, 7, 1700890.
- [307] S. Waheed, J. M. Cabot, N. P. Macdonald, T. Lewis, R. M. Guijt, B. Paull, M. C. Breadmore, *Lab Chip* **2016**, 16, 1993.
- [308] M.-M. Song, Y.-M. Wang, X.-Y. Liang, X.-Q. Zhang, S. Zhang, B.-J. Li, *Soft Matter* **2019**, 15, 6615.
- [309] Z. Zhang, N. Corrigan, C. Boyer, *Angewandte Chemie – International Edition* **2022**, 61, e202114111.
- [310] G. Ge, Y.-Z. Zhang, W. Zhang, W. Yuan, J. K. El-Demellawi, P. Zhang, E. Di Fabrizio, X. Dong, H. N. Alshareef, *ACS Nano* **2021**, 15, 2698.
- [311] Y.-Z. Zhang, Y. Wang, Q. Jiang, J. K. El-Demellawi, H. Kim, H. N. Alshareef, *Adv. Mater.* **2020**, 32, 1908486.
- [312] M. M. Perera, N. Ayres, *Polym. Chem.* **2020**, 11, 1410.
- [313] S. Joshi, K. Rawat, C. Karunakaran, V. Rajamohan, A. T. Mathew, K. Koziol, V. Kumar Thakur, A. S. S. Balan, *Appl. Mater. Today* **2020**, 18, 100490.
- [314] F. Momeni, S. M. Mehdi Hassani, N. X. Liu, J. Ni, *Mater. Des.* **2017**, 122, 42.
- [315] S. Miao, N. Castro, M. Nowicki, L. Xia, H. Cui, X. Zhou, W. Zhu, S.-J. Lee, K. Sarkar, G. Vozzi, Y. Tabata, J. Fisher, L. G. Zhang, *Mater. Today* **2017**, 20, 577.
- [316] X. Kuang, D. J. Roach, J. Wu, C. M. Hamel, Z. Ding, T. Wang, M. L. Dunn, H. J. Qi, *Adv. Funct. Mater.* **2019**, 29, 1805290.
- [317] M. Hayashi, *Polymers (Basel)* **2020**, 12, 1322.
- [318] G. Zhu, Y. Hou, J. Xu, N. Zhao, *Adv. Funct. Mater.* **2021**, 31, 2007173.
- [319] D. Puppi, F. Chiellini, *Appl. Mater. Today* **2020**, 20, 100700.
- [320] Z. Chen, M. Yang, M. Ji, X. Kuang, H. J. Qi, T. Wang, *Mater. Des.* **2021**, 197, 109189.
- [321] Q. Shi, K. Yu, X. Kuang, X. Mu, C. K. Dunn, M. L. Dunn, T. Wang, H. Jerry Qi, *Mater. Horiz.* **2017**, 4, 598.



**Ignazio Roppolo** is an assistant professor at Politecnico di Torino, Italy, leader of the laboratory specifically focused on light-induced 3D printing. He has published more than 90 papers, among which more than 40 specifically on 3D printing, and his publications were cited more than 2800 times. In his research activities, he aims at gathering chemistry, physics, material's science, and advanced manufacturing and design for fabricating advanced devices, which can be then applied to multiple fields.



**Matteo Caprioli** obtained his Ph.D. in materials science and technology at the Polytechnic of Turin achieved with a thesis on 3D printed hydrogels with self-healing properties. His research activity, performed in the frame of a joint research project with Prof. Shlomo Magdassi's group at the Hebrew University of Jerusalem, was focused on soft materials with smart properties based on water-based resins for digital light printing. Currently, he is working as a strategic innovation consultant for the sustainable development of companies.



**Candido Fabrizio Pirri**, is a professor at Politecnico di Torino, Head of “Materials and Processes for Micro & Nanotechnologies” (MPMNT) group, and Director of the Center for Sustainable Future Technologies (CSFT) of Italian Institute of Technology. He has published over 480 papers, his publications were cited more than 10000 times. His research activities span on many branches of nanotechnologies: from energy to sensors, from biomedical fields to advanced manufacturing, including the development of advanced devices.



**Shlomo Magdassi** is a professor at The Hebrew University of Jerusalem’s Institute of Chemistry, and academic director of Center for Functional and 3D Printing. His research centers on micro-nanomaterials, with a focus on their applications in functional 2D and 3D printing. He has published more than 350 papers, edited four books, and holds approximately 300 patents. His research outcome includes the creation of commercial activities, start-up companies, licensing agreements, and worldwide sales. He was awarded with the 2022 Johann Gutenberg Prize by the Society for Imaging Science and Technology, and he is also a Fellow of the National Academy of Inventors.